OPTIMIZING THE ELECTROCHEMICAL PERFORMANCE OF IMIDAZOLIUM-BASED POLYMERIC IONIC LIQUIDS BY VARYING TETHERING GROUPS

By

Zhe Jia

A DISSERTATION

Submitted to
Michigan State University
in partial fulfillment of the requirements
for the degree of

Chemistry – Doctor of Philosophy

2014

ABSTRACT

OPTIMIZING THE ELECTROCHEMICAL PERFORMANCE OF IMIDAZOLIUM-BASED POLYMERIC IONIC LIQUIDS BY VARYING TETHERING GROUPS

By

Zhe Jia

Increasing efforts have been made in the area of sustainable alternative energy devices in the past few decades in order to develop high efficiency, low-cost electrochemical devices with sufficient long-term stability. Due to the drawbacks of conventional organic liquid electrolytes, such as leakage, volatility, flammability, and toxicity, the synthesis of solvent-free electrolyte materials has been studied world-wide.

Among all the alternatives, polymer electrolytes are of great interest and have attracted many research groups. Solid-state polymer electrolytes and in particular, polymer ionic liquids (PILs), considered to be promising candidates, have been under studied widely. Ionic Liquids (ILs), defined as organic/inorganic salts with m.p. lower than 100 °C, offer good chemical stability, low flammability, negligible vapor pressure and high ionic conductivity. PILs, as the polymerized state of ILs, not only present some of the unique properties of ILs, but also benefit from the intrinsic properties of polymers, such as better thermal and chemical stability, enhanced mechanical properties, and tunable solution properties. The constrained structure of PILs may help to overcome fabrication and leakage problems associated with simple liquid electrolytes, but typically also leads to lower ionic conductivity. Once polymerized, the ionic conductivity of PILs drops substantially, usually by several orders of magnitude compared to the corresponding monomers. Therefore, to improve PILs chain mobility is crucial. Previous

studies suggest that a flexible tethering group should make the polymer backbone less rigid and increase electrolyte ion mobility.

To investigate how tethering groups affect both electrochemical performance and physical properties of free ILs and PILs, we first report the synthesis and characterization of a novel class of imidazolium (Im) based IL model compounds and their corresponding PILs. Poly(ethylene oxide)s (PEOs), considered to be promising candidates for this purpose, were attached as tethering groups to imidazolium cations in order to optimize the T_g and ionic conductivities. Previous research on oligomer/polymer electrolytes showed that attaching PEO to the imidazolium cation lowered the T_g of ILs and increased their conductivity. PEO is also chemically stable, dissolves metal ions, and when incorporated into ionic liquids, provides a solvent free electrolyte. A series of IL model compounds and PILs were first synthesized with various lengths of PEO attached on the imidazole. The thermophysical and electrochemical properties of ILs and PILs, including density, viscosity, conductivity and thermal properties were characterized in order to investigate the effect of tethering groups.

To My Beloved Family

ACKNOWLEDGMENTS

TABLE OF CONTENTS

LIST OF TABLES

LIST OF FIGURES

LIST OF SCHEMES

KEY TO ABBREVIATIONS

σ	conductivity
ε	dielectric constant
η	viscosity
γ	strain
γ_0	stain amplitude
τ	stress
μ	ion mobility
Λ	molar conductivity
G'	storage modulus
G''	loss modulus
G^*	complex modulus
q	ion charge
γ-BL	γ-butyrolactone
ATRP	atom transfer radical polymerization
AC	alternating current
Bpy	bipyridine
CTAB	cetyltrimethylammonium bromide
CV	cyclic voltammetry
DC	direct current
DMC	dimethyl carbonate
DSC	differential scanning calorimetry

DSSC	dye-sensitized solar cell
EC	ethylene carbonate
EIS	electrochemical impedance spectroscopy
EMC	ethyl methyl carbonate
EO	ethylene oxide
FTIR	Fourier transform infrared spectroscopy
LCST	lower critical solution temperature
IL	ionic liquid
LIB	lithium ion battery
LiTFSI	lithium bis trifluoromethanesulfonyl imide
LVR	linear viscoelastic region
NMP	nitroxide-mediated polymerization
NMR	nuclear magnetic resonance
PAN	poly(acrylonitrile)
PC	propylene carbonate
PDMS	poly(dimethyl siloxane)
PDI	polydisperse index
PEG	poly(ethylene glycol)
PEGMA	poly(ethylene glycol) methyl ether methacrylate
PEGDME-500	polyethylene glycol dimethyl ether (average molecular weight 500)
PEI	poly(ethylene imine)
PEO	poly(ethylene oxide)
PGPS	poly(ethylene oxide) grafted polysiloxane

PIL	polymer ionic liquid
PMMA	poly(methyl methaacrylate)
POE	poly(oxythylene)
poly(PEGMA)	polymer of poly(ethylene glycol) methyl ether methacrylate
POO	poly(oxymethylene-oligo-oxyethylene)
POM	poly(oxymethylene)
PPO	poly(propylene oxide)
PVAc	polyvinyl acetate
PVC	poly(vinyl chloride)
PVdF	poly(vinylidene fluoride)
PVS	poly(vinyl sulfone)
RAFT	reversible addition-fragmentation chain transfer radical polymerization
r.t.	room temperature
SEI	solid electrolyte interface
Silica-initiator	surface-imitator coated silica nanoparticle
Silica-poly(PEGMA)	PEGMA homopolymer coated silica nanoparticles
Silica-copolymer	PEGMA copolymer coated silica nanoparticles
T_b	boiling point
T_d	decomposition temperature
T_g	glass transition temperature
T_m	melting point
TEM	transmission electron microscopy
TFSI	bis(trifluoromethane)sulfonimide

TGA   thermogravimetric analysis

VFT   Vogel-Fulcher-Tammann

1. Chapter 1   Introduction

1.1   General background

In the Intergovernmental Panel on Climate Change (IPCC) 2013 annual report, it is pointed out that greenhouse gases emissions have likely been a major cause of global warming since the mid-20th century and that greenhouse gas (i.e. carbon dioxide, methane, chlorofluorocarbons and nitrous oxide) from fossil fuel use made up 56.6% of total greenhouse gas emissions in 2004.[1] Concern is increasing regarding fossil fuel use, both about the short and the long term supplies. As human dependence on energy rises to unprecedented levels, the sustainability of the energy supply is one of the greatest challenges. The search for efficient renewable energy sources and advanced energy storage devices is drawing the attention of many researchers.[2] A particular challenge is the development of high efficiency, low-cost electrochemical devices with sufficient long-term stability.

1.2   Electrolytes

Electrolytes which function as the inner charge carrier between two electrodes, are crucial components of batteries, cells or capacitor-needed electronics.[2] The majority of electrolytes consist of salts dissolved in solvents. The ions in the solutions conduct electricity working under applied voltage, thus transporting charge. The solvent can be aqueous solvent (i.e. water) or non-aqueous solvent (i.e. organic liquid).[3]

The choice of a particular salt might vary as a function of its thermal stability or electrochemical properties. In general, the salt should possess a relatively low lattice

energy to guarantee efficient ion dissociation in the chosen solvent.[4] As reviewed in previous literature, an ideal electrolyte solvent needs to meet several fundamental requirements:[5]

(1) a high dielectric constant (ε) that can efficiently dissolve salts;

(2) a low viscosity (η) to allow effective ion transportation;

(3) a relatively large electrochemical window to ensure chemical stability during cell operation;

(4) melting point $\ll$ boiling point so that it will stay in the liquid phase over a wide temperature range;

(5) safety issues, such as low toxicity, high flash point, resistance to oxidation and polymerization, etc.

1.2.1   Conventional liquid electrolyte
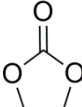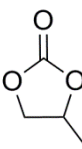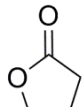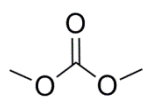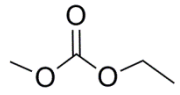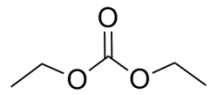
Conventional liquid electrolytes for lithium ion batteries (LIB)s are usually composed of two parts: a lithium salt (e.g. $LiPF_6$, $LiAsF_6$, $LiBF_4$, $LiPF_3(C_2F_5)_3$, $LiN(CF_3SO_2)_2$, $LiClO_4$), and a mixture of nonaqueous organic small molecules—alkyl carbonate solvents, such as ethylene carbonate (EC), propylene carbonate (PC), dimethyl carbonate (DMC), ethyl methyl carbonate (EMC), or lactones such as γ-butyrolactone (γ-BL).[6]

Non-aqueous organic solvents are needed to establish a wide enough redox window for the electrolyte. The powerful reducing anodes and oxidizing cathodes in LIBs make protic solvent unusable in a working cell, despite their great capability in dissociating salts, because the reduction of any active proton or the oxidation of its

2

corresponding anion would fall inside the range of cathode and anode potentials needed for charging in the rechargeable LIBs.[7] Meanwhile, in order to generate sufficient ion dissociation, the non-aqueous organic solvent molecules need to be highly polar in structure, making the alkyl carbonates ideal for this purpose.[8] These carbonate compounds usually have a high dielectric constant, enabling them dissolve various lithium salts.[5] Moreover, such low molecular weight organic compounds are generally low in viscosity, resulted in relatively high ionic conductivity (10^{-3} to 10^{-2} S/cm)[8]; this range, however is still about an order of magnitude lower than aqueous alkaline electrolyte (10^{-2} to 10^{-1} S/cm)[4]. The aspect that makes them particularly attractive is their electrochemical stability. They are also capable of the rapid formation of a stable passivating layer at the solid electrolyte interface (SEI),[9] which is extremely important for the durable performance of electrochemical devices.[6]

The initial cell developed in 1991 employed $LiPF_6$ dissolved in PC and DEC mixture as electrolyte, while the combination of EC and γ-BL were later introduced in 1992, followed by MEC, methyl propionate (MP) and DMC in 1993.[10] Since then tremendous efforts have been made to further optimize the electrochemical performance of carbonate electrolytes. Two major types of alkyl carbonate compounds have been employed: cyclic esters (e.g. PC, EC) and linear esters (DMC, EMC). The former have higher permittivity, attributed to their high polarity, but they are higher in viscosity due to strong intermolecular forces; the latter are lower in viscosity because of increased freedom coming from the rotation of alkyl groups, but they are less chemically stable.[6] **Table 1-1** shows some physical properties of common carbonates used as electrolyte solvents.[11]

Table 1-1   Examples of common conventional small molecule electrolytes and their corresponding physical properties

Common electrolyte solvents	Structure	m.p. (°C)	b.p. (°C)	Viscosity (η) /cp [a]	Density (g/cm^3) [b]
EC		36.4	248	1.93	1.3214
PC		-48.8	240	2.53	1.2047
γ-BL		-43.5	204	1.73	1.199
DMC		4.6	91	3.12	1.071
EMC		-43	203	0.66	1.007
DEC		-74.3	126	0.75	0.969

[a] Viscosity data was taken at 40 °C. Water at 20 °C has a viscosity of 1.0020 cP, 1 cP = 1 mPa·s. [b] Density was measured at room temperature.

However, these alkyl carbonate small molecules are highly flammable compounds, leaving cells prone to combustion.[12] Moreover, the mobile liquid nature of these organic small molecules not only raises problems for sealing in the packaging process, but also raises the issue of leaking during cell operation, which could cause severe damage to the

working cell and devices it powers.[13] The problem is particularly significant under thermal abuse conditions (external heating, flame attack, hot combustion, etc). A previous study of electrolytes composed of $LiPF_6$ dissolved in various common organic carbonates suggests that the electrolyte thermal decomposition reaction happened autocatalytically, which could cause serious thermal runaway issues with functioning cells.[14] Some other common drawbacks related to liquid electrolytes, including narrow operating temperature range, electrode corrosion, and growth of dendritic lithium, could also lead to system failure.[15]

With the heavy dependence on LIBs nowadays, safety issues associated with electrolytes have sparked increasing interest among researchers. To develop intrinsically safe electrolyte, the replacement of flammable liquid organic electrolyte solvent is necessary.[16]

1.2.2   Solid polymer electrolytes

Polymer based electrolytes are of growing interest in high energy density electrochemical device applications mostly due to their combined advantages of superb solid-state electrochemical stability and intrinsic plastic polymer material properties, which are believed to circumvent problems regarding sealing and leaking.[17] They are thus viewed as highly promising candidates as improved electrolyte materials. Here, polymer electrolytes refer to solid solutions that dissolve alkali metal in a polymer matrix. Polyelectrolytes are polymers where charged sites, either cation or anion, are bonded onto polymer backbones used for electrolytes (see more in **Section 1.2.5**).

As discussed in the previous section, in analogy with conventional liquid electrolytes, an inorganic salt of low lattice energy is necessary to facilitate ion dissociation.[18] However, the choice for a suitable host polymer in potential solid-state electrolyte applications also needs to meet some fundamental prerequisites:[19]
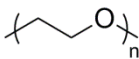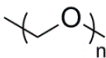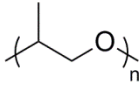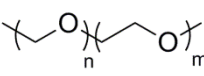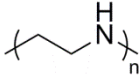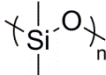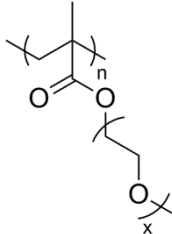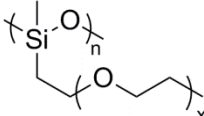
(1) a polar structure to be able to effectively coordinate ions;

(2) a low cohesive energy (the amount of energy needed to completely remove a unit volume of polymer molecules from their neighbors to infinite separation) to assist solvation;

(3) a highly flexible polymer chain to enable facile ion transport.

To fulfill these requirements, several polymers based on polyamines and polyethers have undergone extensive studies. Among all the alternatives, poly(ethylene oxide) (PEO) based polymers have so far been identified as the most promising candidates.[20]

Table 1-2   Examples of some common polymer electrolyte-salt and their corresponding properties[21]

Polymer	Structure	Electrolyte [a]	Conductivity (S/cm) [b]
Poly(ethylene oxide) (PEO)		$(PEO)_8$-$LiClO_4$	10^{-8}
Poly(oxymethylene) (POM)		POM-$LiClO_4$	10^{-8}
Poly(propylene oxide) (PPO)		$(PPO)_8$-$LiClO_4$	10^{-8}
Poly(oxymethylene-oligo-oxyethylene) (POO)		$(POO)_{25}$-$LiCF_3SO_3$	3×10^{-5}
Poly(ethylene imine) (PEI)		PEI-$LiClO_4$	10^{-3}
Poly(dimethyl siloxane) (PDMS)		PDMS-$LiClO_4$	10^{-4}
Poly(methoxy poly(ethylene oxide) methacrylate)		$(PMG)_{22}$-$LiCF_3SO_3$	3×10^{-5}
PEO-grafted polysiloxane (PGPS)		PGPS-$LiClO_4$	10^{-4}

[a] Electrolyte complexes are examples cited from literature. [b] Conductivity was measured at room temperature (25 °C).

1.2.2.1 Poly(ethylene oxide) based polymer electrolyte

PEO (or in some references is denoted as poly(oxyethylene) (POE)) refers to a polymer with –CH_2CH_2O– repeating unit, often being synthesized through ring opening polymerization of ethylene oxide. While low molecular weight oligomer is commonly termed poly(ethylene glycol) (PEG), high molecular weight polymer can be obtained through ring-opening cationic or anionic polymerization.[22] As the molecular weight of PEO rises, the physical appearance turns from a viscous liquid into a pale white solid at room temperature. Normally, PEO has a low glass transition temperature (ca. -60 °C), and favors a high degree of crystallinity (almost 80%), with a melting point at around 60 °C.[23] Previous work has shown that PEO is prone to crystallization, choosing its most stable conformation—the 7_2 helix conformation, with a repeating unit of seven ethylene oxide segments, comprising two turns over a fiber period of 1.93 nm.[24] It has also been observed by Takahashi *et al*.[25] that PEO could yield a planar zigzag conformation under external tension cause by macroscopic stretching. **Figure 1-1** shows the work done by the Baker group where the ethylene oxide repeating unit in PEO/PE (polyethylene) micro building blocks adopt different crystallization conformations induced by different conditions.[26]
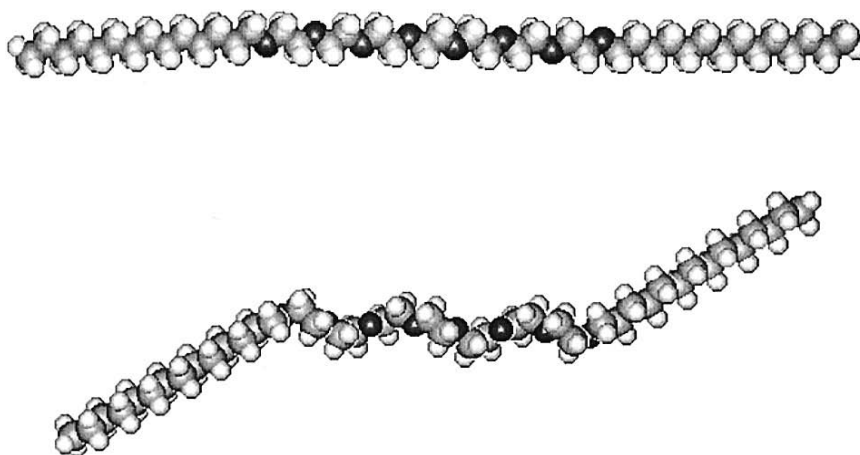
Figure 1-1 PEO crystallization conformations: planar zigzag (top) and 7_2 helix (bottom), obtained by crystallization from methanol and hexane, respectively[26] (Copyright 2014 American Chemical Society. Reproduced with permission)

The discovery of alkali metal ions forming complexes in PEO matrix was first reported by Wright in 1973,[27] followed by the observation of Na and K salts conducting in PEO and reported in 1975.[28] However, the suggestion to utilize this system as a solid-state electrolyte did not appear until 1978.[29] Since the first all solid-state battery based on PEO and Li ion electrolyte, which also was the first solvent free electrolyte system discovered, was reported in 1979 by M. B. Armand,[30] the active and systematic study of PEO based polymers as solid-state electrolytes, including synthesis, characterization methods and related technological applications, has been vigorously pursued for several decades.[31]

The popularity of PEO and its derivatives as host polymer electrolytes for solid-state ionic studies is largely owing to their formation of stable complexes and the relatively high degree of lithium ion dissociation in the polymer matrix, compared with other polymer candidates for the same purpose.[32] The polar oxygen atom in the ethylene

9

oxide repeating unit provides sites where the polymer chain can dissolve/complex with cations.[15] Furthermore, PEO chains are arranged in helical conformations with a hollow core that presents ideal distances for oxygen–lithium interactions.[33] A previous study of PEO-LiClO$_4$ revealed that the cations were encapsulated within the PEO helix while the anions were stacked outside.[34]

The generally accepted mechanism for ion transportation in PEO complexes was proposed by Ratner (**Figure 1-2**): the high polarity of the ethylene glycol repeating unit, caused by ion-dipole interactions between the alkali cation and oxygen atoms, enables cation dissociation in the polymer network, resulting in a solvation-desolvation process.[35] Molecular dynamics simulations indicate that the PEO/Li ion complexes form through approximately five ethylene oxide repeating unit coordinating with one lithium ion.[36] As a result of this complexation, lithium ion mobility is significantly decreased. Moreover, its transportation in the polymer matrix is highly coupled with the segmental movement of the polymer chain in the amorphous phase.[37] Therefore, the ion movement can be described as the motion of the lithium ion "hopping" between PEO complexation sites aided by the segmental movement of polymer chains.
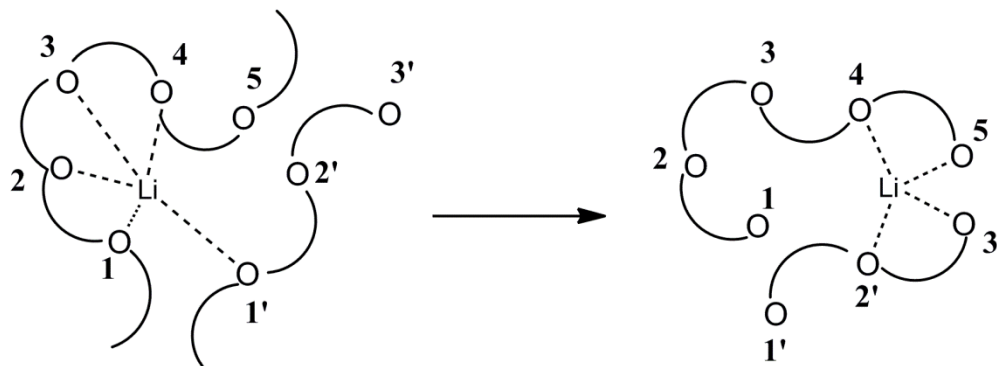
Figure 1-2   Schematic representation of lithium ion transportation in PEO polymer complex, as proposed by Ratner[35] (Copyright 2014 American Chemical Society. Reproduced with permission)

The original work done by Armand points out that fast ion transport only occurred within the polymer amorphous phase, where conductivity could be two to three orders of magnitude higher than in the crystalline phase.[38] Therefore, to obtain a larger fraction and higher degree of amorphosity of the host polymer seems to be a key goal to optimize ionic conductivity. PEO based polymers crystallize below 70 °C—mostly associated with the m.p. of the polymer.[32] PEO is amorphous when above its melting point. Therefore, tremendous efforts have been made to prevent crystallization and to maintain a high degree of polymer amorphosity.

On the other hand, an important property in defining conductivity is T_g, the point at which the amorphous PEO changes from a flexible, rubbery state to a brittle, glassy state. The temperature dependence of ionic conductivity often correlates with the temperature dependence of segmental movement (i.e. T_g). A low T_g generally reflects flexibility of the polymer chain, offering faster ion transportation. Hence, intensive investigation has been made in search of "low T_g" host polymers.

11

It has been reported that room temperature conductivity of a polymer electrolyte should be above 10^{-4} S/cm for practical applications.[20] However, because of PEO's tendency to crystallize, the conductivity is relatively low at room temperature ($\leq 10^{-6}$ S/cm). **Table 1-3** reports some polymer salt complexes investigated in previous studies, along with their conductivity data.[17,23,39-41]

Table 1-3   Conductivity data of some polymer salt complex

Polymer electrolyte	Conductivity (S/cm)	Temperature (°C)
$(PEO)_x-LiClO_4$	1×10^{-7}	27
$PEO-LiN(CF_3SO_2)_2$	1×10^{-4}	25
$PEO\text{-}LiBF_4$	1×10^{-6}	25
$PEO\text{-}NH_4I$	1×10^{-5}	23
$(PPO)_{12}\text{-}NaCF_3SO_3$	1×10^{-5}	45

In addition to their relatively low room temperature conductivity, another defect associated with PEO-salt systems is the fairly low lithium transference number (t^+)—the fraction of the total charge carried through electrolyte by Li^+, which is usually in the range of 0.2 – 0.4,[3] indicating that the anion is the dominant species transporting charge. This, however, can be improved by choosing large, highly delocalized organic anions (e.g. $TFSI^-$). This issue will be further discussed in Chapter 2.

In conclusion, the development the solid polymer electrolytes has seen huge breakthroughs over the decades, but the practical application of PEO based polymer electrolytes requires a compromise between the ionic conductivity and acceptable mechanical properties. Novel materials are desired for this aim.

1.2.2.2 Ionic conductivity of polymer electrolytes

Ionic conductivity (σ) is defined as the product of the charge carrier concentration (n), ion charge (q), and ion mobility (μ):

$$\sigma = n \cdot q \cdot \mu \qquad \qquad \textbf{Equation 1-1}$$

The physical description of ionic conductivity generally falls into two categories: Arrhenius behavior or Vogel-Fulcher-Tammann (VFT) behavior.[15,42] The Arrhenius equation is described as followed[17]:

$$\sigma = \sigma_0 exp\left(-\frac{E_a}{RT}\right) \qquad \qquad \textbf{Equation 1-2}$$

where σ_0 is a pre-exponential factor correlated to the number of charge carriers, and E_a is the activation energy that can be calculated from the linear best fit of log σ against 1/T. This type of behavior is associated with ion hopping decoupled with long-range motions in the matrix, typically observed in amorphous polymers or polymer glass phases below T_g, ceramic ion conductors, *etc.*[42]

Since the phase of the electrolyte is highly dependent on temperature, the most widely used models to describe the temperature dependence of ion conductivity in polymer electrolyte is the VFT equation[23,30]:

$$\sigma = \sigma_\infty exp\left(-\frac{B}{T - T_0}\right) \qquad \qquad \textbf{Equation 1-3}$$

where σ_∞ is the infinite temperature conductivity, B is the fitting parameter related to the activation energy of ion conduction, while T_0 is the equilibrium glass transition temperature close to T_g that is associated with polymer chain mobility. Higher conductivity value will be obtained as difference between operation temperature (T) and

T_0 increases. Consequently, the VTF equation provides theoretical guidance for developing low T_g host polymer materials.

The VTF behavior is most relevant for polymer electrolytes.[42] It is commonly observed not only in polymer electrolytes, but also gel electrolytes[43] and ionic liquids[44]. The Arrhenius plot for VTF behavior is usually non-linear. It is based on empirical observation, and ionic hopping movement within the polymer matrix is coupled with segmental movement of polymer chains.[15] However, it is worth pointing out that this model is restricted to cases where ion pairs are completely dissociated in a homogeneous amorphous phase.[45]

1.2.2.3 Conductivity measurement – AC impedance spectroscory

Electrochemical impedance spectroscopy (EIS) is typically employed to measure the ionic conductivity of polymer electrolytes. Ohms law describes the resistance, R (unit in Ω, $\Omega = 1/S$), as a function of current, I (A), and applied voltage V:

$$R = V/I \qquad\qquad \textbf{Equation 1-4}$$

Conductivity (σ, unit in S/cm) is defined as the reciprocal of resistivity (ρ, unit in $\Omega\cdot$cm):

$$\sigma = 1/\rho \qquad\qquad \textbf{Equation 1-5}$$

Since R is measured by AC impedance, and

$$R = \rho\cdot l/A \qquad\qquad \textbf{Equation 1-6}$$

where l (cm) refers to the measured sample distance and A (cm^2) is the cross-section area of tested sample.

Therefore, conductivity can be described as:

$$\sigma = 1/\rho = l/(R \cdot A) \qquad \qquad \textbf{Equation 1-7}$$

with the unit in S/cm.

During the impedance measurement, electrolyte is typically sandwiched between two electrodes, and an AC potential is applied over a broad frequency range, from 5 mHz to 1.3 MHz. The sample cell used in this work is made of two steel disks as symmetrical electrodes. Under the applied voltage, a current is generated passing through the electrodes (as a capacitor) and the polymer electrolyte (as a resistor). This current is inversely proportional to the impedance (Z) of the cell and is frequency dependent. For the convenience of calculation, the complex impedance is expressed as:

$$Z = Z' - iZ'' \qquad \qquad \textbf{Equation 1-8}$$

where Z' is the real part ($Z' = Z \cos\theta$), Z'' is the imaginary part ($Z'' = Z \sin\theta$) and i is the imaginary symbol.

The electro response of measured cell can be described as an equivalent circuit. As **Figure 1-3** shows, C_1 and R_1 refer to the capacitance between two electrodes and resistance of electrolyte respectively; while C_2 and R_2 is the capacitance and resistance between electrode and electrolyte respectively. Therefore, the capacitance (C) can be calculated as

$$C = \varepsilon_r \varepsilon_0 A/d \qquad \qquad \textbf{Equation 1-9}$$

where ε_r is dielectric constant, ε_0 is permittivity of free space, A refers to the area of the two electrodes and d is the distance between electrodes.
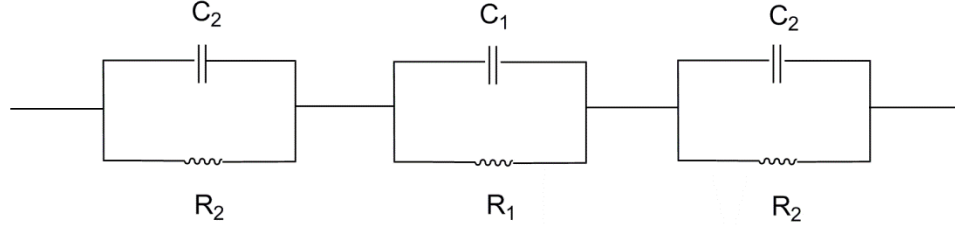
Figure 1-3   Equivalent circuit of the cell used in AC independence measurement

Since the distance between two electrodes (d_1) is far more than the distance between the electrode and electrolyte (d_2), $C_1 \ll C_2$. The impedance of a capacitor (X_C) is calculated by **Equation 1-10**:

$$X_C = -1/\omega C \hspace{4cm} \textbf{Equation 1-10}$$

where ω is the angular frequency and C is the capacitance. Since $C_1 \ll C_2$, $X_{C1} \gg X_{C2}$. Therefore, during a measurement, there are several possible circumstances:

1) At $\omega = 0$, X_{C1} and X_{C2} approach infinite, the total impedance is $Z_{tot} = R_1 + 2R_2$.

2) As ω increases, X_{C1} decreases and is close to 0, $Z_{tot} = R_1$.

3) At ω approaches infinite, X_{C1} and X_{C2} are close to 0.
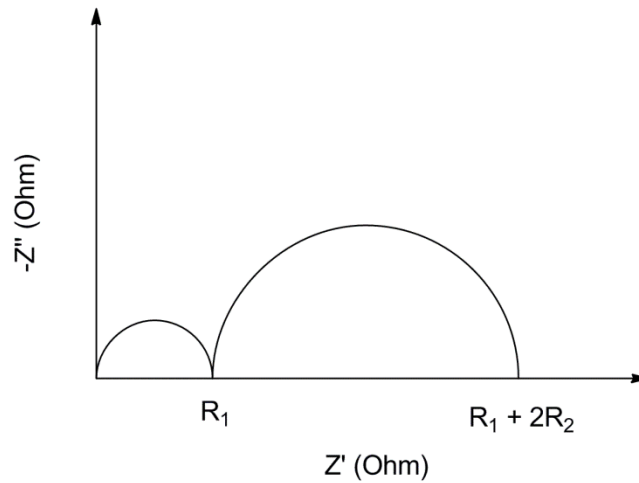
Figure 1-4   The Nyquist plot in the ideal case

16

The data collected at a series of frequencies is plotted as the imaginary part (y axis) versus the real part (x axis) in a so-called Nyquist plot. Ideally, the plot of the equivalent circuit should be presented as **Figure 1-4**. However, ω at both 0 and infinity are immeasurable, so an example of a typical Nquist plot shows in **Figure 1-5**. R_b (bulk resistance) can be read from a plot as the point where the imaginary part returns to zero and intercepts the x axis. Both of the components, electrodes and electrolytes contribute to the measured resistance. Since the two electrode disks are made of much more conductive material, the resistance produced from the electrodes is generally negligible, and R_b can be viewed as the resistance of the electrolyte. Therefore, the conductivity value can be calculated through **Equation 1-7**.
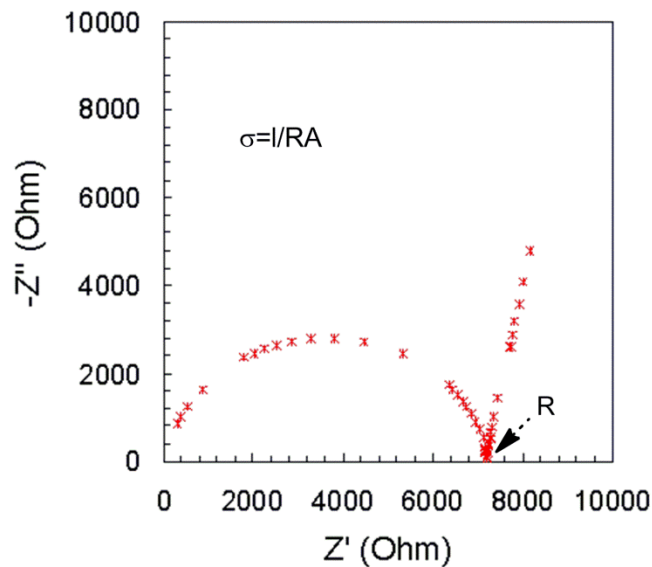
Figure 1-5   An example of a Nyquist plot obtained from EIS

1.2.3 Gel polymer electrolytes

The distinction between a gel polymer electrolyte and a polymer electrolyte is that the former usually refers to a polymer-solvent-salt system, where the role of polymer is to serve as a low-molecular-weight solvent stiffener instead of an overall host matrix for the electrolyte.[17] In gel electrolytes, organic small molecules serve as the major solvent to dissolve the inorganic salts, while the polymer is swollen by the organic solvent, offering dimensional stability and mechanical support.

Work on gel polymer electrolytes was first reported by Fenullade and Perche in 1975.[46] In their original report, several aprotic organic solvents (e.g. PC, PAN, THF, NMP, etc.) were used to dissolve lithium salts, and a thermosetting self-supporting polymer was then added as a gelator. The result was very inspiring. The formation of the gel held the electrolyte in a quasi solid-state, yet still maintained high ionic conductivity, close to the value the liquids electrolytes. Since the discovery of gel electrolyte, a vast number of host polymers, such as PEO[47], poly(vinylidene fluoride) (PVdF)[48], poly(acrylonitrile) (PAN)[49], poly (vinyl chloride) (PVC)[50], poly(vinyl sulfone)[51], poly(methyl methacrylate) (PMMA)[52], etc. have been synthesized and explored in these system (**Table 1-4**).

Table 1-4   Some polymer gel electrolyte systems and their conductivity value.[15,21]

Polymer host	Gel electrolyte	Conductivity (S/cm) [a]
Plasticized liner PEO	$(PEO)_8$-$LiClO_4$ (EC:PC, 20 mol%)	10^{-3}
Crosslinked PEO	$(PEO)_8$-$LiClO_4$ (PC, 50 wt%)	8×10^{-4}
PVdF	PVdF-$LiN(CF_3SO_2)_2$ (EC:PC, 75 wt%)	1.5×10^{-3}
PEI	PEI-$LiClO_4$	10^{-3}
Acrylates (ethylene glycol dimethacrylate (EGDMA))	EGDMA-$LiClO_4$ (PC, 1M)	2×10^{-3}
PAN	PAN-$(EC:PC:LiClO_4)$ 38-33:21.8 mol%	10^{-3}
PMMA	PMMA-EC/PC-$LiClO_4$	10^{-3}
PVC	PVC-EC/PC-$LiClO_4$	10^{-3}

[a] Conductivity measurement was taken at 20 °C.

The reported room temperature conductivity of a gel polymer can be up to 10^{-3} S/cm, mostly due to the greater salt dissociation in the presence of liquid solvent. The host polymer exhibits a more amorphous phase owing to the plasticizing effect of the organic liquid. This results in a much lower T_g, which can be further decreased with increasing liquid content. The volume fraction of liquid electrolyte can be as high as 85%.[53] However, the thermal and mechanical properties may be compromised with escalating temperature. So far, the only commercially available gel polymer electrolyte system was developed in 1996, the Bellcore/Telcordia lithium battery based on a fluorinated polymer—PVdF and $LiPF_6$.[54]

1.2.4 Composite polymer electrolyte

Composite polymer electrolytes refer to nano-sized filler particles dispersed into polymer electrolytes, where the inorganic filler can provide mechanical support.[55] Upon the introduction of inorganic fillers, typically inorganic oxide particles (e.g. Al_2O_3, TiO_2, SiO_2, ZrO_2, etc.), crystallization of the host polymer is somewhat inhibited, resulting in a higher amorphosity.[55-57]

In work first done by Weston *et al*. in 1982, α-Al_2O_3 was introduced as a filler to the PEO-LiClO$_4$ syetem.[58] In the original report, they observed that the addition of up to 10 vol% α-Al_2O_3 filler had an almost negligible effect on ionic conductivity but gave significant mechanical stability even at temperatures higher than 100 °C. Not only are enhanced mechanical properties observed, but later study also revealed that the formation of composites could lead to an increase in ionic conductivity, presumably owing to the inhibiting of polymer crystallization.[59,60] Although enhanced mechanical properties might seem an obvious effect of the addition of inorganic fillers, the discovery of the improved ionic conductivity was not made until the filler particles were of nanometer size.[61] These ideas were widely explored after Croce *et al.*'s work was published in Nature, where PEO-LiClO$_4$ was incorporated with TiO_2 and Al_2O_3 particles 5.8-13 nm in size.[55] They observed that nano-sized ceramic powders performed as solid plasticizers in host PEO matrix, kinetically inhibited crystallization over annealing, and resulted in conductivities around 10^{-4} S/cm at 50 °C and 10^{-5} S/cm at 30 °C. Since then, with intensive ongoing research in this area, systems with room temperature conductivity as high as 10^{-4} S/cm and excellent mechanical properties have been created and employed in LIBs.[20] **Table**

1-5 lists some common composite fillers used for polymer electrolytes (examples are taken from reference 16).

Our group has been a leader in developing inorganic filler composite polymer electrolytes. Baker, Khan and Fedkiw[62-65] incorporated fumed silica nanoparticles into PEO based electrolytes. Not only electrochemical performance, but also the rheological response is rather different from those of pure polymer electrolytes. With the formation of composite polymer electrolytes, they show fairly good mechanical property and electrolyte/electrode interfacial stability, yet still give reasonable ionic conductivity.

In a similar approach, our group has developed a novel method by chemically bonding polymers onto silica nanoparticles. Composite polymer electrolytes, PEO-based polymers, ionic liquids[66] and triphenylamine based hole transporting materials[67] have been tailored onto silica nanoparticles. The details of this study are examined in Chapter 3.

Table 1-5   Some composite polymer electrolytes and their conductivity.

Polymer-salt	Filler	Conductivity (S/cm)	Temperature (°C)
PEO-LiI	Al_2O_3	10^{-4}	r.t.
PEO-LiBF$_4$	superacid-ZrO_2	10^{-6}	r.t.
PEO-LiClO$_4$	α-Al_2O_3	10^{-5}	25
PEO-NaI	SiO_2	5×10^{-6}	25
PEO-LiClO$_4$	SiC	10^{-7}	30
PEO-NH$_4$I	Al_2O_3	8×10^{-4}	70
PEO-LiClO$_4$	SiO_2	10^{-5}	r.t.
PEO-NH$_4$HSO$_4$	SiO_2	6×10^{-5}	r.t.
PEO-LiCF$_3$SO$_3$	γ-$LiAlO_4$	3×10^{-6}	30
PEO-LiClO$_4$	$BaTiO_4$	10^{-3}	70
PEO-LiClO$_4$	TiO_2	2×10^{-5}	30
PEO-LiClO$_4$	Al_2O_3	10^{-5}	30
PEO-LiBF$_4$	TiO_2	10^{-5}	r.t.
PEO-LiBF$_4$	ZrO_2	10^{-5}	r.t.
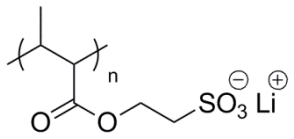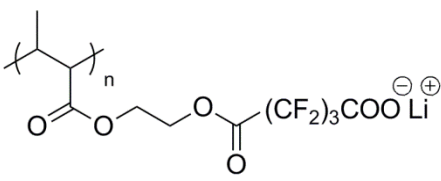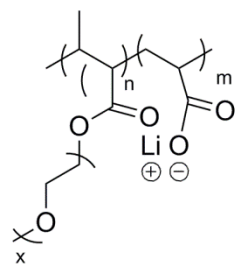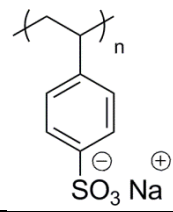
1.2.5 Polyelectrolyte

Polyelectrolytes and polymer electrolytes differ in that the former have charged groups—either cations or anions—covalently bonded to the polymer backbone, while both cations and anions are mobile in the latter systems. The motivation for synthesizing polyelectrolytes in LIBs is to develop "single ion conductors". Such systems are expected to have lithium transference number near unity,[68] due to the anion being attached onto backbone, leaving the lithium cation as the sole charge carrier under applied voltage, and thereby increasing the power density in LIBs. Moreover, polyelectrolytes would avoid not only a low lithium transference number, but also lead to accumulation of anions on the anode side, resulting in concentration polarization during charge/discharge process.[69]

The idea of immobilized anions as single ion conductors was first demonstrated by Bannister *et al.* in 1984, where poly(lithium 2 sulfoethyl methacrylate) (entry 1 in **Table 1-6**) was blended with PEO to form a lithium-salt complex.[70] Conductivity was obtained around 10^{-5} S/cm at 100°C. Since then, Shriver's group (entry 4 in **Table 1-6**)[71] and Tsuchida's group (entry 3 in **Table 1-6**)[72] further pursued the idea by introducing other polymer backbones as polyelectrolytes. Tsuchida was able to reported single ion conductors based on poly[(oligo(oxyethy1ene) methacrylate)-*co*-(alkali-metal methacrylates)] and achieved a remarkable lithium transference number as high as 0.99. However, immobilization of the anion led to a serious drop in ionic conductivity—about one order of magnitude loss.[73] In most of the cases, room temperature conductivities are reported within the range of $10^{-6} \sim 10^{-5}$ S/cm.

Despite the above difficulties, ongoing research aims to develop novel polyelectrolytes as single ion conductors with sufficient ionic conductivity for practical LIB applications.

Table 1-6   Some examples of early stage polyelectrolytes used as single ion conductors[74]

Polymer	Structure
Poly(lithium 2-sulfoethyl methacrylate)	
Poly(lithium 2-(4-carboxy hexafluoro-butanoyl-oxy) ethyl methacrylate)	
Poly(oligo(oxyethylene methacrylate)-co-(lithium methacrylates))	
Poly(sodium styrene-p-sulfonate)	

1.3   Ionic Liquids (ILs)

Ionic Liquids (ILs), also known as molten salts, are defined as organic/inorganic salts with m.p. lower than 100 °C.[75] In some occasions, salts with melting points below room temperature, considered to have special applications, are called room temperature ionic liquids. As salts in the liquid state, the intrinsic properties of ILs are strongly influenced by the electrostatic interactions between ions, which result in unique features such as chemical stability, low flammability, negligible vapor pressure and high ionic conductivity. [76-78] Therefore, they are considered to be promising candidates for various applications, including green solvents for organic reactions[79], catalysts in synthesis[80], separation agents in analytical chemistry[81], nanotechnology[82], biotechnology[83], and, most importantly, electrolytes in energy devices[84].

1.3.1   Discovery and revolution of ILs

The field of ILs was first introduced by Paul Walden in 1914, where he observed the formation of ethylammonium nitrate salt ($EtNH_3^+$ NO_3^-, m.p. at 13−14 °C) by neutralizing ethylamine with concentrated nitric acid.[85] In his original report, he chose low melting points anhydrous salts for the study and observed these organic molten salts at low temperatures ($\leq$ 100 °C), compared with inorganic molten salts which melt at much higher temperatures (c.a. 300 – 600 °C). He also pointed out that the degree of ion dissociation would largely depend on the intrinsic properties of binary salts. Discussions and debates on "ionicity" (how ionic a given IL is at room temperature) are still currently ongoing.[86]

25

Though Walden's discovery occured in 1914, ILs did not attract much scientific attention and the field was silent for twenty years until a patent claimed halide salts of nitrogen-containing bases published in 1934, which described a cellulose dissolution employing a molten pyridinium salt above 130 °C.[87] However, the technological importance of ILs was not fully recognized until a breakthrough study made by Osteryoung's group in 1975, where the detailed study of physical and chemical properties of [C$_4$py]Cl-AlCl$_3$ system made from 1-butylpyridium chloride and aluminum (III) chloride was reported (**Scheme 1-1**).[88] This system was found to be in the liquid state at room temperature—melting below 20 °C. The paper also first pointed out that the discovery of a "room temperature, strong Lewis acid, molten salt system offers a new choice of media in which to study the chemical and electrochemical properties of a variety of compounds".[85] Inspiring as it was, the system has the serious limitation that the cation is prone to reduction, giving a very narrow voltage range which prevented its potential use in batteries or cells. In 1982, Wilkes and his co-workers developed a new system using 1-ethyl-3-methylimidazolium chloride and aluminum (III) chloride ([C$_2$mim]Cl-AlCl$_3$), yielding a much wider liquid range at 30 to 60 mol% AlCl$_3$.[89]

[C$_2$py]$^+$ [C$_4$py]$^+$ [C$_2$mim]$^+$
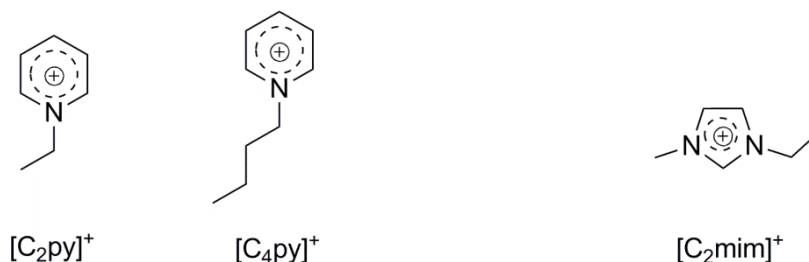
Scheme 1-1   Cations of ILs studied by Osteryoung *et al.* (left) and Wilkes *et al.* (right).

However, one problem associated with these AlCl$_3$-based IL systems was their requirement for preparation in a glove box, owing to their moisture sensitivity. This feature hindered their potential practical application in batteries.[90] In 1992, Wilkes *et al.* were able to synthesize new IL systems still featuring [C$_2$mim] cation that could be directly prepared on the bench. These systems replaced the aluminates with anions, such as acetate (CH$_3$COO$^-$), nitrate (NO$_3$$^-$) and tetrafluoroborate (BF$_4$$^-$).[91] The study of water and air stable diakylimidazolium ILs also led to the discovery of more hydrolytically stable anions upon ion exchange. This was a breakthrough in the field that led to the development of modern ILs, and opened up an era research in the field. In 1996, Grätzel's group developed ILs with more hydrophobic anions, including trifluoromethanesulfonate (CF$_3$SO$_3$$^-$), bis((trifluoromethyl-sulfonyl) amide) (N(CF$_3$SO$_2$)$_2$$^-$) and tris(trifluoromethanesulfonyl)methanide (C(CF$_3$SO$_2$)$_3$$^-$).[92] These hydrophobic ILs not only resolve the problems of reactions with water but also have a wide electrochemical window, which expands their possibilities in electrolyte applications.

Early stage research showed that the melting points of ILs with chloride anions are significantly above room temperature, which seriously limits their practical use. Kapustinskii's theoretical study on lattice energies indicated that increasing anion size could remarkably lower IL melting point.[93] Another factor that could impact melting temperature is the absence/presence of H bonding in the lattice, as noted for the case of 1-alkyl-3-methylimidazolium salt in 1986.[94] Hence, the early studies provided guidelines in designing IL analogues for specific applications. Most ILs developed nowadays are

27

compromised of an organic heterocyclic cation and an inorganic anion; **Scheme 1-2** presents some commonly used ion structure.[90]

Most commonly used cations:

1-alkyl-3-methyl-imidazolium

N-alkyl-pyridinium

N-alkyl-*N*-methyl-piperidinium

tetraalkyl-ammonium

tetraalkyl-phosphonium

N-alkyl-*N*-methyl-pyrrolidinium

1,2-diakyl-pyrazolium

N-alkyl-thiazolium

trialkyl-sulfonium

Some commonly used anions:

water-immiscible ⟶ water-miscible

$PF_6^{\ominus}$

$(CF_3SO_2)_2N^{\ominus}$

$BF_4^{\ominus}$

$CF_3SO_3^{\ominus}$

$CH_3COO^{\ominus}$

$CF_3COO^{\ominus}$ $NO_3^{\ominus}$

$Cl^{\ominus}$ $Br^{\ominus}$ $I^{\ominus}$

Scheme 1-2   Some commonly used IL cations and anions

1.3.2   ILs used as electrolytes

ILs are viewed as superb electrolyte materials, mostly due to their ionic nature which offers high ionic conductivities (within the range of 10^{-4} to 8×10^{-2} S/cm at room temperature) and wide electrochemical windows (usually 4 ~ 5V, up to 5.7 V vs. Pt

28

electrode).[95,96] Besides other advantages like non-volatility and good solubility, later studies revealed that ILs have a wide range of operation temperature, up to 200 – 300 °C.[76,97] In addition, ILs' non-flammability effectively resolves the problem associated with conventional organic alkyl carbonate electrolytes. The use of ILs greatly reduces the risk of thermal runaway during cell operation, which is a significant safety asset for large-scale applications in open markets. The major obstacle in commercializing IL-based systems is their high viscosity, which not only causes problems related to purification, but also makes them less suitable for electrolyte applications.[98]

In 2002, MacFarlane's group published a Science paper that introduced IL based electrolytes for π-conjugated polymer electrochemical devices, which greatly improved the performance speed, cycle ability and long-term stability.[99] Since then, ILs have been widely explored in various electrochemical devices, including LIBs, DSSCs, fuel cells and supercapacitors.[84] However, their main downsides are their high viscosity, inefficiency in wetting particle pores and poor electrochemical performance at low temperature. But their excellent qualities have still motivated many researchers to design new ILs seeking to overcome these obstacles and enable their use as electrolytes in various devices.[100]

Figure 1-6 Three major types of IL and the designs for specific applications[76] (Copyright 2014 Nature Materials. Reproduced with permission)

In solid polymer electrolyte systems, the solvents are polar polymers where cations are dissolved via a solvation/desolvation process; on the other hand, in gel polymer electrolytes, high molecular weight polymers are swollen in organic solvent and solely used as stiffeners for mechanical support. However, the IL electrolytes differ from both the above systems where no solvent is present, leaving ions dissociated merely through melting, where thermal disorders of the salt lattice.[5] When a lithium salt $[Li^+][X^-]$ is dissolved in an IL system $[A^+][X^-]$, it is likely to form a new IL $[Li^+][A^+][X^-]$, incorporating both cations.[101] ILs possess high ionic conductivity. Especially for imidazolium based ILs, conductivity values can be as high as 10 mS/cm, equivalent to the best current organic solvent based electrolytes. Moreover, it is worth mentioning that the structures of both cations and anions are particularly important in defining the overall properties of ILs. These diverse variables provide a broad range of different ILs for specific applications.

Among all the cations, imidazolium and pyrrolidinium based ILs are the most used for LIB electrolytes. Both cations are versatile scaffolds for ILs. The former has the highest ionic conductivity, while the latter is higher in chemical stability. **Figure 1-7** presents the cyclic voltammetry of imidazolium, piperidinium and pyrrolidinium based ILs with TFSI$^-$ (N(SO$_2$CF$_3$)$_2$$^-$) counterions and dissolved LiTFSI salt.[100,102] The piperidinium and pyrrolidinium based ILs give remarkable anodic stability (> 5 V) and wide electrochemical windows.
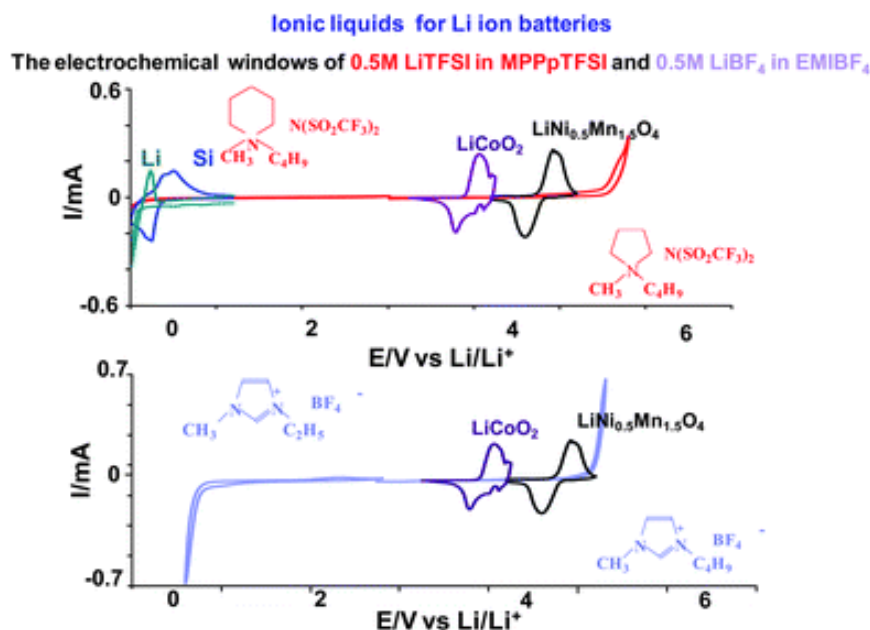
Figure 1-7   Steady-state CV response of a Pt electrode in three IL solutions, as indicated. The CV presentations include insets of steady-state CVs of four electrodes, as indicated: Li, Li–Si, LiCoO$_2$, and LiMn$_{1.5}$Ni$_{0.5}$O$_4$ (Copyright 2014 Royal Society of Chemistry. Reproduced with permission)

Among all the choices for IL anions, TFSI$^-$, also known as NTf$_2$$^-$, (bis(trifluoromethane)sulfonamide) is of great interest (**Scheme 1-3**). LiTFSI salt is well-

known as "lithium imide", commercialized by 3M, and was first employed in rechargeable LIBs in 1984 by Foropoulos *et al.*[103] Even though LiTFSI has not been used in any commercial available LIBs, it is a promising alternative and widely used in ILs as a lithium ion source owing to its unique properties.[104] As shown in **Scheme 1-3**, the TFSI anion is stabilized by the extremely electron-withdrawing CF_3SO_2 group in which the negative charge is well delocalized via resonance structures and linked by flexible S-N-S bonds. It can generate a fluid IL when combined with an imidazolium cation. For instance, the ethylmethylimidazolium TFSI ionic liquid has a m. p. as low as -15 °C, presents an impressive ionic conductivity that can compete with the best organic electrolyte solutions, and shows negligible vapor pressure up to 300 – 400 °C.[105]
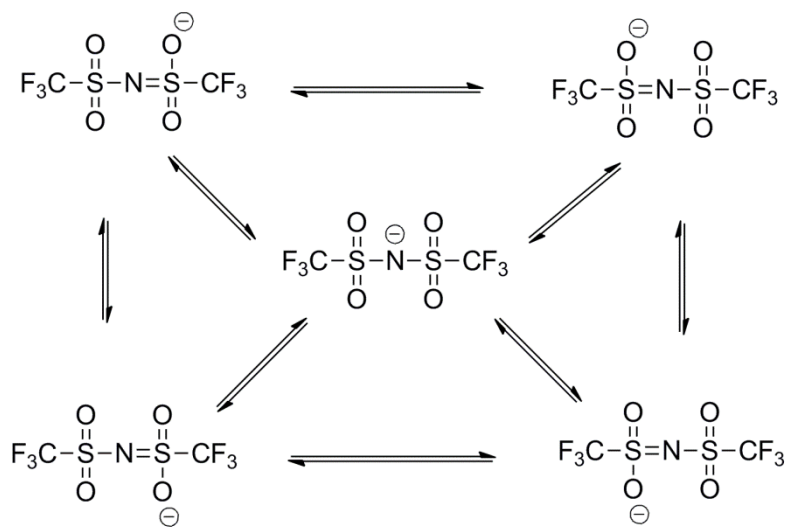
Scheme 1-3   TFSI anion in resonance structures

As mentioned in **Section 1.2.2**, anions are very likely to migrate within the polymer matrix under applied voltage, which is not beneficial in cell operation because of the decline in device performance and possible damage to the electrode surface. Anions

with large size and highly delocalized negative charge, such as TFSI⁻, are desirable to preventing anion migration.[15] Moreover, TFSI based ILs are also found to be useful incorporated with polymer electrolytes as the presence of such a highly delocalized anion could act like plasticizer, resulting in a more flexible polymer chain to facilitate ion transportation.[106] A previous study on PEO-LiTFSI complex indicated that polymer electrolytes containing TFSI anion gave much lower crystallinity, and higher ionic conductivity and lithium transference number.[106]

1.4   Polymer Ionic Liquids (PILs)

PILs, as the polymerized analogues of ILs, not only retain some of the unique properties of ILs, but also benefit from the intrinsic properties of polymers, such as better thermal and chemical stability, enhanced mechanical properties, and tunable solution properties.[107] Here, "PILs" refer to polymers with organic cations or anions bonded to the backbones and therefore restricted in mobility compared to their mobile counter ions, a situation different from other systems with free ILs[101,108] or in which ILs are dissolved in the polymer matrix[97,109,110] where both ions and counter ions are mobile.

1.4.1   Major types of PILs

There is no clear definition for categorizing PILs, but they are generally put into three major types: a) polycation PILs containing cationic moieties in the polymer backbone and free counter anions, b) polyanion PILs containing anionic backbone moieties and free counter cations and c) zwitterionic PILs with both cationic and anionic moieties in the polymer backbone.
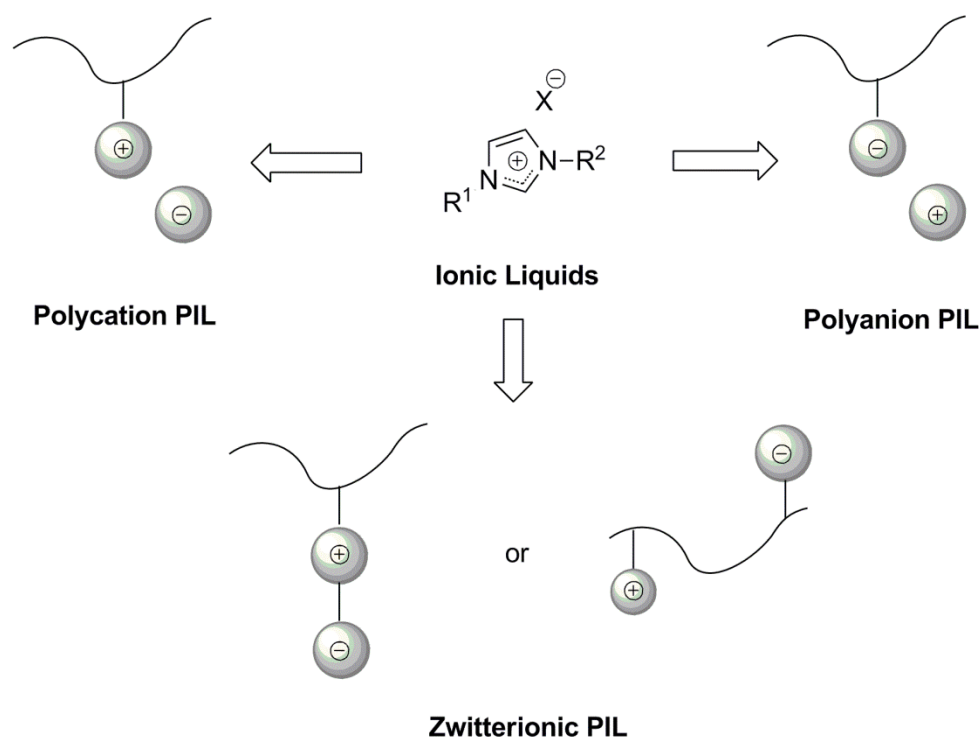
Scheme 1-4   Schematic illustration of major types of PILs

1.4.1.1   Polycation PILs

The majority of PILs synthesized so far are polycation PILs with cations bonded in the polymer structure and free counter anions. This family offers a variety of choices of cations, free anions and polymer backbone for combination in designing PIL for specific applications. The typical polymer backbone building blocks used are vinylic[75,111], styrenic[112] and methyl acrylic[113,114]. **Scheme 1-5** shows some examples of common polycation PILs from the literature.[107] Imidazolium[77,115], ammonium[113,116,117], pyridinium[118,119], pyrrolidinium[120-122] and guanidinium[123] based cationic structure have been widely investigated.

R = H, or alkyl group
X = Halide, SCN, BF_4, PF_6, TFSI, etc.
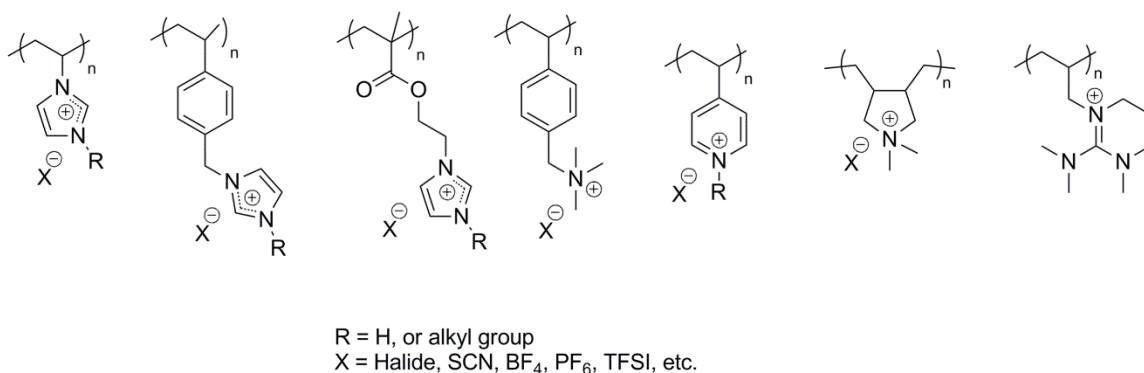
Scheme 1-5 Examples of some common polycation PILs

Among all the potential candidates, imidazolium based cations are the most popular IL cationic moiety mostly due to their unique property in effectively coordinating metal atoms, which make them extremely versatile in various areas including biphasic reaction catalysis, electrochemical actuator membranes and diluents, separation science membranes, and water purification agents.[77] Moreover, imidazolium cation PILs offer thermal stability, high ionic conductivity, wide electrochemical windows, and most importantly, highly tunable properties that can be adjusted via combination of various alkyl group attached to the imidazolium ring and counter anions.[124,125] The structure is particularly tunable due to its intrinsic amphoteric behavior, acting as both a proton acceptor and a proton donor. The imidazole ring is easily ionized during quaternization reactions onto the tertiary nitrogen, leaving a positive charge delocalized on the imidazolium ring.

There are two major methods in synthesize the targeted PILs: direct polymerization of functionalized IL monomers, and chemical modification on existing PILs, as illustrated in **Scheme 1-6**. The study of PIL synthesis was pioneered established by Ohno, who made various IL monomers by anion exchange reactions from 1-vinyl-3-alkyl

imidazolium halides to different counter anions, followed by direct polymerization (the top route in **Scheme 1-6**).[75,115,126-128] Another method involves polymerization from an initial IL monomer, followed by anion exchange on the resulting PIL (the bottom route in **Scheme 1-6**). For both routes, various polymerization techniques were used, including conventional radical polymerization[126,129-131], controlled radical polymerization (e.g. ATRP[132], RAFT[133-135]), step-growth polymerization[136], ring-opening polymerization[137] and others[138,139].
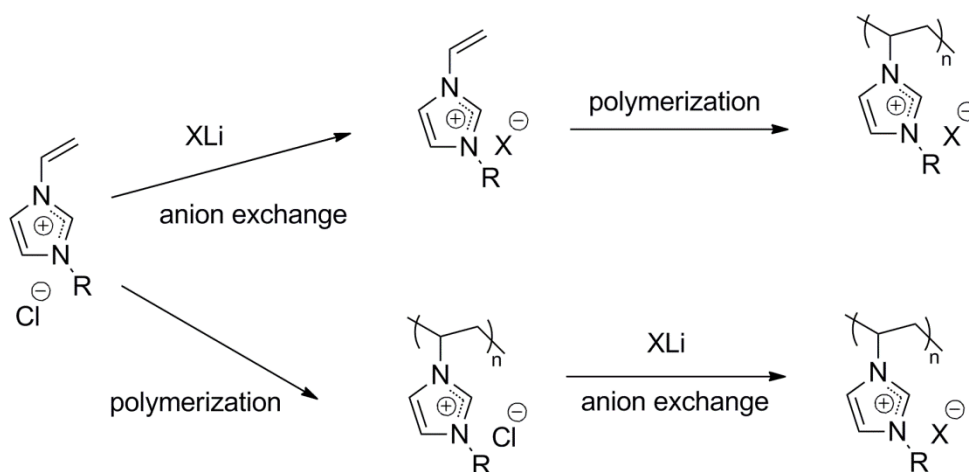
Scheme 1-6   Schematic illustration of synthesis route for 1-vinyl-3-alkyl imidazolium based PILs

Both routes in **Scheme 1-6** have their pros and cons and their selection is usually determined by the target PIL and its specific application.[140] The direct polymerization of functionalized IL monomers (top route) is a straightforward strategy, and typically leads to the formation of a homogenous polyelectrolyte with the IL moiety in the polymer repeating unit and a free counter ion.[97] This direct polymerization method also can be used to design copolymer architectures. However, the involvement of monomer side

chain can cause potential difficulties during synthesis and purification, and/or interfere with control in polymerization conditions.

In contrast to direct polymerization, modification of existing polymers (bottom route) enables the formation of PIL according to the structure, monomer composition and degree of polymerization of its polymer precursor. This method allows the design of PILs with a larger scope of polymer building blocks and architecture.[77] In terms of chain assemble, it is usually synthetically less complicated but it is potentially limited by the challenge of quantitative ion exchange after functionalization.

Various free counter anions, including chloride, bromide, tetrafluoroborate (BF_4^-), hexafluorophosphate (PF_6^-) and bis(trifluoromethane)sulfonamide ($TFSI^-$), are frequently used in combination with polycations in adjusting PIL structure according to their intended uses.

1.4.1.2 Polyanion PILs

The pool of polyanion PILs reported to date is much smaller than that of polycation PILs, presumably due to the difficulties in synthesizing various types of anionic monomers.[107] However, there are still intensive efforts being made to explore the area. In analogy to polycation PILs, the synthesis of polyanion PILs is usually performed via direct polymerization of functionalized polymerizable IL monomers. Poly(vinyl sulfonate), poly (acrylamido)-2-methylpropane sulfonate, poly(styrene sulfonate), poly(acrylic acid) and poly(vinyl phosphonic acid) are the common polymer building blocks employed here.[128,141-143] The anion monomers are partnered with alkyl-imidazolium or tetraalkylammonium counter cations, and polymerized through free

37

radical polymerization that resulted in polyanion PILs. **Scheme 1-7** shows the structure

of some common polyanion PILs and the choice of free counter cations.
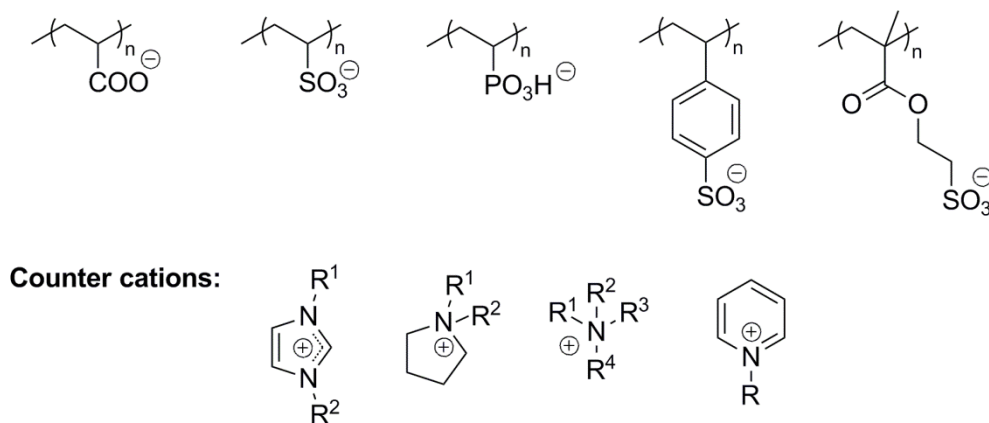
Scheme 1-7   Examples of some common polyanion PILs

Ohno's group did the pioneering work in preparing polyanion PIL electrolytes.[144]

In 2004, they reported a new class of PILs with various polyanionic backbones and

imidazolium counter cation. As shown in **Scheme 1-8**, the IL monomers were obtained

via salt formation between of ethylimidazole and acrylic acid (**AC**), styrene sulfonic acid

(**SS**), vinylsulfonic acid (**VS**) and vinylphosphonic acid (**VP**). Anions were embedded in

polymer backbones to minimize anion migration for electrolyte operation under applied

voltage, while imidazolium cations were chosen to maintain high ionic conductivity.

Table 1-7 presents the results of glass transition temperature and ionic conductivity

measurements of both monomer ILs and PILs. Even though the room temperature

conductivity was satisfactory, these PILs surprisingly present low T_g, suggesting a

flexible polymer backbone. This work offers possibilities to utilize polyanion PILs as

novel electrolytes.
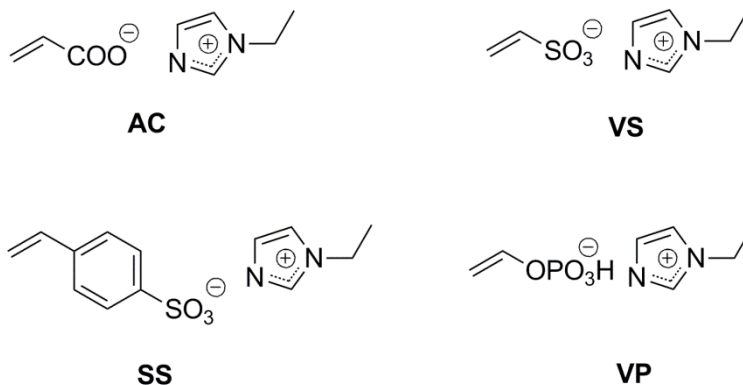
Scheme 1-8   Monomer structures studied by Ohno *et al*.

Table 1-7   Thermal properties and ionic conductivity of ILs and their corresponding

PILs

	T_g (°C)		σ (S/cm) [a]	
	Monomer	Polymer	Monomer	Polymer
AC	-61	-32	1.4×10^{-4}	1.2×10^{-6}
SS	-77	n/a [b]	8.7×10^{-5}	1.1×10^{-8}
VS	-95	-63	9.0×10^{-3}	1.1×10^{-4}
VP	-78	-56	1.5×10^{-4}	2.9×10^{-5}

[a]: Ionic conductivity results were obtained at 30°C. [b]: Not detected.

1.4.1.3   Zwitterionic PILs

Zwitterionic PILs, with both cationic and anionic in the same repeating unit, were also synthesized and explored by researchers. In 2001, Ohno's group reported the synthesis and electrolyte characterization of zwitterion PILs.[129] **Scheme 1-9** presents the four zwitterion PIL monomers studied in this work. The ionic conductivity values were all below 10^{-9} S/cm, indicating that as expected, the PILs themselves almost contained no

charge carriers. This is because both cation and anion are attached on polymer backbones and cannot move under potential gradient. However, when equimolar amounts of LiTFSI salt were added into the PIL systems, it was fully dissociated and served as charge carrier, which increased lithium transference number by minimizing solvent (zwitterion PIL) transportation. The electrolytes containing equimolar LiTFSI present conductivity in the range of 10^{-8} to 10^{-9} S/cm, and give a relatively high value of 10^{-5} S/cm at 50°C.
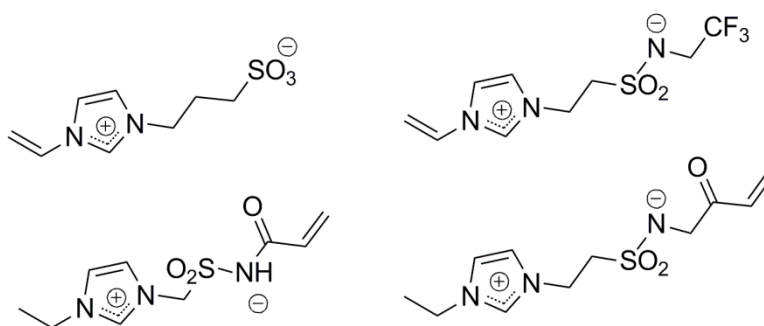
Scheme 1-9   Monomer structures of zwitterion PILs studied by Ohno *et al*.

1.4.2   Physical and electrochemical properties of PILs
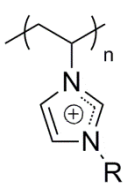
Understanding the physical properties of PILs is crucial in designing structures for specific use, since they behave very differently from neutral polymers owing to the electrostatic interactions. Both cations and anions are useful tools in tuning the properties for resulting PILs.

1.4.2.1   Solubility

The strong influence of PILs solubility mainly comes from the anions, particularly for the polycation PILs free counter anions.   As summarized in **Table 1-8**, the solubility

40

of poly(1-vinyl-3-ethylimidazolium) X^- in different solvents was studied.[145] The replacement of halide anions with PF_6^- or BF_4^- makes a PIL immiscible in water, but soluble in other polar aprotic solvents, such as acetone, DMF or DMSO.

Table 1-8 Solubility of poly(1-vinyl-3-ethylimidazolium) X^- in different solvents

	X^-	H_2O	MeOH	Acetone	THF	EtAc	$EtImi^+TFSI^-$
	Br^-	+	+	−	−	−	−
	BF_4^-	−	+ −	+	−	−	−
	PF_6^-	−	−	+	−	−	−
	$TFSI^-$	−	−	+	+	−	+
	$CF_3SO_3^-$	−	+	+	−	−	+
	$(CF_3CF_2SO_2)_2N^-$	−	+	+	+	+	+

Rogers' research on imidazolium based ILs suggests that ILs with hydrophilic anions (e.g. halide) are miscible with any proportion of water, and their properties are therefore very sensitive to the addition or removal of water. On the other hand, for ILs with hydrophobic anions (e.g. PF_6^-, $TFSI^-$), water has limited impact their properties.[125] Similar solubility and hydrophobicity behaviors were observed on PILs with imidazolium, pyridinium and guanidinium cationic moiety.[111,145,146] In most cases, anions are varied to manipulate the water miscibility of PILs. However, the use of cations to modify solubility was also reported in several occasions.[92,147,148]

1.4.2.2 Thermal stability

Since PILs have no obvious vapor pressure, the first thermal event during heating PILs is decomposition. Previous studies suggest that thermal stability is strongly

dependent on the PIL salt structure. [125] Generally, most PILs have a high thermal stability—their onset thermal decomposition temperatures are in the range of 200 – 400 °C. The choice of anion also strongly influences its thermal stability. From TGA (thermogravimetric analysis) experiments, the relative stability of ILs with various anions is halide anion $< BF_4^- < CF_3^- < PF_6^- < TFSI^- < CF_3SO_3^-$.[149] A similar trend is observed for the corresponding PILs (exemplified in **Figure 1-8**).[150] Halide anions significantly lower the thermal stability with the onset decomposition temperature at least 100 °C below the ones with non-halide anions.[92] However, cation size does not have a clear-cut effect on thermal stability. In 1999, Holbrey *et al.* reported on the phase behavior of ILs as a function of increasing alkyl chain length on the imidazolium cation. These authors found that there is no obvious change even when the attached chain length was dramatically increased.[151]
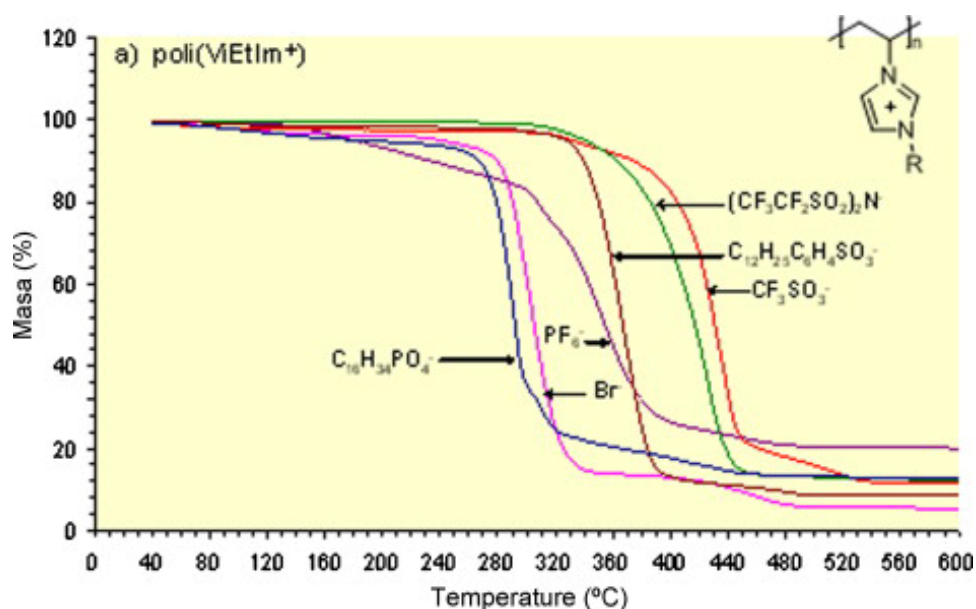
Figure 1-8   TGA of poly(1-vinyl-3-ethylimidazolium)X⁻ in N_2 (Copyright 2014 Elsevier Science. Reproduced with permission)

1.4.2.3 Glass transition and melting

In most of cases, neutral solid-state polymers show a glass transition temperature, changing from a flexible, rubbery state to a brittle, glassy state, and may or may not show a melting temperature upon heating. However, due to the electrostatic interactions, PILs show thermal transition behaviors quite different from neutral polymers.

Ngo *et al.*'s pioneering work on the thermal properties of imidazolium based small molecule ILs indicated that melting points dropped with increasing degree of asymmetry in the cations, due to the larger side chains that likely provide increased degrees of freedom.[149] Through the work done by Huddleston *et al.*, several imidazolium based ILs were analyzed.[125] Melting points for most of the ILs were not observed, where cations and anions could be reorganized after passing the glass transition. In most cases, the PILs are in a non-crystalline amorphous phase, presumably due to the nature of the highly mobile counter ions that prevent the polymers from crystallizing. Therefore, no melting point is obtained.[107]

Since PILs are a combination of both polymers and ionic liquids, the T_g of PILs depends not only on their polymer backbone structure but also on the nature of counter ions. As discussed in previous sections, low T_g is crucial for practical electrolyte applications. Intensive investigation has been made into study the T_g of various PILs. Long's group[152] and Gavrilova's group[153] studied the T_g of poly(trimethylammonium-2-ethyl) X^- (**Table 1-9**) and poly(1-vinyl-3-ethylimidazolium) X^- (**Table 1-10**) PILs respectively. In each of the cases, T_gs were highly dependent on the free counter anion. Generally, anions of larger size (e.g. TFSI$^-$) resulted in lower T_g, presumably owing to

the disturbance of polymer packing that introduced more "disorder". In addition, several groups reported difficulties in obtaining T_g through DSC (differential scanning calorimetry).[150] The reasons are not fully understood yet, but a combination of DSC with other measurements (e.g. thermomechanical study, dielectric relaxation) was recommended.

Table 1-9 T_g of poly(trimethylammonium-2-ethyl) X^- PILs
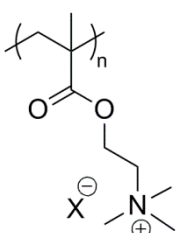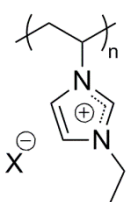
	X^-	Cl^-	BF_4^-	PF_6^-	$CF_3SO_3^-$	$TFSI^-$
	T_g (°C)	164	130	164	70	38

Table 1-10 T_g of poly(1-vinyl-3-ethylimidazolium) X^- PILs

	X^-	Br^-	$(CN)_2N^-$	$CF_3SO_3^-$	$TFSI^-$
	T_g (°C)	235	19	173	60

1.4.2.4 Ionic conductivity

As will be discussed in **Section 1.4.3**, an important application of PILs is as solid state electrolytes for modern electronic devices. Therefore, ionic conductivity is a crucial characteristic in evaluating a PIL. Tremendous efforts have been made to optimize the electrochemical performance of PILs by various research groups. Several features,

including polymer structure, counter ions, T_g, morphology, viscosity, *etc.*, can impact the ionic conductivity of PILs.[154]

As with other solid-state polymer electrolytes, the general relationship between T_g and ionic conductivity in PILs is that lower T_g results in higher conductivity, as expected since more flexibility in the polymer chain should assist ion transportation. As discussed in section **1.4.2.3**, larger anions (e.g. TFSI$^-$) generate lower T_g, leading to higher conductivity. The relevant theory was first established by Ohno in 1999.[130] He synthesized PEO based methacrylate with imidazolium cations, where both chloride and TFSI anion were selected as counter anions (**Scheme 1-10**). For both IL monomers and PILs, the one with the TFSI anions presents lower T_g and higher room temperature ionic conductivity (**Figure 1-9**). Even though ionic conductivity dropped after polymerization, owing to the more constrained structure, the PIL with the TFSI anion still offers an excellent conductivity value of 1.2×10^{-4} S/cm at 30 °C. This is attributed to the larger anion size, resulting in a weaker interaction of ether oxygen in the polymer pendent chain, leading to a lower T_g.

X = Cl; TFSI
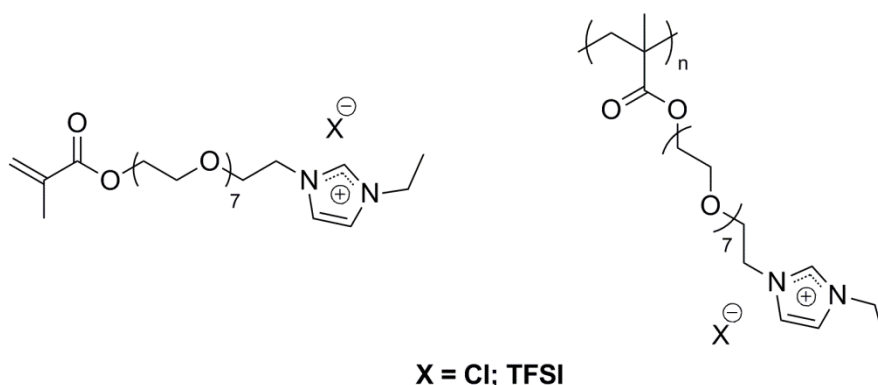
Scheme 1-10 IL monomer structure (left) and the corresponding PILs (right)

45
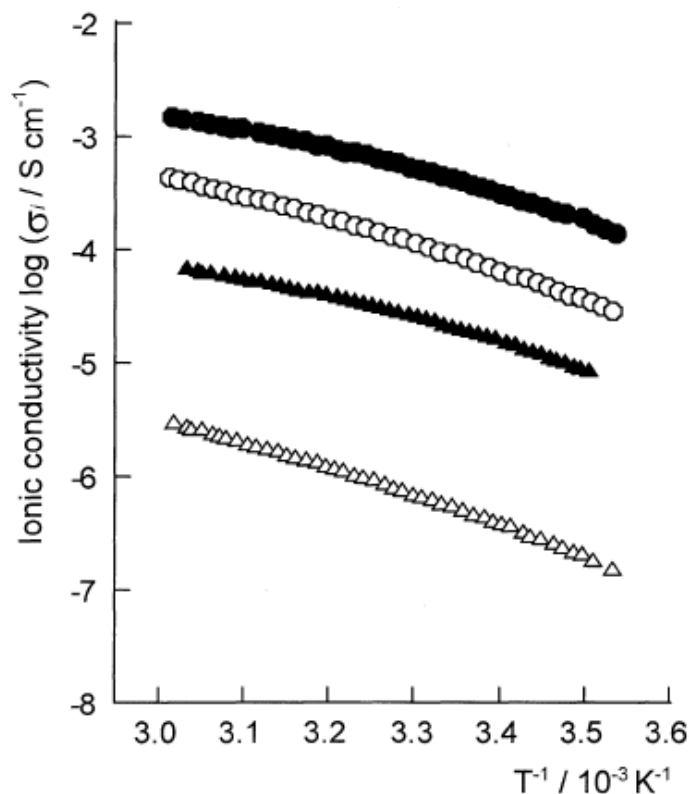
Figure 1-9 Temperature dependence of ionic conductivity of IL monomers (● = TFSI; ▲ = Cl) and the corresponding PILs (○ = TFSI; △ = Cl) (Copyright 2014 The Chemical Society of Japan. Reprinted with permission)

Not only do anions greatly impact ionic conductivity, cations also exhibit a strong influence. The pioneering work was again done by Ohno's group. A paper published in 2006 reported several PILs with variations in attached cations, including imidazolium, pyrrolinium, pyrrolidinium, and piperidinium.[120] The PILs, comprised methacrylate as the polymer backbone and alkyl spacers between backbone and cation sites, were synthesized via free radical polymerization (**Scheme 1-11**). The conductivity results

revealed that the imidazolium cation presents the highest ionic conductivity among all the

other cations (**Figure 1-10**).

a: $R_1 = CH_3$, $R_2 = H$
b: $R_1 = C_2H_5$, $R_2 = H$
c: $R_1 = C_2H_5$, $R_2 = CH_3$
d: $R_1 = C_4H_9$, $R_2 = H$

e

f

g: $R_3 = CH_3$
h: $R_3 = C_2H_5$
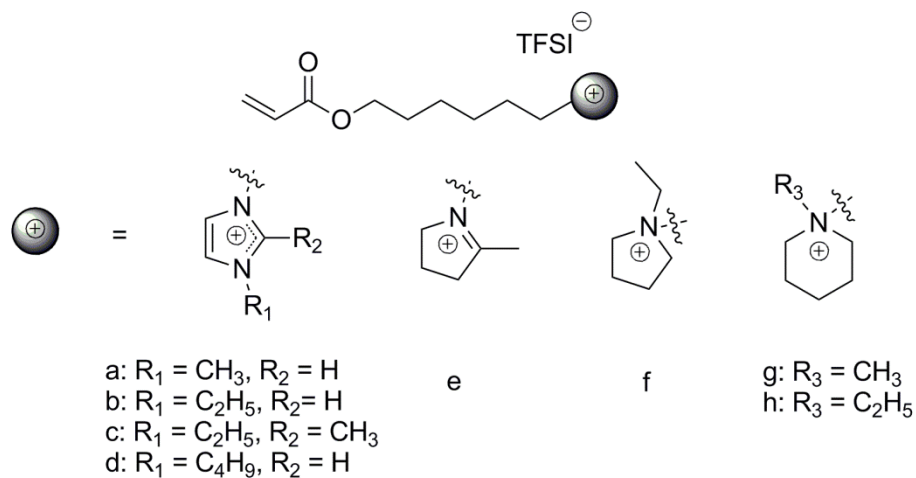
Scheme 1-11 Monomer structure with various cations
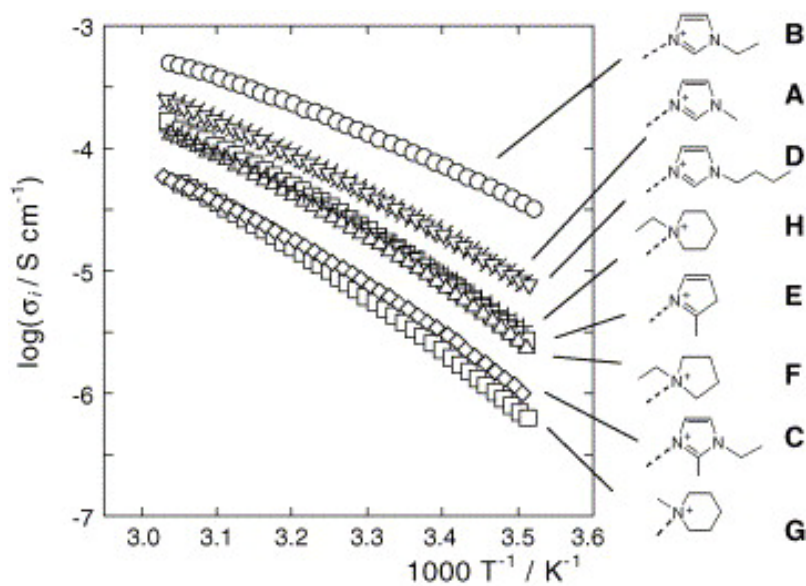
Figure 1-10   Temperature dependence of ionic conductivity of PILs with various

cations (Copyright 2014 Elsevier Science Ltd. Reprinted with permission)

1.4.3   PILs as electrolytes

PIL electrolytes can be synthesized as polycations with free counter anions, as polyanions with free counter cations, or as polyzwitterion structures carrying both cation and anion moieties in polymer backbone. Moreover, various polymer structures (e.g. random/alternating/block copolymers) and macromolecule architectures (e.g. branched, dendritic, and ramified) can potentially be used in PILs. All of these provide numerous pathways for the design of PIL electrolytes.[107]

As discussed previously, PILs benefit from both ILs' unique properties and polymers' intrinsic characteristics, which are particularly useful for electrolyte materials. Owing to the liquid nature of small molecule ILs, they can suffer leakage issues as well as inconvenience for processing and packaging during cell operations. Hence, a more suitable electrolyte for practical use in electronic devices would exist in the form of a solid-state film like ion conductive polymers.[155,156] Another major problem associated with ILs is that under the potential gradient of an applied external voltage ILs transport not only target ions (i.e. salt dissolved in ILs), but their own ions, which are essential as part of the solvent in the system. Therefore, when ILs are used as solvents for electrolytes, enhancement of the transference number of the desired conducting ion is required. To solve this problem, PILs can be employed to replace ILs. Because the ionic sites are covalently attached to the polymer backbone, they do not migrate under applied voltage along with the target ions. Given these unique features offered by PILs, a lot of attempts have been made to gain advantages by combining ILs and polymers.[154]

As mentioned previously, imidazolium is one of the most versatile building blocks in synthesis of IL-based electrolytes for electrochemical devices, owing to its

excellent ionic conductivity. It also can be extremely useful as a scaffold in PILs. Acrylate imidazolium IL monomers (**Scheme 1-12**), with imidazolium as the pendent group of the polymer backbone, were reported by Firestone's group.[157] The study indicates that the alkyl spacer between imidazolium and acrylate moiety impacts the polymer packing behavior; a more flexible polymer chain leads to higher ionic conductivity.
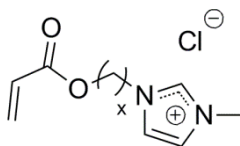
Scheme 1-12 Acrylate imidazolium IL monomers (x = 8 or 10)

As mentioned previously, Ohno's group has been quite active; they have published reports on several imidazolium based polymerizable functionalized ionic liquid monomers, synthesized with imidazole rings either as pendent groups or in the polymer backbone: **A**) vinyl imidazolium[115,126], **B**) methacrylate backbone with short PEO tethering group as spacer[75,130], **C**) acrylate backbone with short alkyl chain tethering group as spacer[75,120,158], **D**) methacrylate backbone derivatives[128], **E**) polyanion PIL with imidazolium counter cation[131]. The polymerizations were all carried out through conventional free radical polymerization.

Shen *et al.* reported the synthesis of methacrylate imidazolium PIL, in analogy to the ones investigated by Ohno but with BF_4 anion instead of TFSI¯ (**Scheme 1-14**).[159] It is worth mentioning that a controlled radical polymerization technique, atom transfer

radical polymerization (ATRP), was employed in this work. This allowed closer control of the product PILs' molecular weight and architecture.
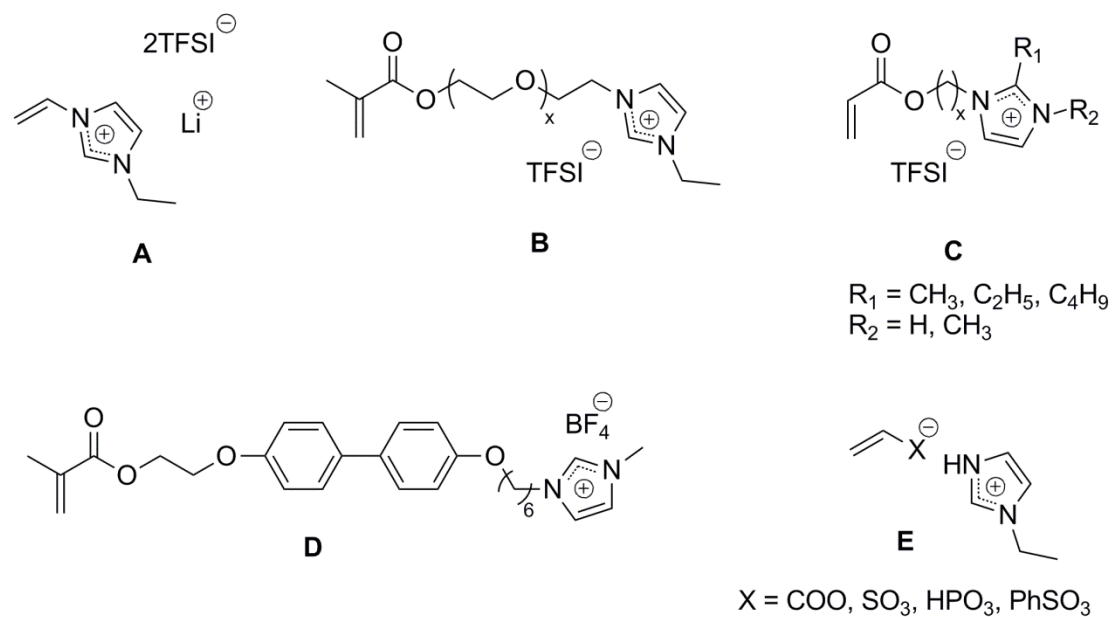
Scheme 1-13 PIL monomer structures studied by Ohno *et al*.
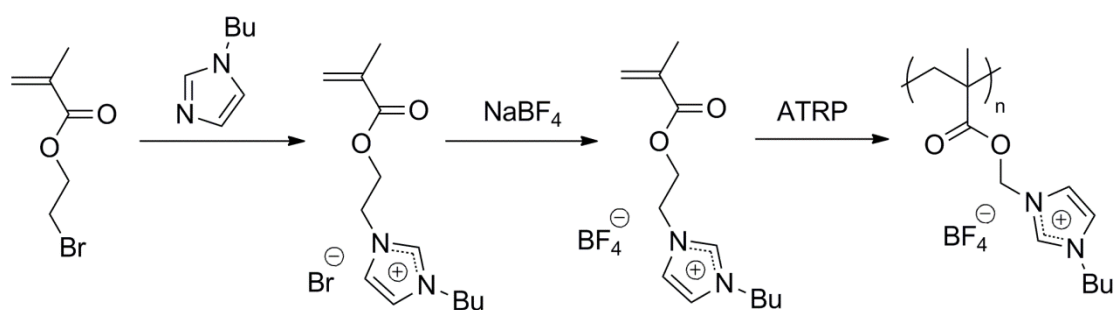
Scheme 1-14 Synthetic route for poly(1-butylimidazolium-3-yl)ethyl methacrylate tetrafluoroborate

2. Chapter 2   Optimizing the Electrochemical Performance of Imidazolium-Based Polymeric Ionic Liquids by Varying Tethering Groups

2.1 Introduction

Development of economical and clean energy sources is perhaps the most crucial technological challenge of the 21st Century. Accordingly, a variety of energy capture and storage devices have emerged in recent decades.[78] Advances in dye-sensitized solar cells (DSSCs), rechargeable lithium ion batteries (LIBs), supercapacitors and fuel cells represent important developments in this area. [78,97,160,161]

Of particular relevance to this work, many studies focus on developing high-efficiency, low-cost electrochemical devices with long-term stability.[5] Electrolytes, which function as the charge carriers between electrodes, are crucial parts of DSSCs, fuel cells, supercapacitors, and batteries. Water is typically unsuitable for such application due to its electrochemical reactivity, and conventional organic liquid electrolytes have drawbacks such as leakage, volatility, flammability, and toxicity.[76] Hence, the synthesis of solvent-free electrolytes has garnered the attention of research groups all over the world.[90,162]

Polymer electrolytes, and especially polymer ionic liquids (PILs), are among the most promising candidates for solid or gel electrolytes.[33,76,107] Ionic Liquids (ILs), organic/inorganic salts with melting points lower than 100 °C,[95] offer chemical stability, low flammability, negligible vapor pressure and high ionic conductivity.[75-77] Most salts have high melting points and are solids at room temperature due to the strong Coulombic attractions between cations and anions. In contrast, salts of bulky organic cations such as

alkylated ammonium, phosphonium, imidazolium, and pyridinium ions are liquid at room temperature.[126] Such salts are thermally stable and useful in various applications. As the polymerized analogues of ILs, PILs not only retain some of the unique properties of ILs, but also benefit from the intrinsic properties of polymers, such as enhanced mechanical properties compared to conventional liquid electrolytes or IL small molecules, and tunable solution properties where the polymer structure can be modified to be soluble/insoluble in certain solvents.[107] In this dissertation, PILs refer specifically to polymers with organic cations or anions bonded to the backbone. These bound ions are less mobile than their counter ions, which is not the case with free ILs[101,108] or with ILs dissolved in a polymer matrix,[97,109,110] where both cations and anions are mobile. In some applications, such as LIBs, conductivity via only the mobile counterion of a polymer, e.g. Li^+ is highly desirable for increasing the device efficiency.

PILs should avoid electrolyte leakage and give superior thermal stability compared to liquid electrolytes. However, because of their high viscosity and the immobilization of cations or anions, PILs have lower ionic conductivities than liquid electrolytes.[163] After polymerization the conductivities of PILs typically decrease several orders of magnitude relative to their monomers.[66]

Ionic conductivity is the product of the ion density (n), ion charge (q), and ion mobility (μ):[162]

$$\sigma = n \cdot q \cdot \mu \qquad \textbf{Equation 2-1}$$

Efforts to optimize polymeric electrolytes therefore typically focus on increasing the mobility of counterions through lowering the polymer glass transition temperature (T_g) and consequently increasing chain flexibility and polymer free volume.[20,21] The T_g and

conductivity are generally inversely related; a low T_g correlates with a high counterion mobility, which leads to a high conductivity.[164] To optimize the electrochemical performance of PILs, Ohno and co-workers introduced alkyl-chain or ethylene oxide (EO) tethering groups on the cationic imidazole ring.[126,127] A flexible tethering group should increase the motion of immobilized ions and disrupt polymer packing both of which should make the polymer less rigid and increase the counterion mobility.

In research with polymerized 1-alkyl-3-vinylimidazolium salts, ionic conductivity increased with the alkyl tether between the vinyl polymer backbone and terminal imidazolium cation.[14,24,25] Longer tether gave low T_g values for the PILs and consequently increased their conductivity. In an effort to investigate how tethering groups affect both electrochemical performance and physical properties of free ILs and PILs, I synthesized and characterized a new class of imidazolium (Im)-based IL model compounds and their corresponding PILs. The different PEO tethered ILs and PILs contain 1, 2, 3, 8, 12, and 17 EO units attached to the imidazolium salts. I selected PEO as the tether because it is chemically stable, dissolves metal ions, and when incorporated into ionic liquids, it provides a solvent-free electrolyte.[35] These PILs exhibit excellent conductivity values of 10^{-4} S/cm at room temperature, which is essentially the minimum conductivity needed for practical applications.[20] Data for ionic conductivity, rheological behavior, T_g, melting temperature, and decomposition temperature clearly demonstrate that increasing the length of the PEO tethering group drastically alters physical properties of PILs and enhances their conductivity. With free ILs, the charge carrier density is the dominant factor affecting conductivity, whereas ion mobility plays a more important role after polymerization.

2.2 Results and discussion

2.2.1 Synthesis of model imidazolium-based ILs

Scheme 2-1 shows the 4-step synthetic route to IL model compounds. During the synthesis of the key intermediates, the PEO substituted imidazoles (**2a-2f**),[164] as the PEO chain length increased, the target compounds became extremely hydrophilic because of the increasing polarity from the addition of electronegative oxygen atoms. This caused problems during purification (see below), yet the yield of the target compounds remained relatively high (> 80%). However, attempts to synthesis longer PEO-chain-substituted imidazole (e.g. PEO-2000 and PEO-5000) were not successful due to the high hydrophilicity of these compounds.

Quaternization occurred via reaction with benzyl chloride. The resulting products were low-viscosity yellow liquids, and extensive washing with diethyl ether ensured removal of the starting materials. Drying under vacuum (100 mTorr) at 70 °C gave purified ILs **3a-3f**, with an imidazolium cation and a chloride anion. Previous studies reveal that the solubility of ILs strongly depends on the anion.[92,147,151] ILs with halide anions are strongly hydrophilic while those with $TFSI^-$ are extremely hydrophobic.[154] Thus, upon the addition of LiTFSI to aqueous solutions containing chloride ILs (**3a-3f**), a two-phase system formed immediately. The exchange of chloride for $TFSI^-$ was allowed to continue overnight to fully precipitate **IL-1** to **IL-8** from DI water.[165] Several intensive wash/redisperse/decant processes ensured the removal of Cl^-. The washing process was repeated until no AgCl was observed upon dissolution of $AgNO_3$ in the water wash. Ion exchange reactions with compounds containing longer tethering groups (**IL-12** and **IL-17**)

resulted in ILs that did not readily precipitate from water. However, **IL-12** and **IL-17**
showed a lower critical solution temperature (LCST) behavior—a commonly observed
phase behavior where polymers are miscible with solvent below the critical temperature,
but two phases form above this temperature. Therefore, purification of **IL-12** and **IL-17**
required heating above 60°C for precipitation from water. The final compounds were
dried under vacuum ($\leq$ 10 mTorr) at 70 °C for at least 48 hours for the complete removal
of moisture. They were then sealed and stored in the glove box.

1a, x=1
1b, x=2
1c, x=3
1d, M=350, x $\cong$ 8
1e, M=550, x $\cong$ 12
1f, M=750, x $\cong$ 17

2a, x=1
2b, x=2
2c, x=3
2d, M=350, x $\cong$ 8
2e, M=550, x $\cong$ 12
2f, M=750, x $\cong$ 17

3a, x=1
3b, x=2
3c, x=3
3d, M=350, x $\cong$ 8
3e, M=550, x $\cong$ 12
3f, M=750, x $\cong$ 17

4a, **IL-1**, x=1
4b, **IL-2**, x=2
4c, **IL-3**, x=3
4d, **IL-8**, M=350, x $\cong$ 8
4e, **IL-12**, M=550, x $\cong$ 12
4f, **IL-17**, M=750, x $\cong$ 17
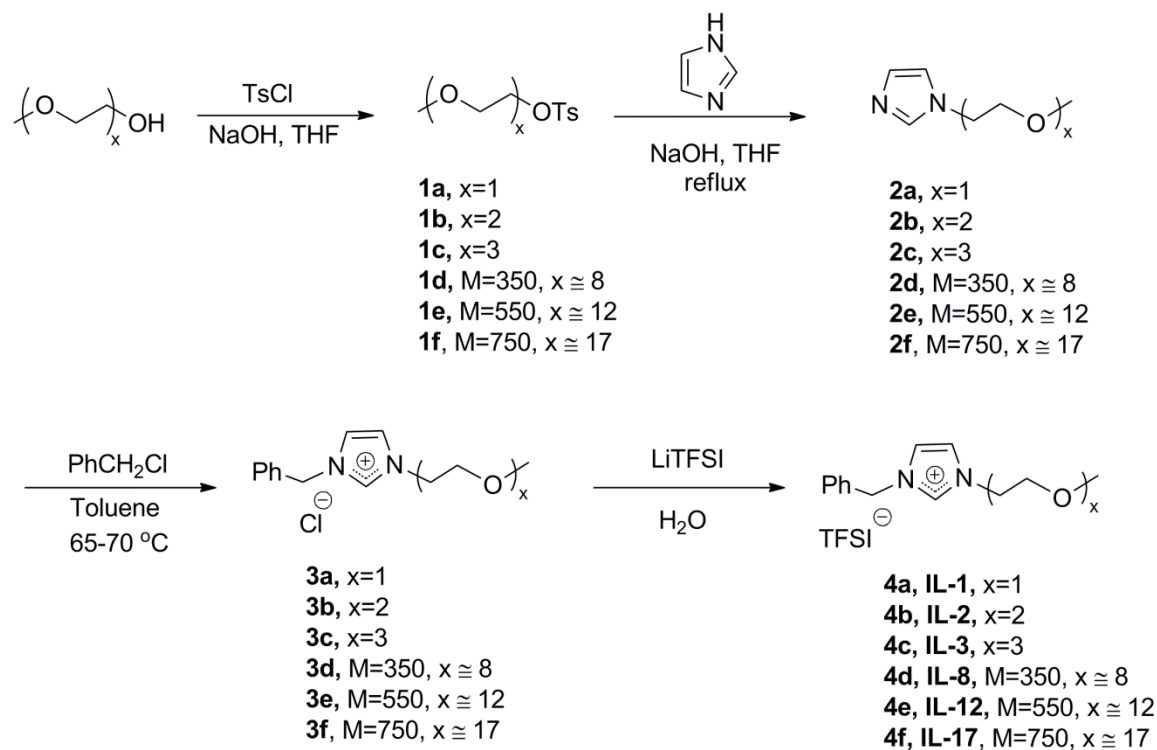
Scheme 2-1   Synthesis of imidazolium-based IL model compounds (M is the number
average molecular weight of the PEO side chain given by the chemical manufacturers;
while x refers to a rough estimation of the number of PEO repeating units attached on the
molecule.)

2.2.2 Synthesis of imidazolium-based PILs

Scheme 2-2 outlines the synthesis of PILs. Using free radical polymerization with AIBN as the radical initiator, I synthesized six PILs with different lengths of the tethering group attached to the imidazolium cation. The synthetic route to the PIL is similar with the one for the model IL compounds, except for the substitution of polymerizable *p*-methylchlorostyrene for benzyl chloride during quaternization. I added hydroquinone during each step in **Scheme 2-2** to prevent polymerization and washed away this inhibitor with diethyl ether before polymerization. Polymers were precipitated with cold methanol and dried under vacuum ($\leq$ 10 mTorr) at 70°C for at least 48 h to remove the remaining solvent. They were then sealed and stored in a N_2-filled glove box. ^{1}H NMR spectroscopy confirmed the structures.
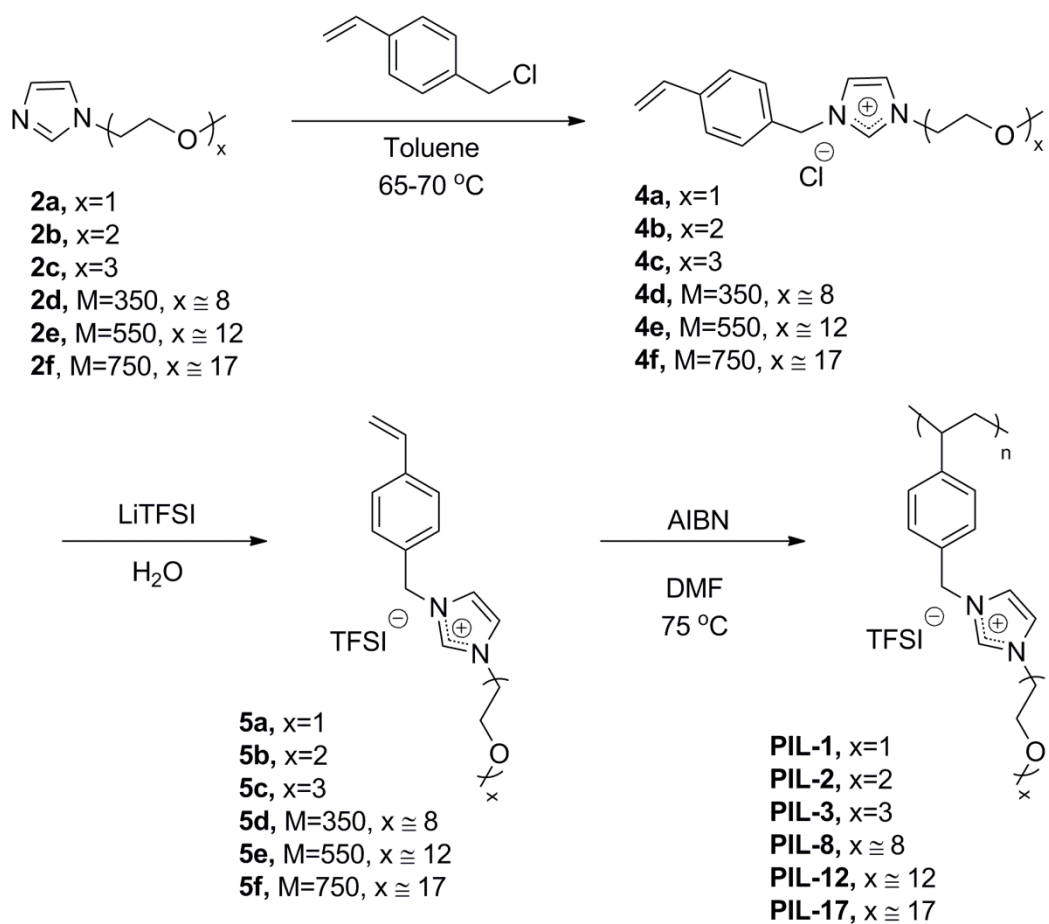
Scheme 2-2 Synthesis of imidazolium-based PILs (M is the number average molecular weight of the PEO side chain given by the chemical manufacturers; while x refers to a rough estimation of the number of PEO repeating units in the molecule.)
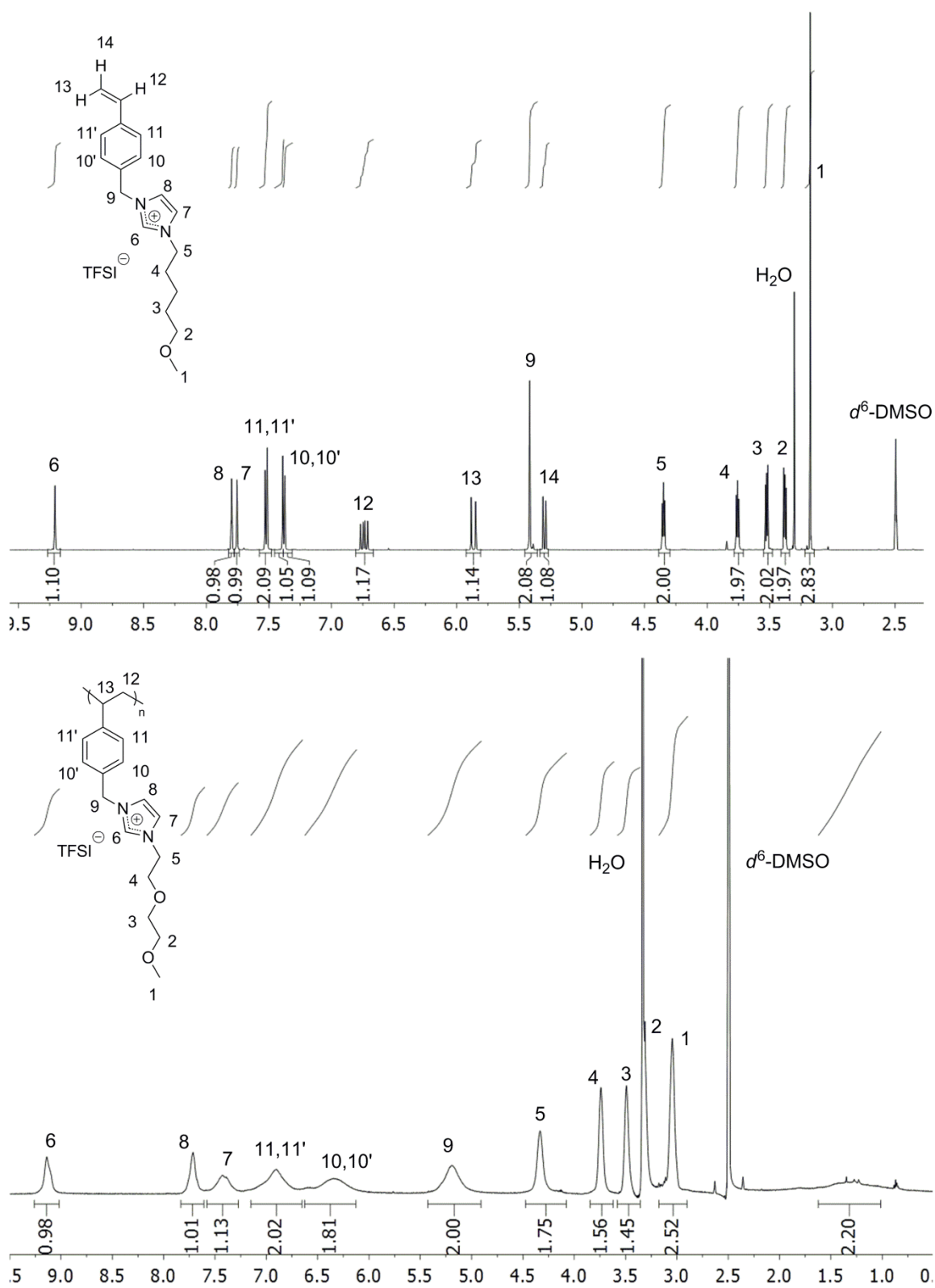
Figure 2-1   NMR spectra of **5b** (top) and its corresponding polymer **PIL-2** (bottom)

Figure 2-1 shows an example NMR spectrum of **PIL-2** (bottom) and its monomer (top). In the polymer spectrum, the signal of proton 2 partially overlaps with the H_2O signal, preventing integration. The signal of proton 13 likely overlaps with the signals of protons 1 and 2. Otherwise, the spectral integration is consistent with the polymer structure.
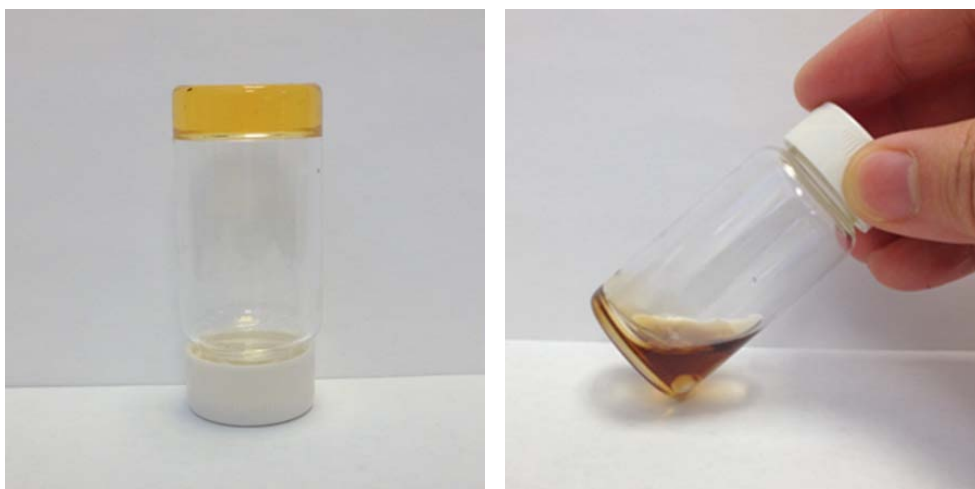
Figure 2-2   Physical appearance of **PIL-1** (left) and **PIL-17** (right)

All the PILs in **Scheme 2-2** are viscous yellowish to brown liquids. Nevertheless, as the length of the PEO side chain increases, the viscosity drops significantly. As **Figure 2-2** shows, **PIL-1** is extremely viscous and solid-like, whereas **IL-17** is much less viscous. PILs with side-chain lengths between those of **PIL-1** and **PIL-17** exhibit intermediate viscosities. **Section 2.2.5** will discuss oscillation rheology tests.

2.2.3 Thermal properties of ILs and PILs

A previous study showed that the thermal stabilities of PILs depend on the nature of their counter anions.[107] Mecerreyes and his co-workers found that for poly(1-vinyl-3-ethylimidazolium) X$^-$, the TFSI$^-$ salt is more stable than the halide salt.[111] One of the main reasons that ILs with "proton-abstracting" anions, e.g. halide anion, are less thermal stable than those with "poorly proton-abstracting" anions, e.g. TFSI$^-$, is the nucleophilic attack by halide anions during thermal degradation at high temperature.[166-168] The onset decomposition temperature for the TFSI$^-$ polymer was at least 100 °C higher than the value for polymers with halide anions.[125]

A similar trend occurs with PEO attached to imidazolium ILs. **Figure 2-3** compares TGA results for imidazolium-based ILs with Cl$^-$ (top) and TFSI$^-$ (bottom) counterions. The onset decomposition temperature of **3a-3f** (Cl$^-$ salts) is around 275 – 325°C, whereas it is 325 – 400°C for ILs after ion exchange of the TFSI$^-$.
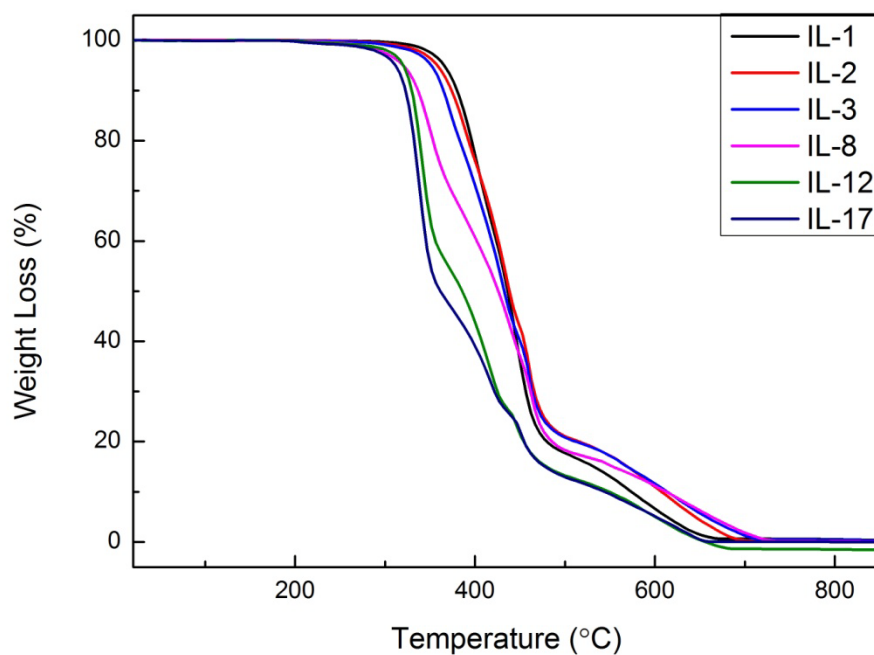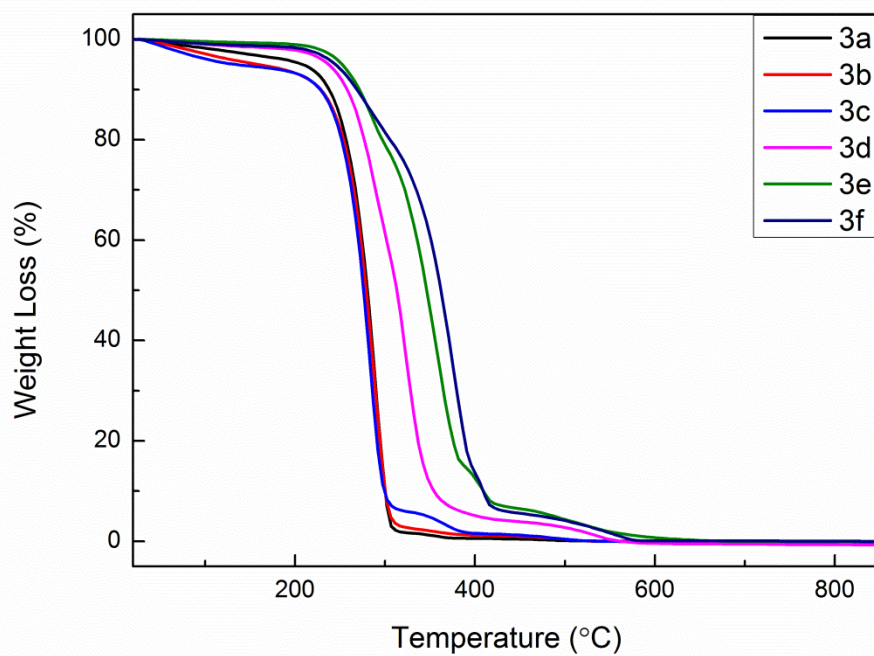
Figure 2-3 TGA of ILs with PEO tethers and Cl⁻ counterions (top) or PEO tethers and TFSI⁻ counterions (bottom) (**Scheme 2-1** shows the structures)

For TFSI⁻ counterions, the onset decomposition temperature decreases with an increase in the number of PEO units attached to the imidazolium cation. **IL-12** and **IL-17**, with tethering groups containing approximately 12 and 17 PEO repeating units, respectively, exhibit onset decomposition temperatures 50 °C lower than **IL-1**and **IL-2**, which have only 1 or 2 repeating units. Interestingly, Cl⁻ salts (**3a** – **3f**) show an opposite trend, i.e. the onset decomposition temperature increases with increasing linker length, where **3a** and **3c**, with 1 to 3 repeating units, respectively, show the lowest thermal stability. The opposite trends for the different anions in terms of stability as a function of the tethering group length may reflect different thermal decomposition mechanisms. Chan and his coworkers suggested that a 1-ethyl-3-methylimidazolium chloride IL decomposed by the attack of highly nucleophilic chloride on the primary alkyl group (S_N2 reaction).[169] Witkamp's group later reported that quantum chemical calculations agree with this thermal decomposition mechanism for 1-butyl-3-methylimidazolium salts (**Scheme 2-3**, top).[170] Therefore, we speculate that for **3a** – **3f** the longer PEO side chain sterically protects the imidazolium cation, to decrease the rate of nucleophilic attack. Witkamp's study further showed that ILs containing non-nucleophilic anions (e.g. TFSI⁻), cannot decompose through dealkylation or proton transfer. According to his calculation, the lowest energy barrier for thermal breakdown is the degradation of TFSI⁻ by SO_2 release, while the imidazolium cation stays intact. Therefore, for 1-butyl-3-methylimidazolium TFSI IL (**Scheme 2-3**, bottom), the thermal decomposition starts with only anion degradation. Thus, a possible explanation for the TGA trends with linker length in **Figure 2-3** is that the TFSI⁻ can interact more closely with the imidazolium

cation with shorter tethering groups. This should yield a higher decomposition temperature for the anion.
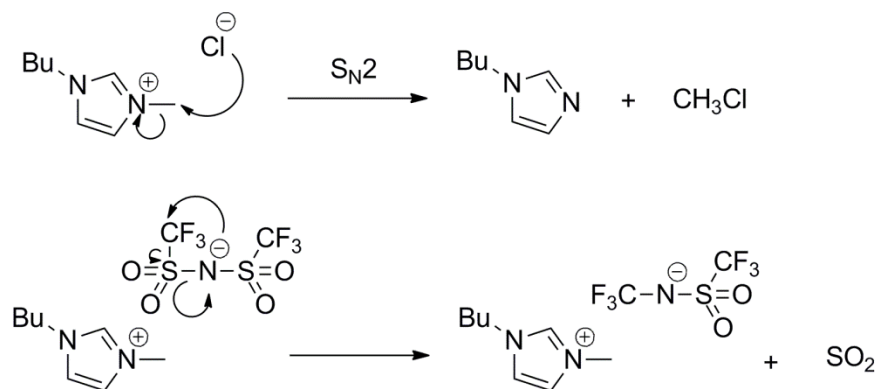
Scheme 2-3   Thermal decomposition mechanism of an imidazolium-based IL with Cl⁻ (top), and TFSI⁻ (bottom) as proposed by Witkamp *et al.*[170]

All TGA data shown here were obtained in air. Literature reports claim that TGA of ILs produces the same decomposition temperatures in N_2 or air, but in the presence of oxygen the decomposition becomes exothermic midway through the TGA weight-loss profile.[92,149] This observation could explain the "shoulder" between 450 – 625 °C on the TGA scans of ILs (**Figure 2-3**, bottom) and PILs (**Figure 2-4**), presumably due to some oxidation reactions that take place during the decomposition of substituted imidazolium cations. The LiTFSI salt shows an onset thermal decomposition temperature around 275 °C and no shoulder at higher temperatures.

PILs (**Figure 2-4**) and ILs (**Figure 2-3**, bottom) show similar degradation patterns, although the PILs show an onset thermal decomposition temperature about 50 °C higher than the ILs. **PIL-1** and **PIL-2** exhibit excellent thermal stability, with an onset decomposition temperature around 425 °C.
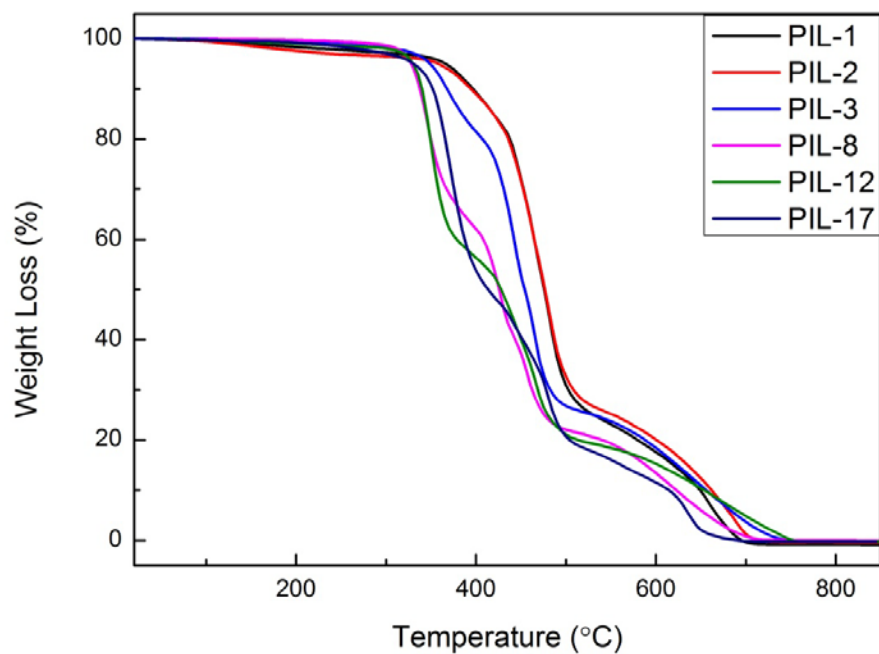
Figure 2-4   TGA of PILs with TFSI⁻ (**Scheme 2-2** gives the PIL structure)

In most cases, the T_g value for a PIL depends on both the counterion and the chemical composition of the polymer backbone.[107] Polymer morphologies are usually amorphous because of the relatively high mobility of counter ions. However, most ILs never solidify because the counterions are highly mobile.

Table 2-1   Tg values obtained from DSC of **3a-3f**, **ILs** and **PILs**

Compound	$T_g(°C)$	Compound	$T_g(°C)$	Compound	$T_g(°C)$
3a	-24	**IL-1**	-60	**PIL-1**	-6
3b	-25	**IL-2**	-59	**PIL-2**	-22
3c	-26	**IL-3**	-56	**PIL-3**	-23
3d	-47	**IL-8**	-50	**PIL-8**	-31
3e	-49	**IL-12**	-48	**PIL-12**	-39
3f	-54	**IL-17**	-51	**PIL-17**	-51
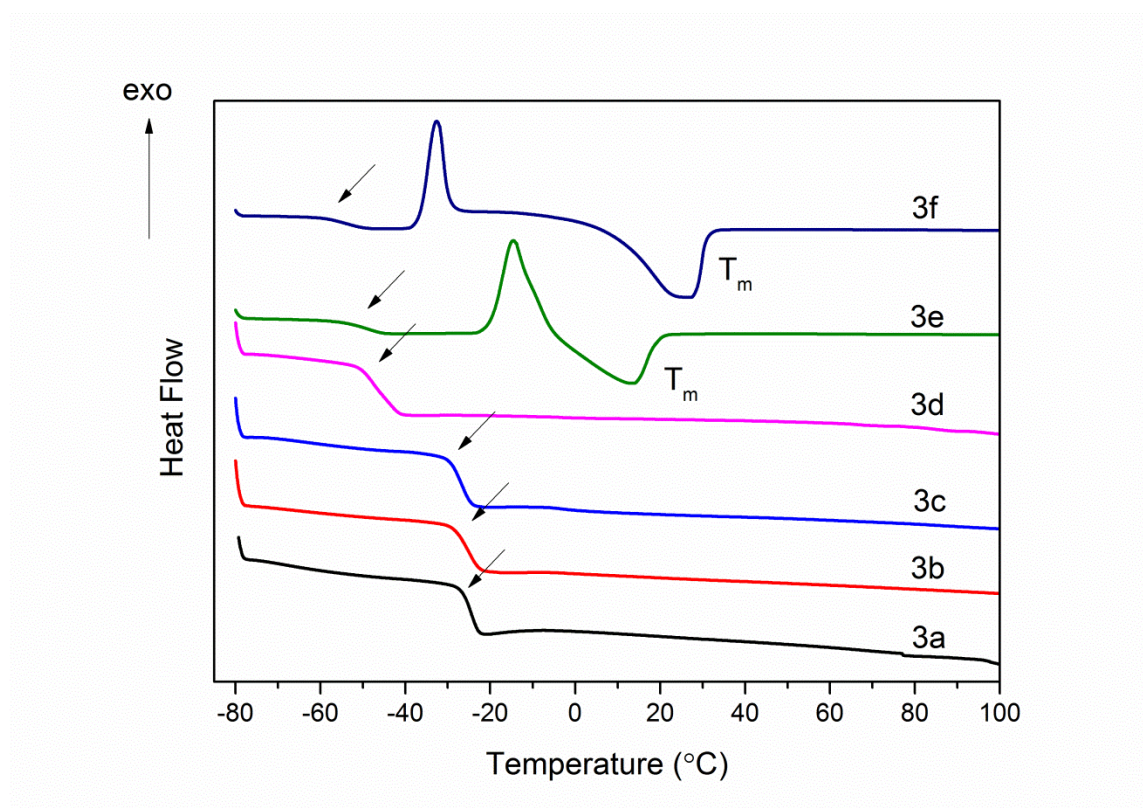
Figure 2-5   DSC of imidazolium-based ILs with Cl⁻ (**3a – 3f**, **Scheme 2-1** shows the structures)

DSC results for the ILs in this work (**Table 2-1** and **Figure 2-5** show example raw data) are consistent with literature reports. The value of T_g drops significantly as the length of the tethering group increases for compounds **3a** – **3f** (**Figure 2-5**). The only ILs or PILs that showed a melting transition were **3e** and **3f**. These compounds have long PEO chains that may crystallize, and unlike TFSI⁻, the Cl⁻ ion is likely too small to disrupt PEO crystallization. When the number of ethylene oxide repeating units is above 8, PEO tends to crystallize as a 7_2 helix.[26] In **Figure 2-5**, both sample **3e** and **3f** show melting in DSC, T_m = 13 and 25 °C, respectively. The sharp exothermic peaks at around -30 °C (**3e**) and -10 °C (**3f**) correspond to cold crystallization, which is a secondary crystallization process where a slow reorganization takes place in the crystalline region to allow the formation of more perfect crystallites.

Table 2-1 also shows a much lower T_g for ILs with TFSI⁻ compared to their analogues with Cl⁻. Long's work on poly(trimethylammonium-2-ethyl) methacrylate X⁻ demonstrated that a larger and less coordinating anion leads to lower-temperature thermal transitions as the result of increased free volume and weaker ion-ion interactions.[152] The low T_g values of ILs with TSFI⁻ stem from both its large size and highly delocalized change. One study introduced TSFI⁻ as a plasticizer for PILs.[150]

From **IL-1** to **IL-17**, varying the tethering group attached to the imidazole ring did not significantly alter T_g (differences <12 °C), suggesting that with larger counterions, increasing the length of the PEO tethering group does not increase disorder in the system. The T_g value is already low and the structure has significant free volume because of TFSI⁻, so long linkers do not greatly increase freedom in the structure.
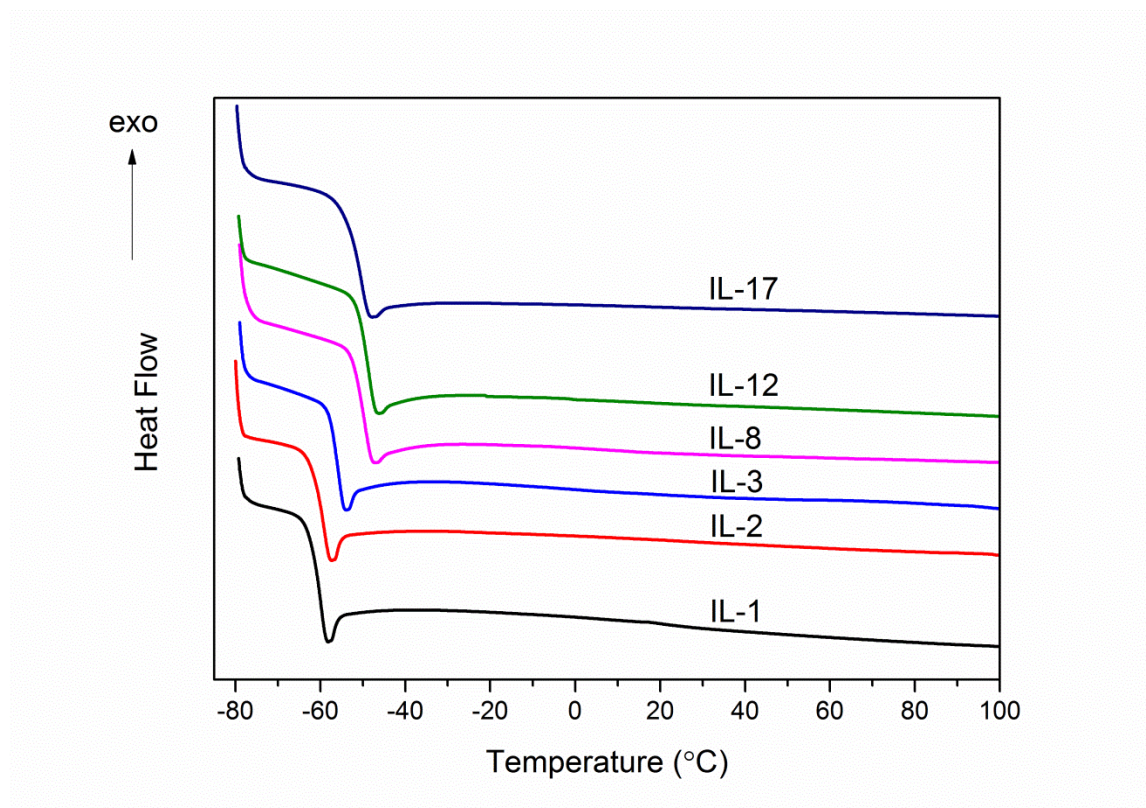
Figure 2-6   DSC of imidazolium-based IL model compounds with TFSI⁻ (**Scheme 2-1** shows structure)

However, once polymerized, the PILs shows higher T_g values than their corresponding ILs, due to the more constrained structure. This observation is more evident with shorter tethering groups (**Figure 2-7** and **Table 2-1**). In addition, with PILs, increasing the PEO side chain greatly reduces T_g, and **PIL-17** exhibits a glass transition of -51 °C, which is 45 °C lower than the T_g for **PIL-1**.
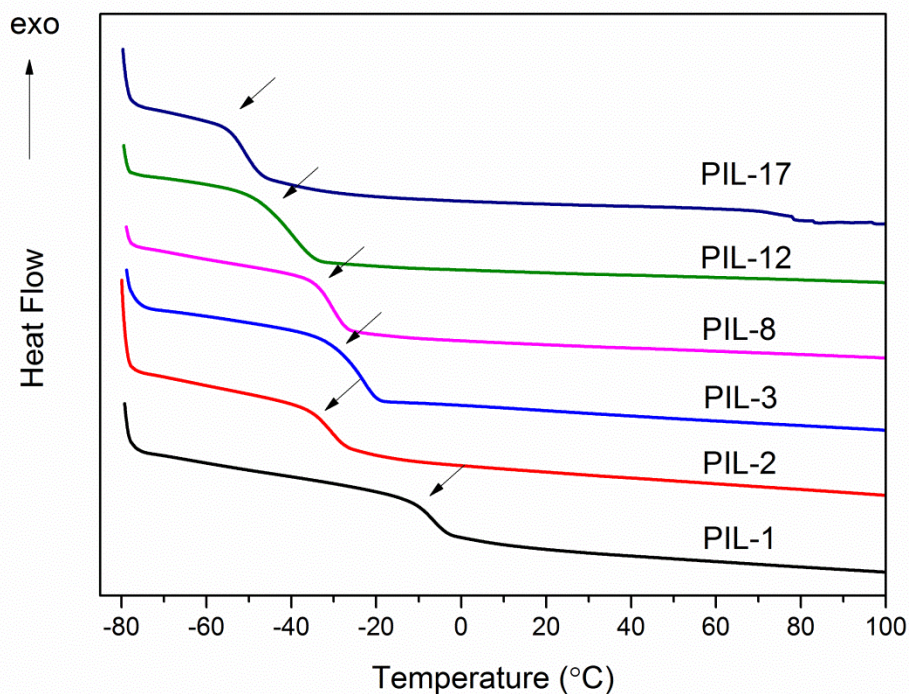
Figure 2-7 DSC of imidazolium-based PILs with TFSI counterions (**Scheme 2-2** shows the structures)

2.2.4 Ionic Conductivity

Ion conduction in polymers is complicated due to the effects of chain motion and free volume, and no model comprehensively describes conductivity.[17] However, the most widely used models for describing temperature-dependent ionic conductivity are the: Arrhenius (**Equation 2-2**) and Vogel-Fulcher-Tammann (VFT) equation (**Equation 2-3**), both of which are used to interpolate ion conduction in disordered systems.

This logarithm of conductivity plotted against 1/T should yield a linear relationship if the conductivity follows the classical Arrhenius equation:

$$\sigma = \sigma_0 exp\left(-\frac{E_a}{RT}\right)$$
Equation 2-2

where σ_0 is a pre-exponential factor correlated to the number of charge carriers, E_a is the activation energy of ion conduction that can be calculated from the linear best fit of log σ against 1/T and k is the Boltzmann constant. This type of behavior indicates ion transport via a simple hopping mechanism decoupled from chain long-range motions.[171]

Unlike the linear Arrhenius behavior, the slight convex curvatures for both **IL** model compounds (**Figure 2-8**) and **PIL**s (**Figure 2-9**) suggests that the ion conduction mechanism corresponds to the Vogel-Fulcher-Tammann (VFT) equation, which explains ion transport in solid polymer electrolytes more generally than the Arrhenius equation. The VTF equation appears in different forms,[172-174] but the most simple and widely used equation is[175]:

$$\sigma = \sigma_\infty exp\left(-\frac{B}{T - T_0}\right)$$
Equation 2-3

where σ_∞ is the infinite temperature conductivity, B is the fitting parameter related to the activation energy of ion conduction, and T_0 is the Vogel temperature where ion transport first occurs, indicating the ideal glass transition temperature. The VFT equation is based on empirical observations and suggests that ion hopping within the polymer matrix is coupled with the segmental movement of polymer chains. This is commonly observed in solid polymer electrolytes above T_g of the polymer matrix, gel polymer electrolytes, and ILs.[171,176,177]

Figure 2-8 presents the temperature-dependent ionic conductivity of **IL**s from 25 – 90 °C, exhibiting typical VFT behavior. In general, lower T_g values result in an increase in σ.[152] Presumably, the lower T_g reflects greater chain flexibility which

facilitates ion transport. The room-temperature ionic conductivity for the **IL** model compounds ranges from 10^{-5} to 10^{-4} S/cm. According to **Equation 2-1**, at a specific temperature, ionic conductivity is defined by the number of charge carriers (n), the charge of the carrier (q) and the ion mobility (μ), where n and μ are the primary variables. With an increasing length of the PEO tethering group, the T_g values of ILs decrease slightly, which could yield a moderate increase in ion mobility; however, the charge carrier density in the system decreases because of the increasing volume of the tether. This should decrease the apparent conductivity.
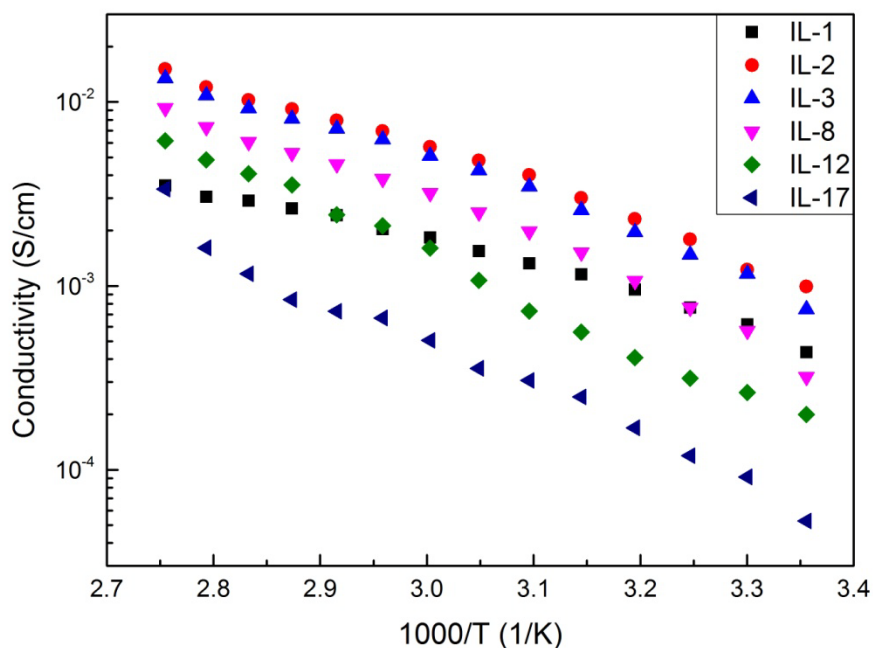
Figure 2-8   Temperature-dependent ionic conductivity of **IL**s (**Scheme 2-1** shows the IL structures)

Table 2-2   Room temperature conductivity, density and molar conductivity of ILs

ILs	IL-1	IL-2	IL-3	IL-8	IL-12	IL-17
Conductivity [a] (S/cm)	4.35×10^{-4}	9.95×10^{-4}	7.48×10^{-4}	3.20×10^{-4}	2.00×10^{-4}	5.27×10^{-5}
Density [b] (g/ml)	2.095 ± 0.005	2.075 ± 0.009	1.970 ± 0.006	1.927 ± 0.008	1.842 ± 0.007	1.784 ± 0.008
Molar conductivity [a] ($S \ast cm^{-2} \ast mol$)	0.103	0.250	0.222	0.131	0.107	0.351

[a]: The conductivity and molar conductivity values were obtained at 25°C. [b]: Densities were measured at 25°C; values were obtained from the average of three measurements.

To further investigate how the concentration of charge carriers affects the conductivity, we employ the molar conductivity (Λ), the ratio of conductivity to molar charge concentration in the electrolyte:

$$\Lambda = \sigma \cdot M/d \qquad \textbf{Equation 2-4}$$

Determination of charge concentration requires a value for density. Huddleston *et al.* reported that IL density depends not only on the nature of the anion, but also decreases with the addition of CH_2 to the alkyl chain attached on cations.[125] We see similar results. **Table 2-2** shows that the density of **IL**s drops with increasing length of the PEO tethering group, which is consistent with results from Krishnan's group.[178] The density decrease is presumably due to the weaker intermolecular interactions when ILs contain relatively large cations. Note that in addition to decreasing mass density, the PEO chains

also dilute the charge carriers. The molar conductivity values in **Table 2-2** show that **IL-17** has the highest molar conductivity despite having the lowest apparent conductivity. Charge carrier density drops as the length of tethered PEO chains increases to 17 EO units, so **IL-17** has the highest molar conductivity, even though it has the lowest conductivity. Therefore, for IL small molecules charge carrier density is the dominant aspect in defining ion conductivity, giving **IL-17** the lowest apparent ionic conductivity.

Figure 2-9 shows that room-temperature ($1000/T = 3.35$) conductivity of PILs is about 100 times smaller than for the corresponding IL model compounds, largely owing to the chain rigidity in polymers. The effect of the tethering group on conductivity is more significant with PILs than with ILs because the tether dramatically decreases the polymer T_g (**Table 2-1**). In spite of its lower charge carrier density, **PIL-17** has a higher ionic conductivity than **PIL-1** because the long tether decreases backbone interactions. **PIL-8** exhibits the highest conductivity among the six **PIL**s, — presumably because the moderate PEO chain length disrupts chain packing but does not dilute the charge carrier concentration as much as longer PEO chains.
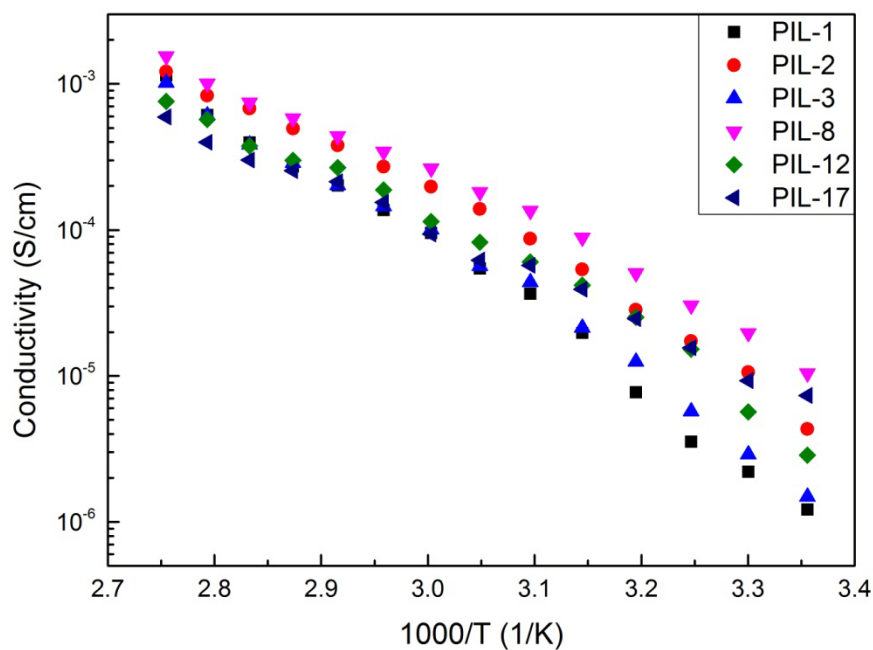
Figure 2-9   Temperature-dependent ionic conductivity of **PIL**s (**Scheme 2-2** shows the PIL structures)

Table 2-3   Room temperature conductivity of **PIL**s

PILs	PIL-1	PIL-2	PIL-3	PIL-8	PIL-12	PIL-17
Conductivity [a] (S/cm)	1.21×10^{-6}	4.33×10^{-6}	1.49×10^{-6}	1.04×10^{-5}	2.87×10^{-6}	7.35×10^{-6}

[a]: The conductivity values were obtained at room temperature (25°C);

Another interesting observation from **Figure 2-9** is that the room temperature conductivities (1000/T = 3.35) for different polymers differ more than values at higher temperature. As temperature increases, the difference in conductivity between various

73

samples becomes smaller. At 90 °C (1000/T = 2.75), **PIL-1**, **PIL-2** and **PIL-3** present

almost identical ionic conductivity values of ~10^{-3} S/cm. One possible explanation for the

similar conductivities at high temperature is a decrease in the polymer viscosities. The

viscosity of **PIL**s drops dramatically at higher temperature, especially for **PIL-1**, whose

ion mobility (μ) increases about 20000 times compared with room temperature. Therefore,

for PILs, ion mobility is the dominant parameter affecting ion conductivity. We examined

polymer rheology to further address changes in polymer viscosity that may affect ion

mobility.

2.2.5   Rheology of PILs

Rheological experiments were conducted using a parallel plate (PP25, plate

diameter of 25 mm) ARES rheometer (ARES-G2) and two PILs, **PIL-1** and **PIL-17**. The

PILs were dried for 48 hours under vacuum (≤ 10 mTorr) at 70 °C prior to all

measurements to ensure the removal of residual solvent or moisture. Dynamic strain

frequency sweep experiments were performed at room temperature (25 °C) with strain

amplitude (γ_0) = 0.5%, to give the variation of viscosity (η), elastic modulus (G',

attributed to energy stored in the sample), and viscous modulus (G'', attributed to energy

dissipated) with oscillation frequency. G' and G'' provide important characteristics of the

at-rest microstructure in a PIL system.[64]

Dynamic rhelogy tests apply a low-amplitude sinusoidal deforemation (γ) to the

sample at some frequency and maximum strain amplitude (γ_0):

$$\gamma = \gamma_0 \sin(\omega t) \qquad\qquad \textbf{Equation 2-5}$$

The sinusoidal stress response (τ) contains both an in-phase component that defines the elastic modulus (G'), and an out-of-phase component that defines the viscous modulus (G''):

$$\tau = G'\gamma_0 \sin(\omega t) + G''\gamma_0 \cos(\omega t)$$ **Equation 2-6**

The strain is not large enough to alter the sample structure (linear viscoelastic region, LVR), so the complex modulus (G^*) should be constant.

$$G^* = G' + iG''$$ **Equation 2-7**

Generally speaking, for a liquid sample G'' dominates, whereas G' dominates for a solid sample. Thus, the complex modulus indicates whether viscous or elastic responses dominate at a given frequency.

The rheological properties of **PIL-1** and **PIL-17** differ greatly. As **Figure 2-2** shows, **PIL-1** is an extremely viscous liquid that is essentially a solid-state electrolyte. Nevertheless, **Figure 2-10** shows that both **PIL-1** and **PIL-17** behave as fluids, as indicated by $G'' > G'$ over the entire range of frequency. **PIL-17**, a much less viscous PIL than **PIL-1** judging by appearance, is essentially a Newtonian fluid, as η is almost independent of frequency. G' and G'' are frequency-dependent, however, with G'' values that exceed G'. **PIL-17** shows typical viscoelastic fluid behavior, represented by linear fits giving $G' \sim \omega^2$ (n ≈ 1.72) and $G'' \sim \omega^1$ (n ≈ 0.97).

The elastic modulus G' provides an indication of the density and association strength of the PIL network. Comparing G' vs. ω for the two PILs, **PIL-1** shows a lower slope than **PIL-17**, consistent with the more solid-like characteristics of **PIL-1**. Previous studies suggest that PILs differ in rheological behavior from neutral polymers because of the electrostatic interactions between cations and anions,[107] and we suspect that the

longer PEO tethering groups of **PIL-17** give rise to both entanglement as well as a decrease in electrostatic interactions. In other words, **PIL-17** behaves more like a polymer because of the longer PEO tethering groups, while **PIL-1** is more like an ionic liquid.
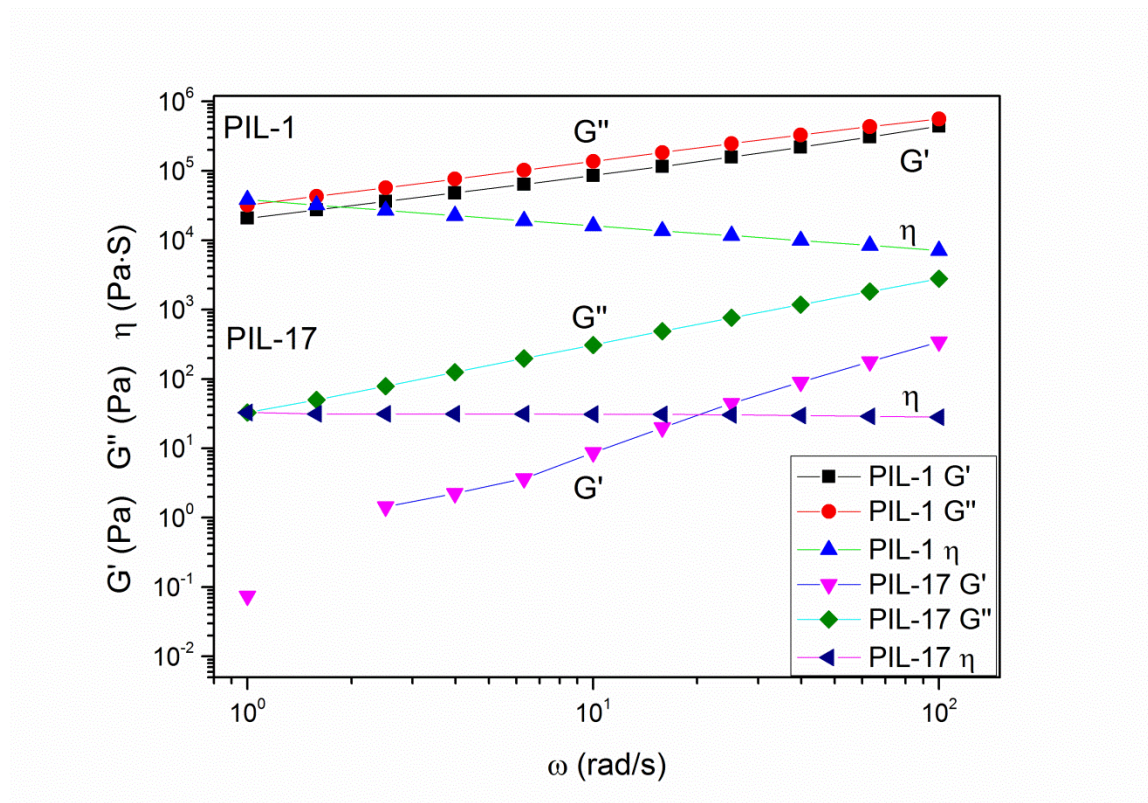
Figure 2-10 Elastic moduli (G'), viscous moduli (G''), and viscosities (η) determined from dynamic strain frequency sweep experiments with **PIL-1** and **PIL-17**

To further investigate the fluid properties of **PIL-1** and **PIL-17**, I determined viscosity as a function of temperature through dynamic temperature ramp experiments. Data were taken from 25 to 90 °C, with a heating rate of 3 °C/min at a constant strain frequency ($\omega = 6.23$ rad/s). The **IL**s show viscosities 1–3 orders of magnitude higher than

those of typical organic solvents.[179] Once polymerized, viscosities of PILs can be even higher. Viscosity, describes the resistance of a fluid to flow due to the inner friction of the liquid, and strong intermolecular interaction within ILs and PILs clearly lead to higher viscosity.

Remarkably, at room temperature the viscosity of **PIL-17** is nearly 4 orders of magnitude lower than the viscosity of **PIL-1,** clearly showing that long PEO tethers decrease the strength of intermolecular interactions in these compounds. This large difference suggests that stronger electrostatic interaction between TFSI⁻ and imidazolium are present with the shorter PEO tethering group. Weaker electrostatic interaction are consistent with greater TFSI⁻ mobility and higher apparent ionic conductivity in **PIL-17** than in **PIL-1**, despite a smaller charge carrier density in **PIL-17**.

Temperature dramatically changes viscosity, which generally decreasing with increasing temperature, often according to an empirical Arrhenius-type equation: [180]

$$\eta = \eta_\infty exp\left(-\frac{E_a}{RT}\right) \hspace{3cm} \textbf{Equation 2-8}$$

where η is dynamic viscosity, η_∞ is the infinite-temperature viscosity (pre-exponential factor), and E_a is the activation energy for the escape of the fluid particle from its "cage" in the stationary fluid. **Figure 2-11** shows the viscosities of **PIL-1** and **PIL-17** as a function of temperature. Both plots of log η vs. 1/T show large linear ranges, with r^2 around 0.999. The decreased viscosities at high temperature are consistent with a large increase in ionic conductivity with increasing temperature. For example, the viscosity of **PIL-1** ranges from 2×10^4 Pa·S at room temperature (essentially a solid) to 400 Pa·S at 90 °C, and ionic conductivity increases three orders of magnitude over the same temperature range. Although it leads to lower conducitivity, high viscosity is beneficial

for the electrolyte containment in devices.[181] Even at 90 °C (1000/T = 2.75), **PIL-1** has a viscosity that is 4×10^5 times higher than that of water at room temperature.

According to Nernst-Einstein equation, conductivity σ of a conventional electrolyte is proportional to ion density (n) and inversely proportional to viscosity (η). However, based on the "hole model" of temperature-dependent ion conduction in IL systems,[182] the fact that attaching imidazolium caions to polymer backbone makes the cation barely mobile, while TFSI⁻ is hopping between one ion pair to the next neighboring site aided by the chain segmental movement. Therefore, the conducting ion density (n) is largely reduced in PILs, and viscosity (η) might play a more important role in determining ionic conductivity. Presumably, it explained the reason why **PIL-17** gives a higher apparent ionic conductivity than **PIL-1**—owing to the less rigid segment movement in the polymer matrix, which leads to higher ion mobility, despite of a smaller charge carrier density.
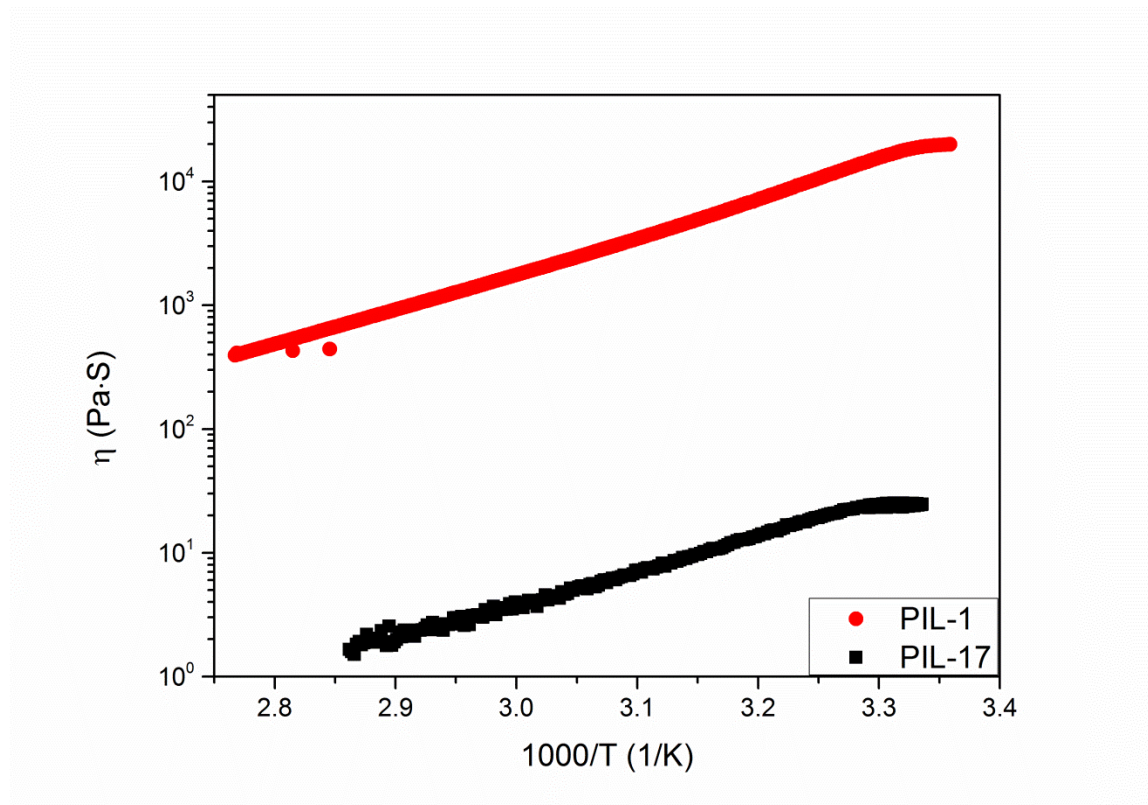
Figure 2-11   Arrhenius plot of viscosity of **PIL-1** and **PIL-17** as a function of inverse of temperature (The viscosity of **PIL-17** at high temperature is too low to detect with the instrument, so the data stop at around 80 °C, 1000/T = 2.83.)

To further examine the rheology of PILs, I performed dynamic strain frequency sweep experiments with **PIL-3**, **PIL-8** and **PIL-12** at room temperature using a cone-and-plate (CP5.7/25, with cone angle at 5.7° and plate diameter at 25 mm) geometry. Compared to the parallel plate configuration, the cone and plate provides homogeneous shear, shear rate and stress in the gap; meanwhile, it requires much less sample loading (ca. 1 mL). However, the cone and plate technique is very sensitive to the gap dimension and thus is not suitable for experiments with temperature ramps.   These experiments employ a higher amplitude strain ($\gamma_0 = 5\%$) than the parallel plate, but the response

should still lie in the linear viscoelastic region (LVR) where the complex modulus (G^*) is constant with varying strain.

Figure 2-12 shows the elastic moduli (G', a measure of the energy stored in PILs) of **PIL-3**, **PIL-8** and **PIL-12** as a function of ω, the strain frequency. As expected, the value of G' varies with the length of the tethering group. **PIL-8**, which exhibits the highest ion conductivity among all the PILs, shows G' values that are more than an order of magnitude lower than corresponding values for **PIL-3** (frequencies >4 rad/S). The relatively constant value of G' for **PIL-8** (slope around 0.3 in **Figure 2-12**) suggests a gel-like behavior. Relative to **PIL-8,** the G' values for **PIL-3** and **PIL-12** show greater frequency dependence, indicative of a more viscous behavior. One possible explanation for differences among **PIL** rheological properties is micelle-like aggregation. Prior studies of alkyl chain tethers on imidazolium-based IL small molecules suggest that when the side-chain reaches a critical length, microstructures form in the fluid (side chains aggregate) to change mechanical properties.[107,178,183] This is also plausible with PEO tethering groups. With short PEO side chains, intermolecular electrostatic interactions may dominate rheological behavior. Increasing the length of tethering groups should weaken the electrostatic interaction to give a decrease in the storage modulus. However, with longer PEO tethers, microdomains may form and the storage modulus may increase again.
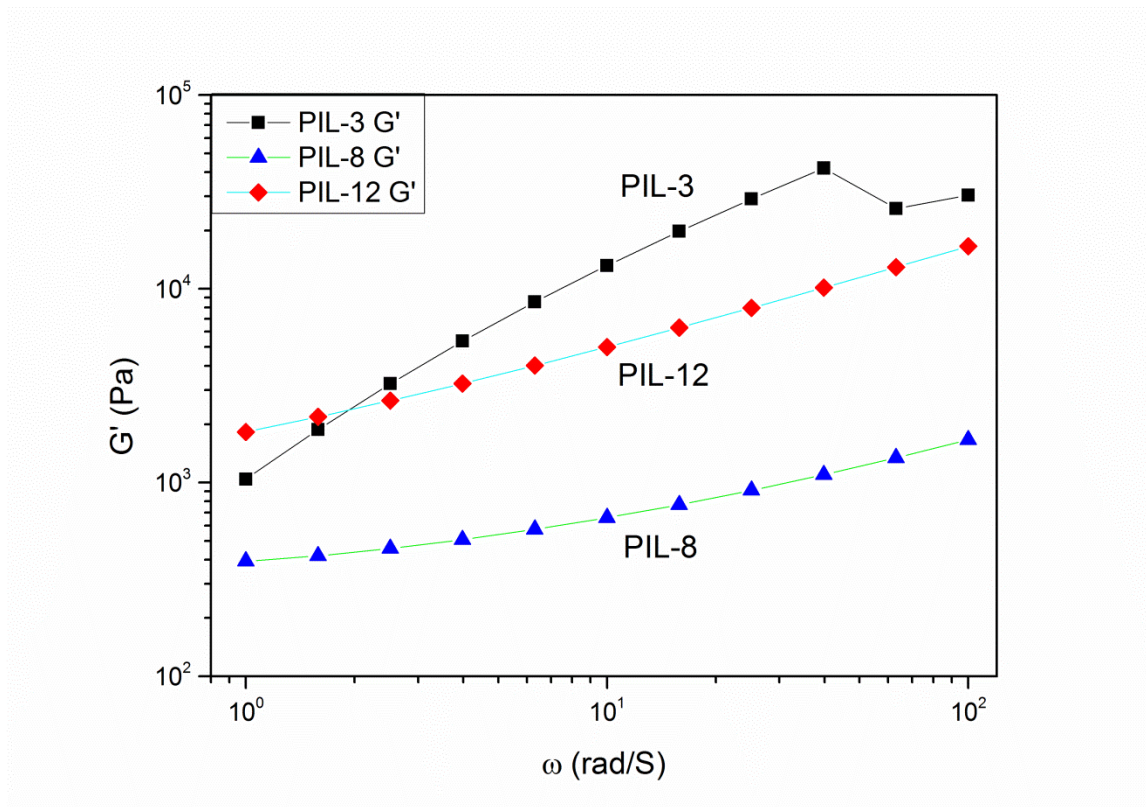
Figure 2-12 Frequency-dependent elastic modulus (G') of **PIL-3**, **PIL-8**, and **PIL-12**

2.3 Conclusions

This chapter examined the ionic conductivity and rheology of six model **IL**s and their corresponding **PIL**s. Both **IL**s and **PIL**s show the VFT type behavior in ion conduction. In the **IL**s, the charge carrier concentration dominates trends in conductivity. Because long tethers decrease the charge density in the liquid, ionic conductivity decreases with the length of PEO chains on imidazolium cations. In contrast, **PIL**s are more rigid structures, so ion mobility affects conductivity in addition to ion concentration. In **PIL**s, long PEO tethers attached to the imidazolium cations lower the polymer T_g, to facilitate ion transport. In rheological studies, the **PIL**s show typical viscoelastic properties that both storage and loss modulus are strong frequency-dependent. As the

length of the PEO tethering group increases, micelle-like aggregates and microdomains may form; therefore, the tethering group can be used to tune both nanostructure and the rheological properties of PILs. Future synthetic work (see more in Chapter 4) will focus on optimization of other tethering groups. With the addition of lithium salt, I will examine these materials as possible electrolytes for Li ion batteries.

2.4   Experimental section

2.4.1   Materials

2-Methoxyethanol (99.8%), di(ethylene glycol) methyl ether ($\geq$99.0%), tri(ethylene glycol) methyl ether ($\geq$99.0%), imidazole (99.0%), benzyl chloride (99.0%), 4-vinyl benzyl chloride (99.0%), and 2,2'-Azobis(2-methylpropionitrile) (AIBN, 98%) were obtained from Aldrich. Tosyl chloride was purchased from Jade Scientific. Poly(ethylene glycol) methyl ethers (with average M.W. values of 350, 550 and 750) were obtained from Acros Organics. 1-Butylimidazole (99.0%) was purchased from Alfa Aesar. Lithium bis(trifluoromethanesulfonyl) imide (LiTFSI, 98%) was obtained from TCI America. All chemicals and solvents were ACS reagent grade and used as received without further purification unless otherwise specified.

2.4.2   Instruments

^{1}H NMR spectra were obtained using a Varian Inova 500 MHz instrument. Differential scanning calorimetry (DSC) of 5 ~ 10 mg samples in hermetic aluminum pans was performed using a TA Instruments DSC-Q2000 calorimeter. Data were

collected between -80 ℃ and 150 ℃, and samples were heated or cooled at a rate of 10 ℃/min under N_2. Thermogravimetric analyses (TGA) were performed in air using a Perkin-Elmer TGA 7 Instrument, with a heating rate of 10 °C/min/ Samples were heated to 850 °C, with the temperature held at 120 °C for 30 min before starting the ramp. Rheology studies were conducted with an ARES rheometer (ARES-G2 rheometer). Frequency sweep experiments were performed at room temperature (25°C) with strain amplitude of 0.5%. Dynamic temperature ramp experiments were also conducted from 25 °C to 90 °C, with a heating rate of 3 °C/min at ω = 6.23 rad/s. Electrical impedance spectroscopy (EIS) analysis was done with a Hewlett-Packard 4192A LF Impedance Analyzer to obtain temperature-dependent ionic conductivity data. Electrolytes were pipetted into a cell, and impedance measurements were performed at 5° C intervals from 30-90 ° C. The sample cell uses two steel disks as symmetrical electrodes separated by a sample 0.6 cm in radius and 0.02 cm in thickness. To avoid moisture, all samples were dried under high vacuum≤ (10 mTorr) at 70 °C for 48 hours, and impedance measurements were conducted in the glove box.

2.4.3   Note on nomenclature

For simplicity, **ILs** and **PILs**, containing PEO side chains are named according to an estimation of the number of EO repeating units in the molecule. For example, **IL-1** refers to 1-(2-methoxyethyl)-3-benzylimidazolium TFSI⁻, with one EO repeating unit in the tethering group. See **Scheme 2-1** and **Scheme 2-2** for structures and details.

2.4.4 Synthesis of ILs

General procedure for the tosylation of poly(ethylene oxide) monomethyl ether. 2-methoxyethyl 4-methylbenzenesulfonate (1a). 2-methoxyethanol (7.6 g, 100 mmol) and tosyl chloride (20.97 g, 110 mmol) were dissolved in THF. NaOH (2.5 equivalents) was then dissolved in water and added dropwise (using an addition funnel) to the THF solution, which was cooled by an ice bath. The reaction was stirred for 30 minutes and left overnight to warm to room temperature. After the removal of solvents under reduced pressure, the product was extracted three times with CH_2Cl_2 and the organic layer was dried over anhydrous Na_2SO_4. After the drying agent was removed by vacuum filtration, the solvent was evaporated under reduced pressure. ^{1}H NMR (500 MHz, $CDCl_3$): δ 2.42 (s, 3H), 3.28 (s, 3H), 3.55 (t, 2H), 4.13 (t, 2H), 7.30 (d, 2H), 7.76 (d, 2H).

2-(2-methoxyethoxy)ethyl 4-methylbenzenesulfonate (1b). Compound **1b** was prepared according to the general procedure for the tosylation of poly(ethylene oxide) monomethyl ether. A colorless liquid (24.78g, 99% yield) was obtained. ^{1}H NMR (500 MHz, $CDCl_3$): δ 2.42 (s, 3H), 3.32 (s, 3H), 3.46 (q, 2H), 3.55 (q, 2H), 3.66 (t, 2H), 4.15 (t, 2H), 7.30 (d, 2H), 7.76 (d, 2H).

2-(2-(2-methoxyethoxy)ethoxy)ethyl 4-methylbenzenesulfonate (1c). Compound **1c** was prepared according to the general procedure for the tosylation of poly(ethylene oxide) monomethyl ether. A colorless liquid (27.51 g, 92% yield) was obtained. ^{1}H NMR (300 MHz, $CDCl_3$): δ 2.42 (s, 3H), 3.34 (s, 3H), 3.50 (m, 2H), 3.57 (m, 4H), 3.59 (m, 2H), 3.66 (t, 2H), 4.13 (t, 2H), 7.32 (d, 2H), 7.76 (d, 2H).

Tosyloxy-PEO(350)-methyl (**1d**). Compound **1d** was prepared according to the general procedure for the tosylation of poly(ethylene oxide) monomethyl ether. A colorless liquid (29.61 g, 86% yield) was obtained. ^{1}H NMR (500 MHz, CDCl$_3$): δ 2.42 (s, 3H), 3.34 (s, 3H), 3.51 (t, 2H), 3.55 (d, 4H), 3.59 (m, 5H), 3.61 (m, 16H), 3.65 (t, 2H), 4.13 (t, 2H), 7.29 (d, 2H), 7.75 (d, 2H).

Tosyloxy-PEO(550)-methyl (**1e**). Compound **1e** was prepared according to the general procedure for the tosylation of poly(ethylene oxide) monomethyl ether. A colorless liquid (17.82 g, 61% yield) was obtained. ^{1}H NMR (500 MHz, CDCl$_3$): δ 2.41 (s, 3H), 3.34 (s, 3H), 3.61 (m, 45H), 4,12 (t, 2H), 7.29 (d, 2H), 7.75 (d, 2H).

Tosyloxy-PEO(750)-methyl (**1f**). Compound **1f** was prepared according to the general procedure for the tosylation of poly(ethylene oxide) monomethyl ether. A colorless liquid (19.60 g, 69% yield) was obtained. ^{1}H NMR (500 MHz, CDCl$_3$): δ 2.41 (s, 3H), 3.34 (s, 3H), 3.58 (m, 65H), 4.12 (t, 2H), 7.29 (d, 2H), 7.75 (d, 2H).

General procedure for the synthesis of 1-(PEO monomethyl ether) imidazole. [164] (**1-(2-methoxyethyl)imidazole**, **2a**). A mixture of **1a** (13.8 g, 60 mmol), imidazole (4.08 g, 60 mmol), and NaOH 50% w/w solution (5.76 g, 60 mmol) in THF (70 mL) was refluxed for two days. After cooling and the removal of solvents in a rotary evaporator, the product was extracted three times with CH$_2$Cl$_2$/H$_2$O and dried with anhydrous Na$_2$SO$_4$. After the drying agent was removed by vacuum filtration, the solvent was removed in a rotary evaporator. A golden-yellow liquid (5.24 g, 69% yield) was obtained. ^{1}H NMR (500 MHz, CDCl$_3$): δ 3.31 (s, 3H), 3.60 (t, 2H), 4.06 (t, 2H), 6.94 (s, 1H), 7.02 (s, 1H), 7.50 (s, 1H).

1-(2-(2-methoxyethoxy)ethyl)imidazole (**2b**). Compound **2b** was prepared from **1b** according to the general procedure for the synthesis of 1-(poly(ethylene glycol) monomethyl ether)imidazole. A golden-yellow liquid (6.73 g, 86% yield) was obtained. ^{1}H NMR (500 MHz, CDCl$_3$): δ 3.33 (s, 3H), 3.47 (m, 2H), 3.54 (m, 2H), 3.70 (t, 2H), 4.08 (t, 2H), 6.95 (s, 1H), 7.00 (s, 1H), 7.50 (s, 1H).

1-(2-(2-(2-methoxyethoxy)ethoxy)ethyl)imidazole (**2c**). Compound **2c** was prepared from **1c** according to the general procedure for the synthesis of 1-(poly(ethylene glycol) monomethyl ether)imidazole. A golden-yellow liquid (6.48 g, 80% yield) was obtained. ^{1}H NMR (500 MHz, CDCl$_3$): δ 3.34 (s, 3H), 3.50 (m, 2H), 3.57 (m, 7H), 3.70 (t, 2H), 4.07 (t, 2H), 6.96 (s, 1H), 7.00 (s, 1H), 7.50 (s, 1H).

1-methyl-PEO(350)-imidazole (**2d**). Compound **2d** was prepared from **1d** according to the general procedure for the synthesis of 1-(poly(ethylene glycol) monomethyl ether)imidazole. A yellow liquid (7.16 g, 93% yield) was obtained. ^{1}H NMR (500 MHz, CDCl$_3$): δ 3.34 (s, 3H), 3.51 (m, 2H), 3.56 (m, 4H), 3.61 (m, 20H), 3.71 (t, 2H), 4.08 (t, 2H), 6.97 (s, 1H), 7.01 (s, 1H), 7.53 (s, 1H).

1-methyl-PEO(550)-imidazole (**2e**). Compound **2e** was prepared from **1e** according to the general procedure for the synthesis of 1-(poly(ethylene glycol) monomethyl ether)imidazole. A yellow liquid (6.83 g, 52% yield) was obtained. ^{1}H NMR (500 MHz, CDCl$_3$): δ 3.34 (s, 3H), 3.52 (m, 7H), 3.60 (m, 38H), 3.71 (t, 2H), 4.08 (t, 2H), 6.97 (s, 1H), 7.01 (s, 1H), 7.54 (s, 1H).

1-methyl-PEO(750)-imidazole (**2f**). Compound **2f** was prepared from **1f** according to the general procedure for the synthesis of 1-(poly(ethylene glycol) monomethyl ether)imidazole. A yellow liquid (7.19 g, 84% yield) was obtained. ^{1}H NMR

(500 MHz, CDCl$_3$): δ 3.33 (s, 3H), 3.51 (m, 8H), 3.60 (m, 55H), 3.70 (m, 2H), 4.07 (t, 2H), 6.96 (s, 1H), 6.99 (s, 1H), 7.51 (s, 1H).

General procedure for the synthesis of 1-methyl-PEO-3-benzylimidazolium (CF$_3$SO$_2$)$_2$N$^-$ (TFSI$^-$).[165] **1-(2-methoxyethyl)-3-benzylimidazolium TFSI$^-$ (IL-1).** Benzyl chloride (5.25 g, 41.5 mmol) was added dropwise to a solution of **2a** (5.24 g, 41.5 mmol) in toluene (25 mL) at room temperature, and the mixture was stirred for 24 h at 65 ºC. A two-phase system formed, and the toluene was removed from the flask by pipette. The remaining liquid was washed three times with diethyl ether, and then placed under vacuum to remove any remaining solvent. A viscous golden-brown liquid **3a** (8.17 g, 78% yield) resulted. To exchange chloride for TFSI$^-$, a solution of **3a** (20 mmol) and an equimolar amount of lithium bis(trifluoromethanesulfonyl)imide were dissovled in 5 mL of DI water and the mixture was stirred overnight at room temperature. The resulted product showed phase separation and precipitated from DI water. The upper liquid was decanted and product was washed with water followed by several intensive wash/redisperse/decant cycles to remove excess unreacted starring materials. The process was repeated until no AgCl was observed upon dissolution of AgNO$_3$ in the water wash, confirmed completed removal of chloride anion. The IL was then collected and placed under vacuum to remove the remaining solvent (6.32 g, 61% yield). ^{1}H NMR (500 MHz, d^6-DMSO): δ 3.30 (s, 3H), 3.65 (t, 2H), 4.30 (t, 2H), 5.28 (s, 2H), 7.17 (s, 1H), 7.33 (m, 2H), 7.38 (m, 4H), 8.74 (s, 1H).

1-(2-(2-methoxyethoxy)ethyl)-3-benzylimidazolium TFSI$^-$ (IL-2). Compound **IL-2** was prepared from **2b** (8.93 g, 81% yield) according to the general procedure for **IL-1**. A viscous golden-brown liquid was obtained (5.98 g, 57% yield). ^{1}H NMR (500

MHz, d^6-DMSO): δ 3.29 (s, 3H), 3.45 (m, 2H), 3.58 (m, 2H), 4.33 (t, 2H), 5.28 (s, 2H), 7.16 (s, 1H), 7.32 (m, 2H), 7.39 (m, 3H), 7.44 (m, 1H), 8.81 (s, 1H).

1-(2-(2-(2-methoxyethoxy)ethoxy)ethyl)-3-benzylimidazolium TFSI⁻ (IL-3). Compound **IL-3** (8.24 g, 81% yield) was prepared from **2c** according to the general procedure for **IL-1**. A viscous golden-brown liquid was obtained (7.18 g, 67% yield). ^{1}H NMR (500 MHz, d^6-DMSO): δ 3.29 (s, 3H), 3.49 (m, 2H), 3.56 (m, 4H), 3.61 (m, 2H), 3.81 (t, 2H), 4.33 (t, 2H), 5.30 (s, 2H), 7.13 (s, 1H), 7.33 (m, 2H), 7.38 (m, 3H), 7.49 (m, 1H), 8.88 (s, 1H).

1-methyl-PEO(350)-3-benzylimidazolium TFSI⁻ (IL-8). Compound **IL-8** was prepared from **2d** (8.92 g, 77% yield) according to the general procedure for **IL-1**. A viscous yellow liquid was obtained (7.54 g, 69% yield). ^{1}H NMR (500 MHz, d^6-DMSO): δ 3.28 (m, 3H), 3.51 (m, 22H), 3.80 (s, 2H), 4.33 (s, 2H), 5.31 (m, 2H), 7.32 (m, 3H), 7.37 (m, 3H), 7.51 (s, 1H), 8.93 (s, 1H).

1-methyl-PEO(550)-3-benzylimidazolium TFSI⁻ (IL-12). Compound **IL-12** was prepared from **2e** (8.32 g, 73% yield) according to the general procedure for **IL-1** with the exception that work-up was facilitated by heating to 65º C to precipitate the IL from DI water. A viscous yellow liquid was obtained (6.97 g, 61% yield). ^{1}H NMR (500 MHz, d^6-DMSO): δ 3.31 (m, 3H), 3.54 (m, 42H), 3.80 (t, 2H), 4.35 (t, 2H), 5.33 (m, 2H), 7.27 (m, 1H), 7.34 (m, 6H), 7.53 (s, 1H), 8.95 (s, 1H).

1-methyl-PEO(750)-3-benzylimidazolium TFSI⁻ (IL-17). Compound **IL-17** was prepared from **2f** (9.23 g, 81% yield) according to the general procedure for **IL-1** with the exception that it was facilitated by heating to 65º C (6.03 g, 53% yield). A pale-yellow liquid was obtained. ^{1}H NMR (500 MHz, d^6-DMSO): δ 3.34 (m, 3H), 3.56 (m,

53H), 3.83 (t, 2H), 4.37 (t, 2H), 5.35 (m, 2H), 7.32 (m, 1H), 7.33 (m, 6H), 7.56 (s, 1H), 9.01 (s, 1H).

2.4.5   Synthesis of PILs

General procedure for 1-methyl-PEO-3-(4-vinylbenzyl)imidazolium TFSI[—].[165]

1-(2-methoxyethyl)-3-(4-vinylbenzy)limidazolium   Cl[—]   (5a). A   small   amount   of hydroquinone (2 – 4 mg) was added to the reaction mixture to inhibit self-polymerization. 4-Vinylbenzyl chloride (4.58 g, 3 mmol) was added dropwise to a solution of **2a** (3.78 g, 3 mmol) in toluene (25 mL) at room temperature, and the mixture was stirred for 24 h at 65 ℃. A two-phase system formed, and the toluene was removed from the flask by pipette. The remaining liquid was washed three times with diethyl ether, and then placed under vacuum to remove any remaining solvent. A viscous golden-brown liquid **4a** resulted, and the chloride was subsequently exchanged with TFSI[—] in the following reaction. A solution containing **4a** (20 mmol) and 1.1 equivalents amount of lithium bis(trifluoromethanesulfonyl)imide (6.31 g, 22 mmol) was prepared in DI water (5 mL) and was stirred overnight at room temperature. After phase separation occurred, the product was collected by decanting upper liquid, followed by washing with water several times and then drying under high vacuum ($\leq$ 10 mTorr) at 70°C for at least 48 hours to remove residual solvent (9.63 g, 63% yield). ^{1}H NMR (500 MHz, d^6-DMSO): δ 3.31 (s, 3H), 3.68 (t, 2H), 4.36 (t, 2H), 5.31 (d, 1H), 5.42 (s, 2H), 5.88 (d, 2H), 6.74(q, 1H), 7.38 (d, 2H), 7.52 (d, 2H), 7.75 (s, 1H), 7.79 (s, 1H), 9.24 (s, 1H).

1-(2-(2-methoxyethoxy)ethyl)-3-(4-vinylbenzyl)imidazolium   TFSI[—]   (5b). Compound **5b** was prepared from **3b** according to the general procedure for **5a**. A

viscous golden-brown liquid was obtained (8.47 g, 57% yield). ^{1}H NMR (500 MHz, d^6-DMSO): δ ^{1}H NMR (500 MHz, d^6-DMSO): δ 3.18 (s, 3H), 3.39 (t, 2H), 3.52 (t, 2H), 3.76 (t, 2H), 4.36 (t, 2H), 5.31 (d, 1H), 5.42 (s, 2H), 5.88 (d, 2H), 6.74(q, 1H), 7.38 (d, 2H), 7.52 (d, 2H), 7.75 (s, 1H), 7.80 (s, 1H), 9.21 (s, 1H).

1-(2-(2-(2-methoxyethoxy)ethoxy)ethyl)-3-(4-vinylbenzyl)imidazolium TFSI⁻ (**5c**). Compound **5c** was prepared from **3c** according to the general procedure for **5a**. A viscous golden-brown liquid was obtained (9.80 g, 65% yield). ^{1}H NMR (500 MHz, d^6-DMSO): δ 3.20 (s, 3H), 3.39 (m, 2H), 3.47 (m, 2H), 3.53 (m, 2H), 3.77 (m, 2H), 4.36 (t, 2H), 5.30 (d, 1H), 5.41 (s, 2H), 5.86 (d, 2H), 6.74(q, 1H), 7.38 (d, 2H), 7.52 (d, 2H), 7.75 (s, 1H), 7.78 (s, 1H), 9.21 (s, 1H).

1-methyl-PEO(350)-3-(4-vinylbenzyl)imidazolium TFSI⁻ (**5d**). Compound **5d** was prepared from **3d** according to the general procedure for **5a**. A viscous yellow liquid was obtained (10.52 g, 61% yield). ^{1}H NMR (500 MHz, d^6-DMSO): δ 3.23 (s, 3H), 3.42 (m, 2H), 3.49 (m, 24H), 3.54 (m, 2H), 3.77 (t, 2H), 4.35 (t, 2H), 5.31 (d, 1H), 5.42 (s, 2H), 5.86 (d, 2H), 6.74 (q, 1H), 7.38 (d, 2H), 7.52 (d, 2H), 7.76 (s, 1H), 7.79 (s, 1H), 9.20 (s, 1H).

1-methyl-PEO(550)-3-(4-vinylbenzyl)imidazolium TFSI⁻ (**5e**). Compound **5e** was prepared from **3e** according to the general procedure for **5a**, with the exception that work-up was facilitated by heating to 65º C to precipitate the product from DI water. A viscous yellow liquid was obtained (10.72 g, 58% yield). ^{1}H NMR (500 MHz, d^6-DMSO): δ 3.22 (s, 3H), 3.41 (m, 2H), 3.47 (m, 44H), 3.54 (m, 2H), 3.78 (t, 2H), 4.34 (t, 2H), 5.29 (d, 1H), 5.40 (s, 2H), 5.85 (d, 2H), 6.73 (q, 1H), 7.37 (d, 2H), 7.51 (d, 2H), 7.75 (s, 1H), 7.77 (s, 1H), 9.19 (s, 1H).

1-methyl-PEO(750)-3-(4-vinylbenzyl)imidazolium TFSI⁻ (5f). Compound **5f** was prepared from **3f** according to the general procedure for **5a**, with the exception that it was facilitated by heating to 65º C. A viscous yellow liquid was obtained (10.13 g, 56% yield). ¹H NMR (500 MHz, d^6-DMSO): δ 3.23 (s, 3H), 3.38 (m, 2H), 3.44 (m, 2H), 3.48 (m, 66H), 3.54 (m, 2H), 3.76 (t, 2H), 4.36 (t, 2H), 5.30 (d, 1H), 5.44 (s, 2H), 5.87 (d, 2H), 6.73 (q, 1H), 7.37 (d, 2H), 7.51 (d, 2H), 7.75 (s, 1H), 7.77 (s, 1H), 9.20 (s, 1H).

Procedure for the polymerization of the 1-poly(ethylene glycol)-3-(4-vinylbenzyl) imidazolium TFSI⁻. Azobisisobutyronitrile (AIBN) was purified by recrystallization from methanol. To remove inhibitor added from the previous reaction, compound **5a** was stirred with ether vigorously for 30 minutes, and the ether was decanted. The process was repeated 3 times, and the product was dried under vacuum to remove ether residue. In a dry Schlenk flask 4.94 g of compound **5a** (17.7 mmol, with inhibitor removed) was dissolved in 20 ml DMF. After three freeze-pump-thaw cycles, 29.1 mg AIBN (0.177 mmol) was discharged into the Schlenk flask under nitrogen. The reaction took place in a nitrogen atmosphere at 75°C with magnetic stirring overnight. Polymerization was quenched by exposure to air. The resulting polymer was precipitated with the addition of cold methanol. A very viscous yellow liquid (2.36 g, 51% yield) was obtained. ¹H NMR (500 MHz, d^6-DMSO): δ 1.31 (s,2H), 3.18 (s, 3H), 3.64 (s, 2H), 4.33 (s, 2H), 5.19 (s, 2H), 6.33 (s, 2H), 6.90 (s, 2H), 7.39 (s, 1H), 7.69 (s, 1H), 9.12 (s,1H).

Poly(1-(2-(2-methoxyethoxy)ethyl)-3-(4-benzyl)imidazolium TFSI⁻) (PIL-2). Compound **PIL-2** was prepared from **5b** according to the general procedure for **PIL-1.** A very viscous yellow liquid (2.73 g, 57% yield) was obtained. ¹H NMR (500 MHz, d^6-

DMSO): δ 1.37 (m, 2H), 2.49 (s, 2H) 3.04 (s, 3H), 3.49 (s, 2H), 3.74 (s, 2H), 4.33 (s, 2H), 5.19 (s, 2H), 6.34 (s, 2H), 6.90 (s, 2H), 7.41 (s, 1H), 7.71 (s, 1H), 9.11 (s,1H).

Poly(1-(2-(2-(2-methoxyethoxy)ethoxy)ethyl)-3-(4-benzyl)imidazolium TFSI⁻) (PIL-3). Compound **PIL-3** was prepared from **5c** according to the general procedure for **PIL-1.** A very viscous yellow liquid (3.18 g, 60% yield) was obtained. ¹H NMR (500 MHz, d^6-DMSO): δ 1.28 (m, 2H), 2.49 (s, 2H) 3.10 (s, 3H), 3.33 (s, 4H), 3.44 (s, 4H), 3.52 (s, 2H), 3.76 (s, 2H), 4.34 (s, 2H), 5.20 (s, 2H), 6.35 (s, 2H), 6.90 (s, 2H), 7.37 (s, 1H), 7.71 (s, 1H), 9.13 (s,1H).

Poly(1-methyl-PEO(350)-3-(4-benzyl)imidazolium TFSI⁻) (PIL-8). Compound **PIL-8** was prepared from **5d** according to the general procedure for **PIL-1.** A very viscous yellow liquid (3.72 g, 65% yield) was obtained. ¹H NMR (500 MHz, d^6-DMSO): δ 1.27 (m, 2H), 3.16 (s, 4H), 3.34 (m, 27H), 3.76 (s, 4H), 4.33 (s, 2H), 5.20 (s, 2H), 6.34 (s, 2H), 6.90 (s, 2H), 7.39 (s, 1H), 7.70 (s, 1H), 9.13 (s,1H).

Poly(1-methyl-PEO(550)-3-(4-benzyl)imidazolium TFSI⁻) (PIL-12). Compound **PIL-12** was prepared from **5e** according to the general procedure for **PIL-1.** A very viscous yellow liquid (3.92 g, 60% yield) was obtained. ¹H NMR (500 MHz, d^6-DMSO): δ 1.29 (m, 2H), 3.28 (s, 4H), 3.34 (m, 44H), 3.77 (s, 2H), 4.34 (s, 2H), 5.20 (s, 2H), 6.35 (s, 2H), 6.93 (s, 2H), 7.39 (s, 1H), 7.70 (s, 1H), 9.20 (s,1H).

Poly(1-methyl-PEO(750)-3-(4-benzyl)imidazolium TFSI⁻) (PIL-17). Compound **PIL-17** was prepared from **5f** according to the general procedure for **PIL-1.** A very viscous yellow liquid (4.02 g, 63% yield) was obtained. ¹H NMR (500 MHz, d^6-DMSO): δ 1.39 (m, 4H), 3.21 (s, 3H), 3.45 (m, 68H), 3.75 (s, 2H), 4.34 (s, 2H), 5.34 (s, 2H), 6.40 (s, 2H), 6.94 (s, 2H), 7.36 (s, 1H), 7.74 (s, 1H), 9.18 (s,1H).

2.4.6 Ionic conductivity measurements

Temperature-dependent ionic conductivity measurements were performed on a home-made cell by electrical impedance spectroscopy (EIS). The data were obtained using a Hewlett-Packard 4192A LF Impedance Analyzer over the frequency range of 5Hz to 13 MHz with an applied sinusoidal voltage amplitude of 10 mV. The sample cell employs two steel disks as symmetrical electrodes. A teflon collar separates the disks and contains a sample 0.6 cm in radii and 0.02 cm in thickness. IL and PIL samples were pipetted into the cell, and impedance determinations were performed at 5 ℃ intervals from 30-90 ℃. The sample was equilibrated at the pre-determined temperature for 15 minutes before each measurement. The resistance (R) was read from a Nyquist plot at the extrapolated point where the imaginary component of the impedance was zero (see chapter 1), and ionic conductivity was calculated using equation (**2-9**):

$$\sigma = 1/\rho = l/(R{\cdot}A) \hspace{3cm} \textbf{Equation 2-9}$$

where l (cm) refers to the measured distance and A (cm^2) is the cross-sectional area. To avoid moisture, all samples were dried under vacuum ($\leq$ 10 mTorr) at 70 °C for at leas t 48 h. All conductivity measurements were conducted in the glove box.

3.   Chapter 3   Composite Electrolytes Comprised of Poly(Ethylene Oxide) and Silica Nanoparticles with Grafted Poly(Ethylene Oxide)-Containing Polymers

3.1 Introduction

The development of sustainable energy-harvesting devices is perhaps the most crucial technological challenge for mankind,[160,184] and dye-sensitized solar cells (DSSCs)[161,185,186] and rechargeable lithium ion batteries (LIBs)[110,156,187] represent important advances in this area. Electrolytes that carry charge between the electrodes of these systems strongly affect device construction and efficiency.[5] Of particular relevance to this work, difficulties in sealing liquid electrolytes in batteries or solar cells and safety issues raised during device operation are driving the development of solid-state electrolytes.[162] One approach for creating highly conductive solid electrolytes employs organic/inorganic nanocomposite materials, which often combine the advantages of both organic and inorganic components.[66] These nanocomposites usually have core-shell architectures comprised of organic polymer shells and inorganic nanoscale cores, to combine the flexibility, and processability of organic polymers with the rigidity and thermal stability of the inorganic component.[188]

Among the candidates for replacing conventional liquid electrolytes, poly(ethylene oxide) (PEO)−based polymers are particularly attractive for LIBs,[189] DSSCs,[190] fuel cells[191] and other solid-state electrochemical devices because these polymers are relatively stable and dissolve high levels of salts due to their high polarity.[33] In 1973, Wright first studied the ionic conductivity of PEO-alkali metal salt complexes.[27]

94

Since that time, many groups worked to develop PEO and its derivative polymers as stable and highly conducting solid polymer electrolytes. However, the ion conduction only occurs in the amorphous PEO phase, where conductivity is two to three orders of magnitude higher than in the crystalline phase,[20] so the ionic conductivities of common PEO-salt systems are not satisfactory because of PEO crystallization.[192] The room temperature conductivity of polymer electrolytes should be above 10^{-4} S/cm for a common applications, but pure PEO-alkali metal salt complexes exhibit conductivities of only 10^{-6} S/cm.[20] Improvements in conductivity require the introduction of disorder to prevent crystallization,[193] and approaches to this end including blending polymers, cross-linking, copolymerization, and plasticizer addition.[33,37]

With the development of controlled living radical polymerization, including atom transfer radical polymerization (ATRP),[194-197] reversible addition-fragmentation chain transfer radical polymerization (RAFT)[198-201] and nitroxide-mediated polymerization (NMP)[202-205], the scope of surface modification with polymers increased dramatically. Researchers have synthesized numerous inorganic/organic composite materials with tailored polymer shells coated on inorganic cores.[206] After anchoring an initiator to the target surface, initiation of polymerization leads to a dense layer of immobilized polymer via a "grafting from" approach.[207-209] Our lab invoked controlled living radical polymerization to grow customized polymers from silica[210] and gold.[211] In particular, Dr. Hui Zhao grafted lithium poly(4-styrenesulfonate) on 7-nm silica particles and used these hybrid particles as single-ion conductors. The protocol gave high polymer content. Although the composite material has a room temperature ionic conductivity of 10^{-7} to 10^{-}

<superscript>6</superscript> S/cm—not significantly improved compared with common single-ion conductors, it exhibits an impressive lithium transference number of almost 1.[212]

The research described in this chapter examines the hypothesis that utilizing controlled polymerization of optimized PEO-based polymers from silica nanoparticles and incorporation of these particles in pure PEO with metal salts will lead to solid or highly viscous materials with high conductivity. The nanoparticle should enhance mechanical strength and may inhibit PEO crystallization to increase conductivity. Grafted copolymers with a significant fraction of short PEG side chains should also lead to a deceased crystallization and increased conductivity.

Scheme 3-1 shows the synthesis of modified electrolytes and their incorporation in PEO. I synthesized several hybrid inorganic/organic electrolytes by first polymerizing poly(ethylene glycol) methyl ether methacrylate (PEGMA) from silica nanoparticles via surface-initiated ATRP. The hydroxyl groups on the surface of the silica particles afford sites for initiator attachment and subsequent PEGMA growth, and grafting of both homopolymers and copolymers from particle surfaces occurs with controlled growth rates and thicknesses. Corresponding free polymers were synthesized in solution via ATRP to monitor macromolecule behavior.
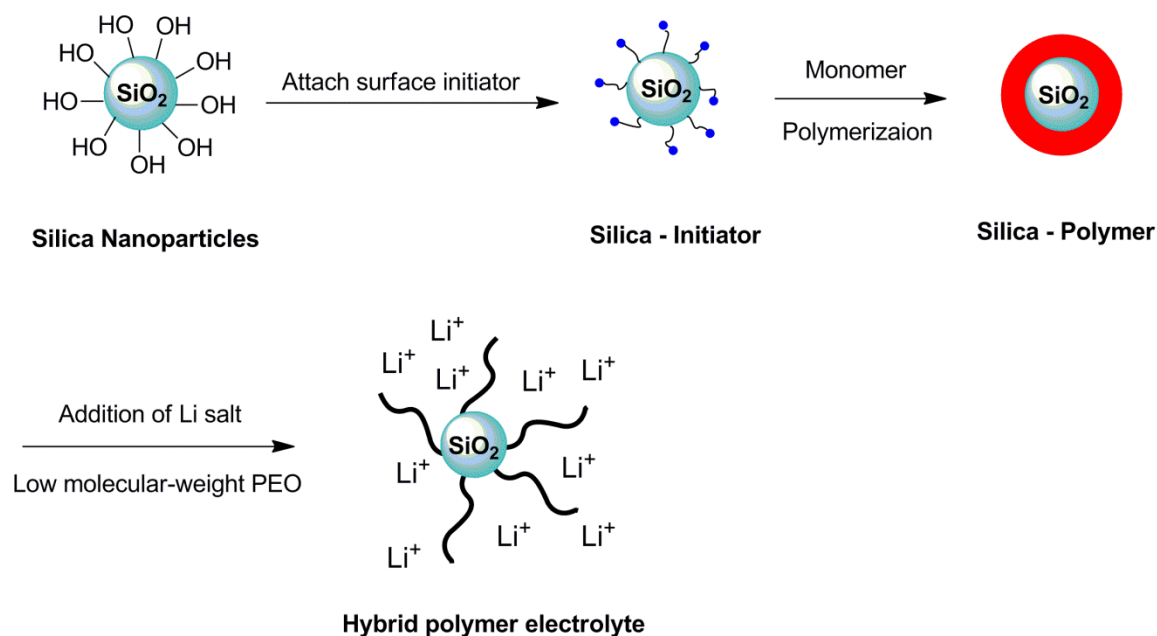
Scheme 3-1 Surface-initiated polymerization from a silica nanoparticle and subsequent formation of a composite electrolyte

One of the target applications of these nanocomposite PEO electrolytes is DSSCs, so we selected LiI as the lithium source during electrolyte preparation. The I^-/I_3^- redox couple is the most common system employed to regenerate dyes in DSSCs. Thus, I prepared electrolytes from the functionalized particles and low-molecular weight polyethylene glycol dimethyl ether (PEGDME) with the addition of LiI and I_2. Upon the introduction of particles in PEGDME, electrolytes formed gels, and with the increasing length of PEO side chains in grafted polymers, the viscosity of the electrolytes increased dramatically. Electrolytes containing silica-poly(PEGMA-1100) solidified. Surprisingly, electrolytes with silica-poly(PEGMA-475) and silica-poly(PEGMA-1100) shows higher ionic conductivity than electrolytes with shorter PEO side chains on the silica coated particles, despite much lower viscosity with shorter side chains. Surface-initiated

copolymerization allows optimization of the ion conductivity of the composite electrolytes via prevention of cystallization. Conductivity values for hybrid silica-copolymer electrolytes ranged from 1.1×10^{-4} to 1.5×10^{-4} S/cm, an order-of-magnitude improvement compared to the homopolymer-coated silica particle electrolytes, and very close to the conductivity of free poly(PEGMA) electrolytes, which have much lower viscosity. The high viscosity of the hybrid electrolytes is attractive for their encapsulation.

3.2 Results and discussion

3.2.1 Synthesis of silica-poly(PEGMA) nanoparticles

The first step in growing polymers from silica nanoparticles is attachment of an ATRP initiator to the surface via silanization (**Scheme 3-2**). Synthesis of the silane-containing initiator, (11-(2-bromo-2-methyl) propionyloxy)undecyl-trichlorosilane, proceeded in two steps according to a literature procedure.[213] Previous members of our research group grew polymers from fumed silica nanoparticles, which are prepared via the flame hydrolysis of $SiCl_4$ (AEROSIL 200 from Degussa, specific surface area (BET) of 200 m^2/g, average particle size 12 nm). This led to the formation of nanometer-scale spherical particles with a branched, chainlike structure ranging 100 to 500 nm in length.[214,215] The surface coverage of silanol groups on AEROSIL 200 is ~ 1.0 mmol/g.[216] Dr. Fadi Asfour prepared single ion conductors from modified AEROSIL 200 silica, but the weight loss of modified particles was only 2.6% (corresponding to 36% surface coverage) from TGA.[74] To increase the ratio of polymer to particle, our strategy is to increase available surface area by using smaller nanoparticles and to grow long-chain polymers from the surface. Therefore, I employed Snowtex silica (Snowtex-XS, Nissan

Chemical Corporation), whose average particle size is about 5 nm as determined from TEM.[217] The Snowtex particles come from the manufacture as an aqueous dispersion in pH 9-10 water, with an average particle size of 4 to 7 nm and a surface area of 302 m^2/g.

To prepare functionalized silica nanoparticles, I followed the procedure published by previous group members.[66,67,212] Silica nanoparticles were first precipitated from alkaline solution to allow immobilization of ATRP initiator in organic solvents. Cetyltrimethylammonium bromide (CTAB) caused particles to precipitate through aggregation by rendering the particle surface hydrophobic. After extensive rinsing to remove surfactant, ATRP initiator was then anchored onto silica surface via silane chemistry. Subsequent surface-initiated ATRP (**Scheme 3-3**) of poly(ethylene glycol) methyl ether methacrylate (PEGMA) (**Table 3-1**) gave the modified particles. Variation of the length of the PEG chain in PEGMA should allow tailoring of particle properties. Polymerization took place at room temperature, using a methanol/deionized water (3:1) solvent and a Cu(I)Br/bipyridine complex as the catalyst. The polymer-coated particles were collected by centrifugation, washed 10 – 15 times with water (recovery by centrifugation each time), and dried under vacuum at 70 °C overnight.
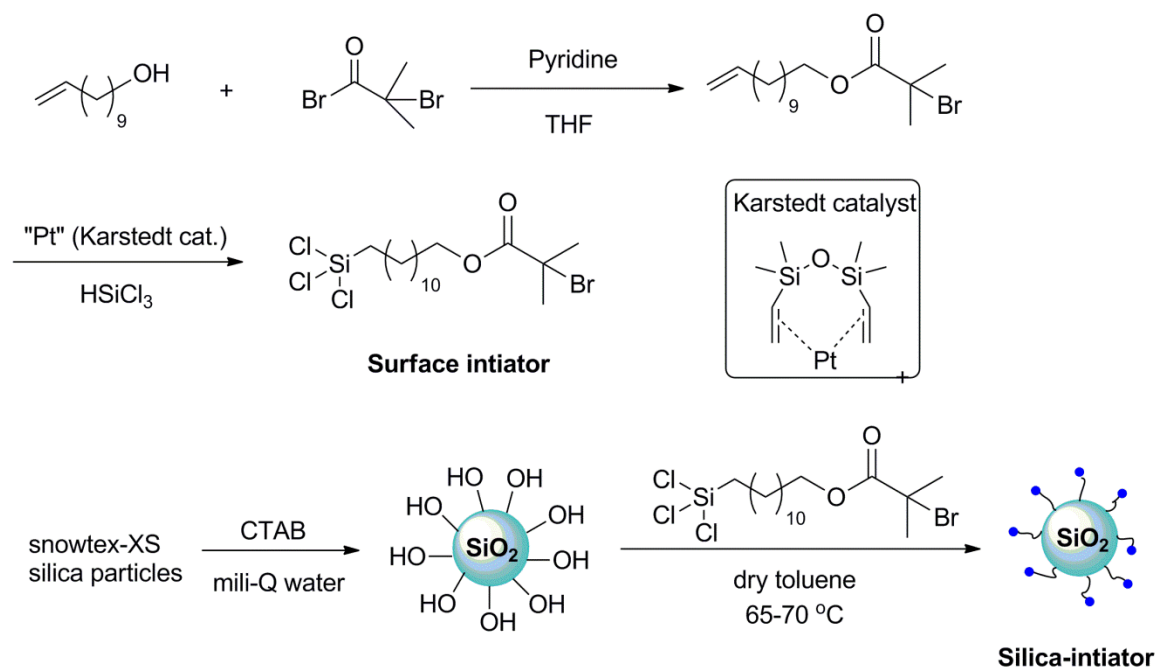
Scheme 3-2 Synthesis of a silane-containing ATRP initiator, and attachment of this initiator to silica nanoparticles
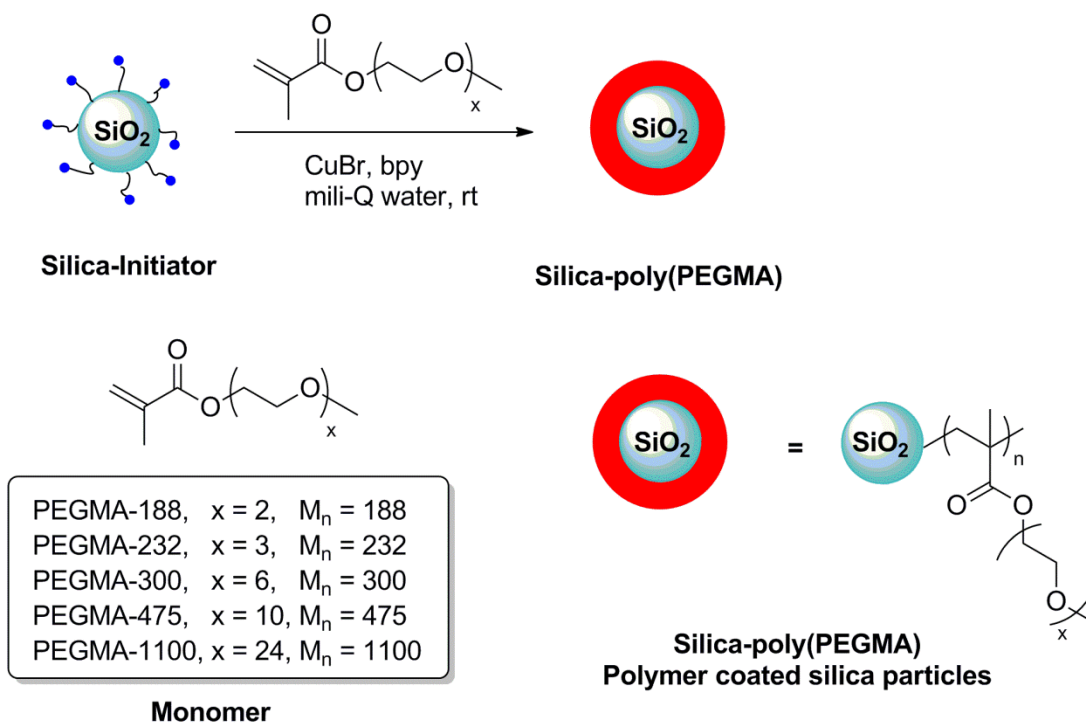
Scheme 3-3 Surface-initiated ATRP of PEGMA homopolymer from silica-initiator nanoparticles to form silica-poly(PEGMA)

Table 3-1 Silica-poly(PEGMA) synthesized in this work

Silica-Polymer	Monomer	x^a
Silica-poly(PEGMA-188)	PEGMA-188, M_n=188	2
Silica-poly(PEGMA-232)	PEGMA-232, M_n=232	3
Silica-poly(PEGMA-300)	PEGMA-300, M_n=300	5-6
Silica-poly(PEGMA-475)	PEGMA-475, M_n=475	8-9
Silica-poly(PEGMA-1100)	PEGMA-1100, M_n=1100	23-24

[a]: x refers to an estimation of the number of PEO repeating units in the monomer, as derived from the average molecular weight given by the manufacturers.

FT-IR spectroscopy confirms the polymer grafting. The FT-IR spectrum (**Figure 3-1**) of bare silica nanoparticles shows a characteristic broad absorption band associated with Si-O-Si stretching (1100 cm^{-1}), and a sharp band at around 800-770 cm^{-1} corresponding to Si-OH stretching. In addition, a C-H stretching band at 3000-2800 cm^{-1} likely stems from residual CTAB. The abundant broad band at 3600-3200 cm^{-1} (**Figure 3-1a**) is due to the hydroxyl groups on the silica surface, which are partly consumed after reaction with the initiator (11-(2-bromo-2-methyl)propionyloxy) undecyltrichlorosilane. After surface-initiated ATRP, the ester carbonyl stretch of the methacrylate appears between 1750 and 1700 cm^{-1}. Another characteristic peak associated with the C-O-C stretching of PEG is present between 1300 and 1100 cm^{-1}. This absorbance along with C-H stretching modes (3000 – 2800 cm^{-1}) become less intense with increasing length of the PEO side chain.
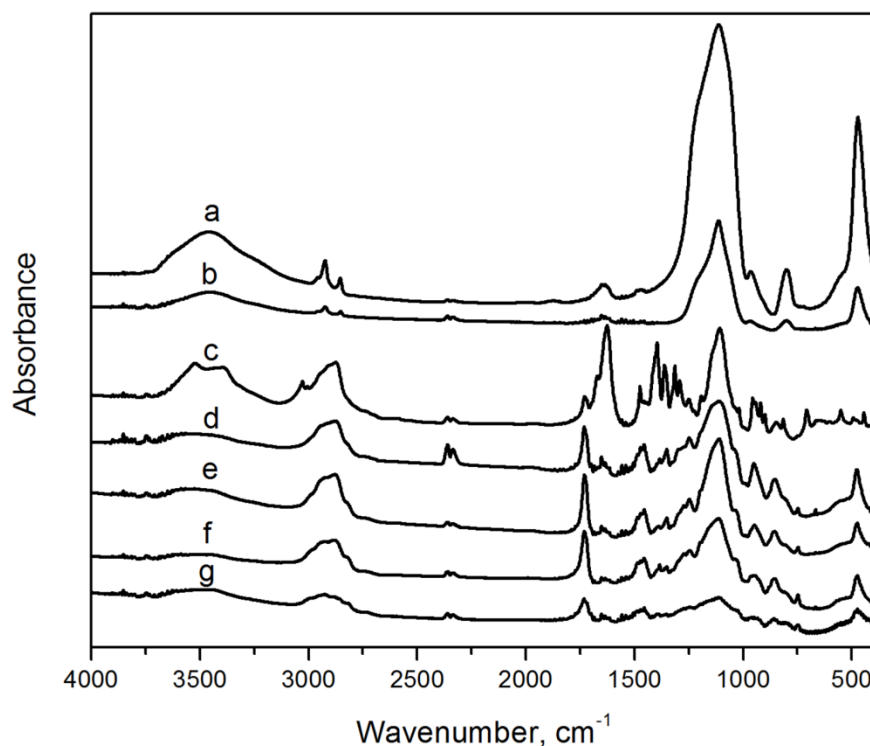
Figure 3-1 FT-IR spectra (KBr) of (a) bare silica particles, (b) silica-initiator nanoparticles, (c) silica-poly(PEGMA-1100) nanoparticles, (d) silica-poly(PEGMA-475) nanoparticles, (e) silica-poly(PEGMA-300) nanoparticles, (f) silica-poly(PEGMA-232) nanoparticles, and (g) silica-poly(PEGMA-188) nanoparticles

TEM images also suggest polymer grafting from nanoparticles (**Figure 3-2**). Bare silica particles precipitated by CTAB show diameters around 16 nm, which is about three times the diameter given by the manufacture. This may reflect some particle aggregation during the extensive wash/centrifugation/redispersion process to remove excess surfactant. After initiator attachment, aggregation became more severe even with ultrasonication during sample preparation. TEM clearly shows the aggregation (**Figure**

103

3-2b). Moreover, **Figure 3-2c** shows that after surface-initiated polymerization, silica-poly(PEGMA) particles can aggregate into a 100-nm particles**.** The dark spots in **Figure 3-2c** are the silica cores, while the abundant gray area between these cores is the poly(PEGMA) shells. The TEM image suggests significant polymer grafting from the silica surface, and thermogravimetric analysis was performed to quantitatively determine the amount of organic content.
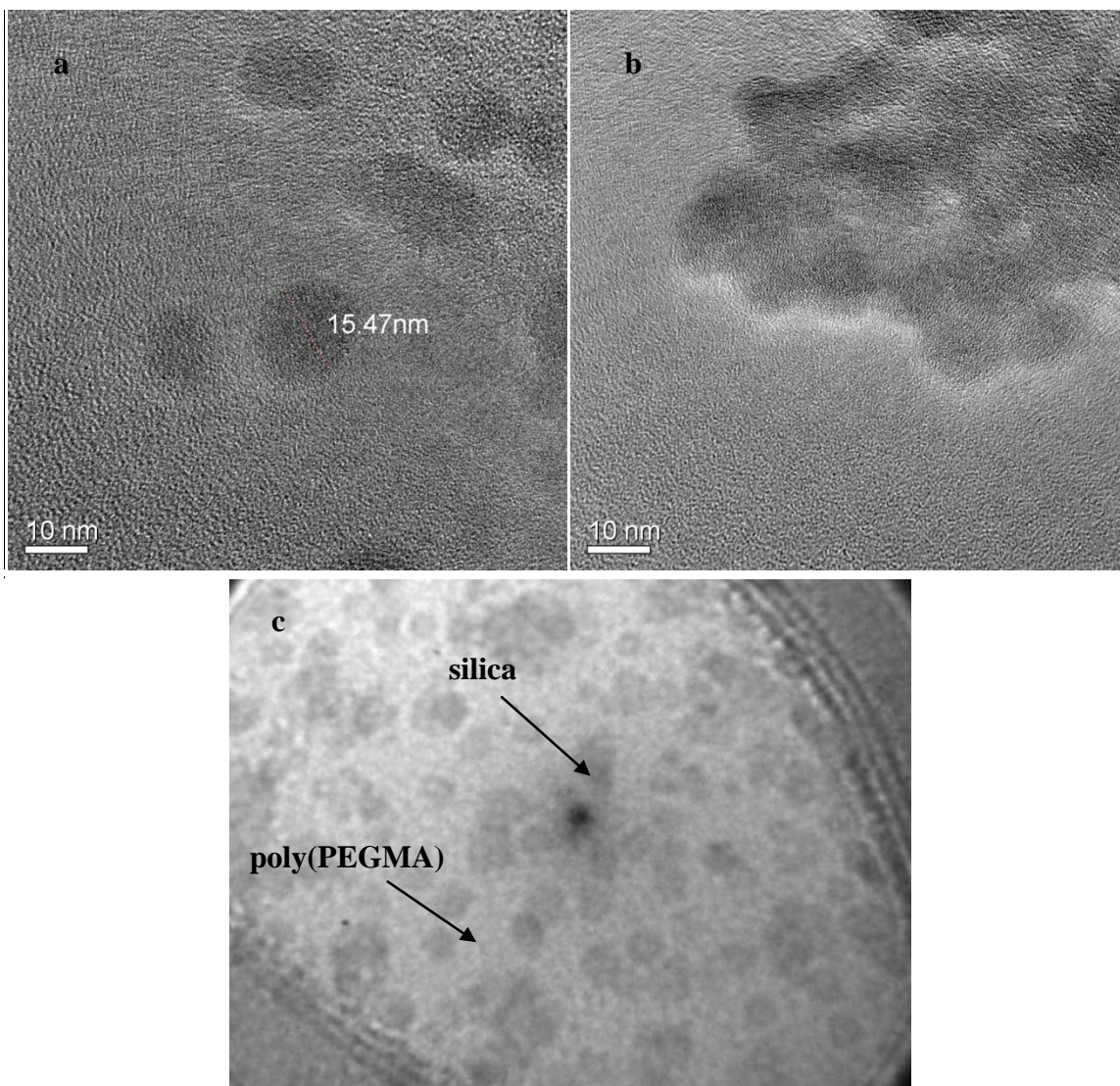
Figure 3-2   TEM images of (a) bare silica particles; (b) initiator-coated silica nanoparticles; (c) polymer-coated silica nanoparticles (All samples were dispersed in water, dropped on an ultrathin carbon film copper grid, and dried before imaging)

3.2.2   Thermal properties of silica-poly(PEGMA) nanocomposites

Thermogravimetric analysis (TGA) allows estimation of the extent of surface-initiated polymerization. TGA occurred in air with temperatures ramped to 850 °C.

Under the presence of oxygen at this high temperature, the organic portion (i.e. polymer and initiator) of the modified particles completely decompose and vaporizes with air flow, to leave behind an inorganic silica core. Therefore, weight loss quantitatively reveals the amount of polymer grafted on silica particles. As **Figure 3-3** shows, the silica-initiator particles exhibit an onset decomposition temperature of 250 °C, with around 25% weight loss up to 850 °C. **Table 3-2** and **Section 3.4.3.2** examine the extent of polymer growth in more detail.
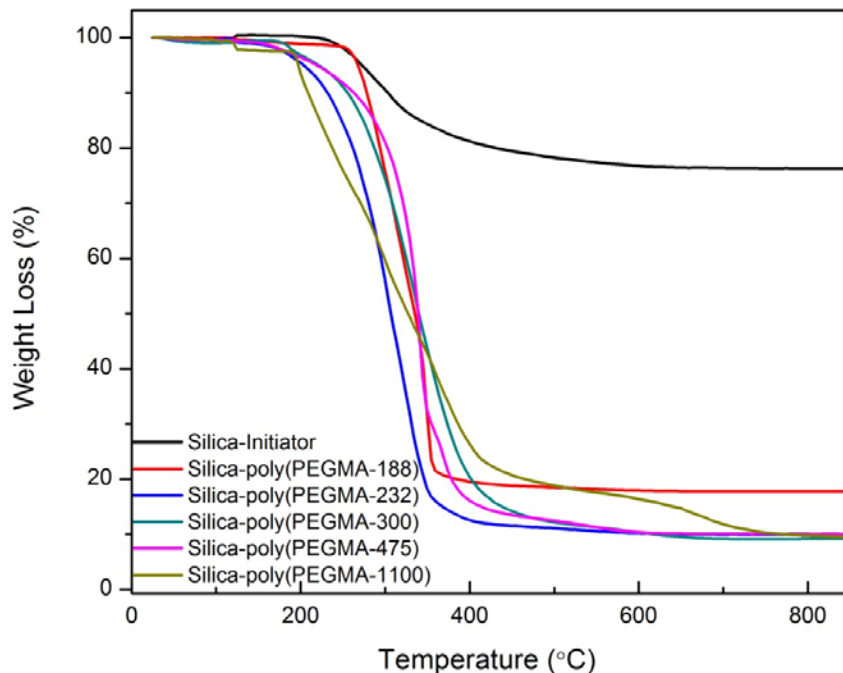
Figure 3-3 TGA data for silica-initiator and silica-poly(PEGMA) nanoparticles

Silica-poly(PEGMA-1100) shows a lower onset thermal decomposition temperature than other poly(PEGMA) coated particles as well as two distinctive decomposition regions, one around 225°C and a shoulder at 450–600°C. This likely

indicates a more complex polymer structure with silica-poly(PEGMA-1100) than other polymers, and may reflect different poly(methyl methacrylate) (PMMA) and PEO phases. A previous study showed that both the onset decomposition temperature and rate of PMMA decomposition depend on the polymer tacticity and molecular weight, and two decomposition temperatures often appear in TGA. PEO decomposition probably occurs through depolymerization and onset decomposition temperatures range from 360 K to as high as 525K.[218] Therefore, the long PEO side chain of silica-poly(PEGMA-1100) likely disturbs the tacticity of the PMMA polymer backbone to decrease the thermal stability compared to other silica-poly(PEGMA) materials with shorter PEO side chains.

As discussed in Chapter 1, high conductivity in solid-state polymer electrolyte requires a low T_g, i.e. flexible chains to facilitate ion transport, and a high T_m, i.e. a wide electrolyte temperature operation range. In DSC, T_m is the onset of an endothermic peak on heating, and the T_g value is the midpoint of a small heat capacity change on heating from the amorphous rubbery state to a brittle, glassy state. The cold crystallization temperature is the onset of an exothermic peak on heating from a subcooled liquid state to a crystalline solid state. The appearance of cold crystallization in a DSC experiment depends on the sample's thermal history.[219]

Table 3-2   DSC and TGA results for silica-poly(PEGMA)

Silica-poly(PEGMA)	T_g (°C)[a]	T_m (°C)[a]	Weight loss [b]	Maximum weight loss[c]
Silica-poly(PEGMA-188)	-49.4	n/a	82.2%	88.2%
Silica-poly(PEGMA-232)	-61.6	n/a	89.2%	90.2%
Silica-poly(PEGMA-300)	-62.4	n/a	90.8%	92.2%
Silica-poly(PEGMA-475)	-70.5	-7.3	89.9%	95.7%
Silica-poly(PEGMA-1100)	n/a	35.7	90.3%	97.7%

[a]: T_g and T_m of silica-polymer nanoparticles were determined from DSC data. [b]: % of weight loss was obtained from TGA. Materials were heated up to 850°C under air. [c]: Maximum weight loss is the theoretical weight loss calculated from monomer to initiator ratio during polymerization. The calculation details are in **Section 3.4.7**.

The T_g of pure PEO ranges from -60 to -30 °C, depending on the number of repeating ethylene oxide (EO) units. Additionally, when the number of EO repeating units is > 8, PEO tends to crystallize,[220] choosing its most stable conformation—the 7_2 helix.[26] Upon crystallization, the polymer chain becomes rigid, and hence the conductivity of PEO-based electrolyte decreases. DSC data (**Figure 3-4**) show that with shorter PEO side chains (e.g. silica-poly(PEGMA-188), silica-poly(PEGMA-232), and silica-poly(PEGMA-300)), no crystallization occurs so a melting temperature is not observed over the operation range. However, for silica-poly(PEGMA-475) and silica-poly(PEGMA-1100), especially the latter, a sharp and strong endothermic peak due to crystallization appears in the DSC curve. **Figure 3-4** and **Table 3-2** show that the value of T_g decreases with the length of the PEO side chain, and the T_g of silica-poly(PEGMA-

1100) is below the range of our instrument (≤ -85 °C) . Below T_g, the polymer is a glass where chains show regions of three-dimensional order, but after passing through glass transition, the polymer softens and becomes rubber like. The T_g correlates with the flexibility of the polymer chains, and greater flexibility should enhance ion conductivity.
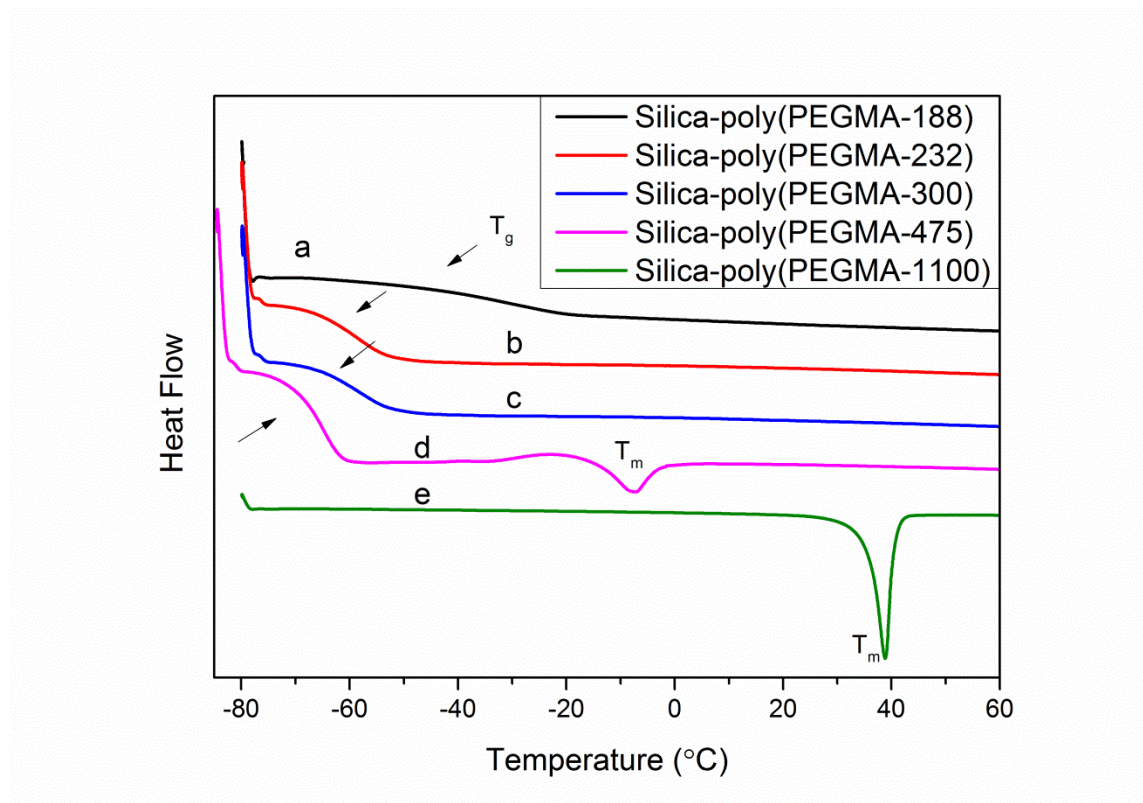
Figure 3-4   DSC results of (a) silica-poly(PEGMA-188); (b) silica-poly(PEGMA-232); (c) silica-poly(PEGMA-300); (d) silica-poly(PEGMA-475) and (e) silica-poly(PEGMA-1100)

3.2.3 Ionic conductivity of electrolytes containing PEO mixed with silica-poly(PEGMA) nanoparticles

Hybrid electrolytes were prepared by dissolving LiI and I_2 (10:1 mole ratio) in poly(ethylene glycol) dimethyl ether (PEGDME-500, M_n = 500), with the mole ratio of PEGDME-500/LiI/I_2 fixed at 100:10:1 (EO to Li ratio of ~ 100:1, PEGDME-500 contains 10 EO units), and subsequently dispersing the silica-poly(PEGMA) nanoparticles into the mixture. The amount of coated nanoparticles added was calculated from TGA data (see **Section 3.4.7** for details) to achieve a total EO:Li ratio in the electrolyte (including EO from PEGDME and silica-poly(PEGMA) of approximately 110:1. Control experiments employed a set of electrolytes consisting of PEGDME-500/LiI/I_2 with no particles but an EO/Li ratio of 110:1. **Figure 3-5** shows that vigorous stirring of functionalized particles in the PEGDME/LiI/I_2 mixture for at least 24 hours resulted in homogeneous electrolytes. For very viscous samples, such as silica-poly(PEGMA-1100), agitation with a Wig-L-Bug facilitated formation of a homogeneous hybrid electrolyte. Upon the introduction of particles, the electrolyte gelled, and with an increasing length of PEO side chains, the viscosity of the electrolyte increased dramatically. Electrolytes containing silica-poly(PEGMA-475) and silica-poly(PEGMA-1100) did not flow.
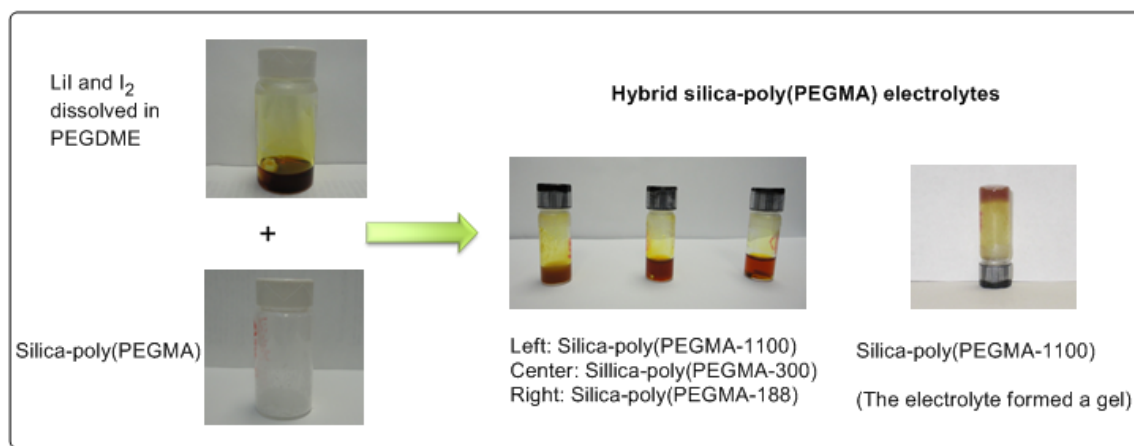
Figure 3-5   Photographs showing electrolytes formed by dispersing silica-poly(PEGMA) in PEGDME containing LiI and I_2

Using electrochemical impedance spectroscopy (EIS), we determined the conductivity of the hybrid polymer electrolytes. **Figure 3-6** shows conductivity values at temperature ranging from 20 °C to 90 °C with 5 °C intervals, plotted versus 1000/T. As expected, the ionic conductivity increased with temperature because of enhanced chain mobility. Room-temperature conductivities (1000/T = 3.41) of all electrolytes containing silica-poly(PEGMA) range from 6×10^{-5} to 1.2×10^{-4} S/cm. Despite its solidification, the electrolyte with silica-poly(PEGMA-1100) shows higher ionic conductivity than other electrolytes with modified silica particles. As discussed previously, three parameters control ionic conductivity: the charge carrier (ion) concentration (n), ion charge (q), and ion mobility (μ). The amount of silica-poly(PEGMA) particles added into PEGDME/LiI/I_2 gave the same EO/Li ratio in all electrolytes, and the silica cores occupy only a small part of the volume because over 90% of the nanoparticle mass is polymer. Hence, the charge carrier concentration for all electrolyte samples should be similar. Because ion transport in the polymer matrix depends on the segmental movement of the

polymer chain in the amorphous phase, and lithium ion coordinates to 4 – 8 oxygen atoms, the relatively high conductivity of silica-poly(PEGMA-1100) has two possible explanations: a lower T_g (i.e. higher chain mobility); or lithium coordination with more oxygen atoms.[35] With shorter PEO side chains, lithium coordination to fewer oxygen atoms might allow formation of Li cation, which will decrease ionic conductivity.

The physical description of ionic conductivity generally falls into two categories: Arrhenius behavior or Vogel-Fulcher-Tammann (VFT) behavior (see **Equation 3-1** in **Section 1.2.2.2**).[42] The slight convex curvatures of hybrid silica-poly(PEGMA) electrolytes plots indicates that the VFT model should give the best fit to the ion conduction mechanism. The VFT equation is the most widely used model to describe temperature-dependence of ionic conductivity in polymer electrolytes. Although this model is based on empirical observation, it is consistent with the free-volume theory in polymers. It suggests that ion hopping is highly coupled with segmental chain movement. For the data in this chapter, all plots show excellent fit with VFT equation, giving r^2 values around 0.99.
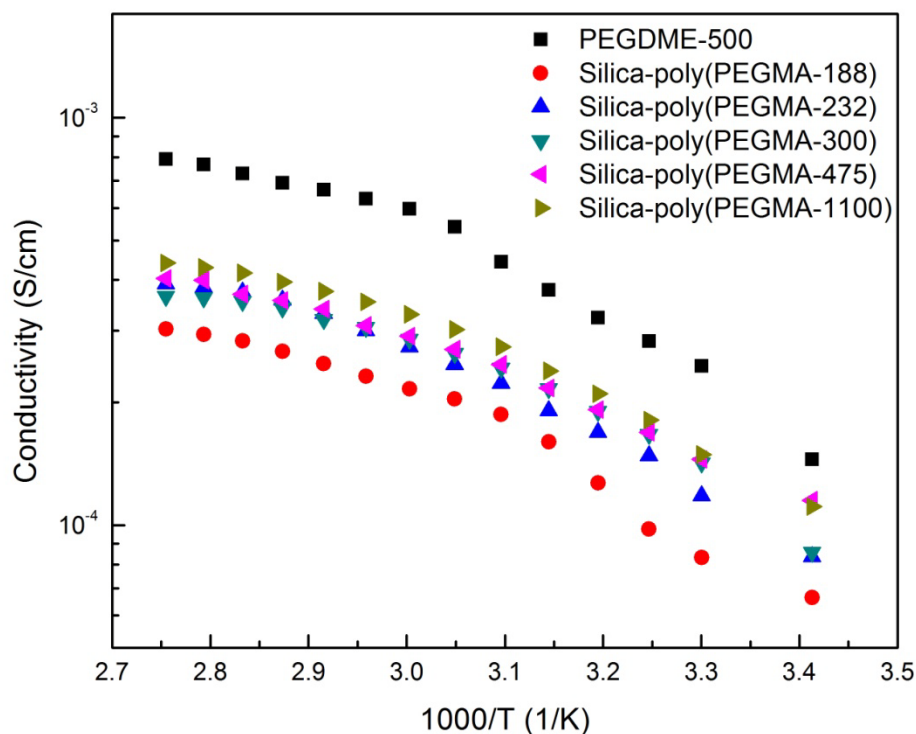
Figure 3-6   Temperature dependent ionic conductivities of electrolytes formed by dispersing silica-poly(PEGMA) in PEGDME containing LiI and I_2 (The figure also shows data for PEGDME/LiI/I_2 without the modified particles.)

3.2.4   Copolymerization to form silica-poly(PEGMA) nanocomposites

Since ion transport only takes place in the amorphous phase, crystallization of long PEO side chains should decrease conductivity.[193] Even though silica-poly(PEGMA-475) and silica-poly(PEGMA-1100) show relatively high ionic conductivity, partial crystallization of PEO side chains might hinder the ion transport in the polymer matrix. Crystallization should be especially detrimental for silica-poly(PEGMA-1100), which has a T_m value around 35 °C. Consequently, decreasing the degree of crystallinity and thus

increasing the ionic mobility, by introducing disorder into the poly(PEGMA-1100) structure should increase conductivity. Methods to decrease crystallinity include blending different polymers, copolymerization, forming cross-linked networks, or addition of plasticizer.[37] Among these methods, copolymerization is particularly attractive for chemically altering the chain tacticity, thereby inhibiting crystallization.[193] Hence, we designed a copolymer with two PEGMA monomers, one with a short PEO side chain to prevent crystallization and one with a longer PEO side chain to complex lithium cation and promote ion transport. As **Scheme 3-4** illustrates, the surface-initiated polymerization strategy is similar to that for coating nanoparticles with PEGMA homopolymers. I synthesized various silica-copolymer nanocomposite materials with different monomer ratios.

Scheme 3-4   ATRP from silica nanoparticles to form PEGMA copolymers

Table 3-3 DSC and TGA data for silica nanoparticles modified with grafted PEGMA copolymers

Silica-copolymer	Monomers		T_g (°C) [a]	T_m (°C) [a]	Weight loss [b]	Maximum weight loss [c]
	A	B				
Silica-copolymer-1	PEGMA-1100 (50%)	PEGMA-232 (50%)	/	38.8	81.9%	96.3%
Silica-copolymer-2	PEGMA-1100 (50%)	PEGMA-300 (50%)	-66.8	21.7	87.5%	96.4%
Silica-copolymer-3	PEGMA-1100 (50%)	PEGMA-475 (50%)	-67.6	18.8	82.2%	96.8%
Silica-copolymer-4	PEGMA-300 (50%)	PEGMA-475 (50%)	-64.9	/	88.2%	93.8%
Silica-copolymer-5	PEGMA-1100 (30%)	PEGMA-232 (70%)	-65.6	23.1	84.8%	90.7%
Silica-copolymer-6	PEGMA-1100 (30%)	PEGMA-300 (70%)	-65.5	8.6	88.8%	90.7%
Silica-copolymer-7	PEGMA-1100 (30%)	PEGMA-475 (70%)	-67.3	19.5	82.5%	92.8%
Silica-copolymer-8	PEGMA-300 (30%)	PEGMA-475 (70%)	-65.3	/	88.2%	89.3%
Silica-copolymer-9	PEGMA-300 (70%)	PEGMA-475 (30%)	-62.2	/	86.1%	87.5%
Silica-copolymer-10	PEGMA-1100 (70%)	PEGMA-300 (30%)	/	36.0	97.4% [d]	94.4%
Silica-copolymer-11	PEGMA-1100 (70%)	PEGMA-475 (30%)	/	35.0	98.1% [d]	94.7%

[a]: T_g and T_m of silica/polymer nanoparticles were obtained from DSC data. [b]: % weight loss was determined from TGA. Materials were heated to 850°C in air. [c]: Maximum weight loss is the theoretical weight loss calculated from the monomer to initiator ratio. [d]: Moisture and some monomer residue with the samples resulted in higher TGA weight loss.
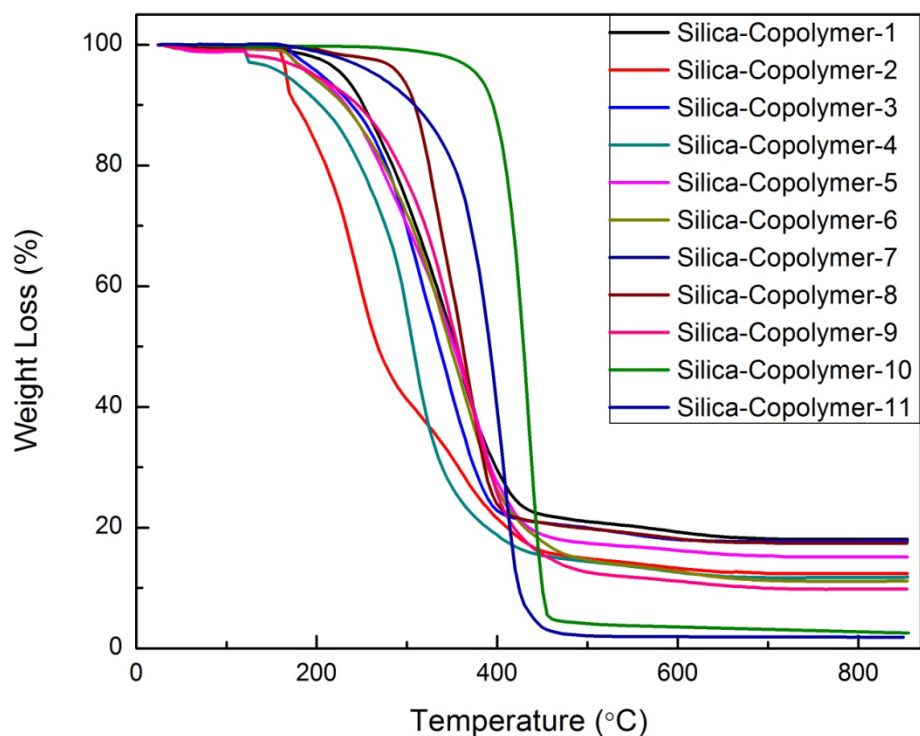
Figure 3-7   TGA of silica-copolymers (**Table 3-3** gives the copolymer compositions)

Silica-copolymers exhibit TGA profiles similar to those of silica-homopolymers (compare **Figure 3-3** and **Figure 3-7**). The onset decomposition temperatures of the silica-copolymers are above 200 °C, and in some cases as high as 400 °C. The formation of copolymers containing PEGMA-1100 and monomers with shorter PEO side chains monomers hinders the crystallization of poly(PEGMA-1100). **Table 3-3** shows decreased T_m values for the copolymers in most cases (**Table 3-2**) shows that the T_m value for the silica-poly(PEGMA-1100) homopolymer is 36°C). Among the copolymers, silica-copolymer-6, with PEGMA-1100 and PEGMA-300 in a 3:7 ratio, shows melting at below room temperature (8 °C). Because PEO is predominantly in the amorphous phase above its melting point, we expect the room-temperature ionic conductivity of hybrid

silica-copolymer-6 electrolyte to exceed the conductivity of the silica-poly(PEGMA-1100) electrolyte. To examine this hypothesis, I prepared hybrid silica-copolymer electrolytes with the protocol discussed previously and determined ionic conductivity as a function of temperature.

Figure 3-8   Temperature dependent ionic conductivities of electrolytes formed by silica-poly(PEGMA) copolymers in PEGMDE containing LiI/I_2. The figure also shows data for PEGDME/ LiI/I_2 without modified particles.

Table 3-4   Room-temperature conductivity of electrolytes containing silica-copolymer

Si-copolymer	Conductivity [a] (S/cm)	Si-copolymer	Conductivity [a] (S/cm)
Si-copolymer-1	1.14×10^{-4}	Si-copolymer-2	1.15×10^{-4}
Si-copolymer-3	1.23×10^{-4}	Si-copolymer-4	1.21×10^{-4}
Si-copolymer-5	1.13×10^{-4}	Si-copolymer-6	1.43×10^{-4}
Si-copolymer-7	1.32×10^{-4}	Si-copolymer-8	1.22×10^{-4}
Si-copolymer-9	1.12×10^{-4}	Si-copolymer-10	1.15×10^{-4}
Si-copolymer-11	1.36×10^{-4}		

[a]: The conductivity and density were measured under room temperature (20 °C, 1000/T = 3.42)

Figure 3-8 presents the temperature-dependent ionic conductivity of electrolytes containing silica-poly(PEGMA) copolymers. These plots for electrolytes containing silica-copolymer also exhibit the VFT behavior, showing excellent fits with VFT equation, which suggests ion transport is highly coupled with segmental movement of polymer chain. Room temperature ionic conductivities for hybrid silica-copolymer electrolytes ranged from 1.1×10^{-4} to 1.5×10^{-4} S/cm, which is approximately two to three times higher than the conductivity of either corresponding electrolyte with silica-poly(PEGMA) homopolymers, even though the highest ionic conductivity was still less than one order of magnitude lower than the reference (PEGDME-500 electrolyte) conductivity. As **Table 3-3** reveals, silica-copolymer-6, which exhibits the lowest

melting point among copolymers with PEGMA-1100 as one of the monomers, gives the highest electrochemical conductivity, which is also higher than the silica-poly(PEGMA-1100) homopolymer electrolyte. In addition, PEGMA copolymer coated particles are excellent gelators. The polymer electrolytes became very viscous with the introduction of the particles. In particular, silica-poly(PEGMA-1100-*co*-PEGMA-300) and silica-poly(PEGMA-1100-*co*-PEGMA-475) solidified easily after mixing with PEGDME/LiI/I_2, and yet, gave reasonably high ionic conductivity.

3.2.5 Synthesis and characterization of free poly(PEGMA) electrolytes

To compare the performance of polymer coated hybrid electrolytes with the corresponding free PEGMA homopolymers and copolymers, I synthesized a series of free polymers (**Scheme 3-5**). All structures were confirmed by ^{1}H NMR. **Figure 3-9** gives the NMR spectrum of poly(PEGMA-232) as an example.
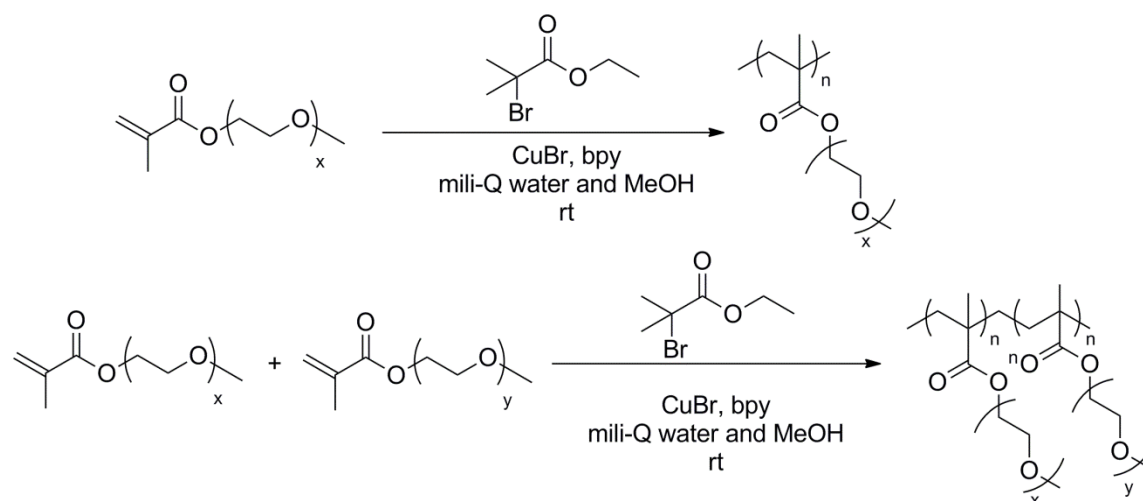
Scheme 3-5 ATRP of free poly(PEGMA) homopolymers (top) and free poly(PEGMA) copolymers (bottom)
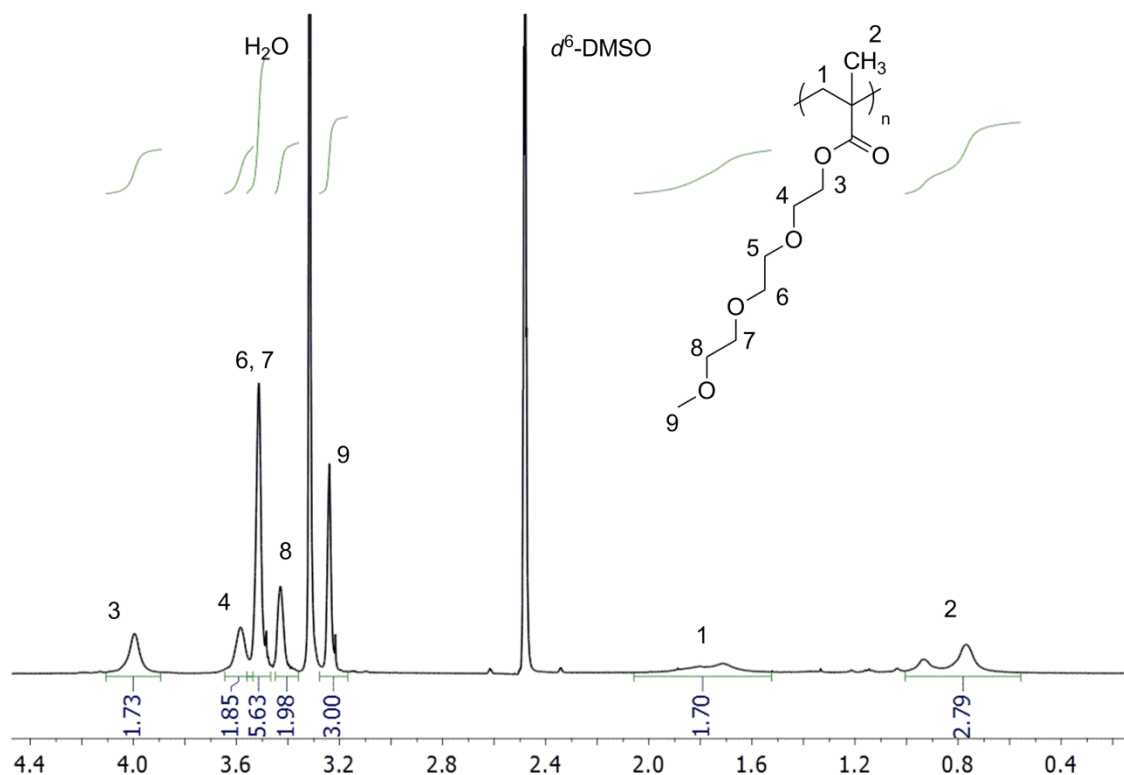
Figure 3-9 NMR spectrum of free poly(PEGMA-232)
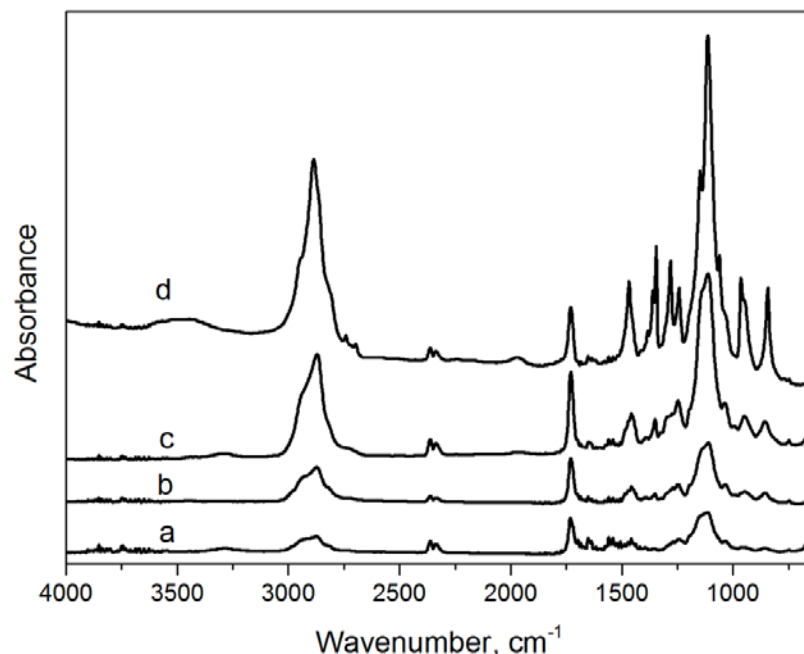
Figure 3-10 FT-IR Spectrum of (a) free poly(PEGMA-232) homopolymer, (b) free poly(PEGMA-300) homopolymer, (c) free poly(PEGMA-475) homopolymer and (d) free poly(PEGMA-1100) homopolymer

As **Figure 3-10** describes, FT-IR spectra of free poly(PEGMA) further confirm polymer structure. The strong and sharp absorbance peak at 1750-1700 cm^{-1} corresponds to the ester carbonyl group. The C-O-C stretching at 1300-1100 cm^{-1} due to the EO repeating unit, which is significantly increases the length of the PEO side chain, along with the broad band at 3000 – 2800 cm^{-1} associated with the sp^3 C-H stretching.

Free polymer electrolytes were prepared via the same protocol for silica-poly(PEGMA) electrolytes (see details in **Section 3.4.7**). **Figure 3-11** shows conductivities of free poly(PEGMA) electrolytes containing LiI/I$_2$ dissolved in PEGDME, with the same EO/Li ratio as for electrolytes with poly(PEGMA)-coated silica. Like

hybrid silica-polymer electrolytes, the plots of electrolytes containing free poly(PEGMA) show good fits to the VFT equation, suggesting the same ion hopping mechanism in both systems. Room-temperature ionic conductivities for free polymer electrolytes ranged from 1.2×10^{-4} to 1.5×10^{-4} S/cm, essentially the same values determined for corresponding hybrid electrolytes. Therefore, compared to the conductivity of free poly(PEGMA) electrolyte with the same EO/Li ratio, immobilizing poly(PEGMA) on silica particles has a negligible effect on ionic conductivity. However, immobilization of the poly(PEGMA) on silica leads to solid electrolytes that should be much more amenable to encapsulation in devices.
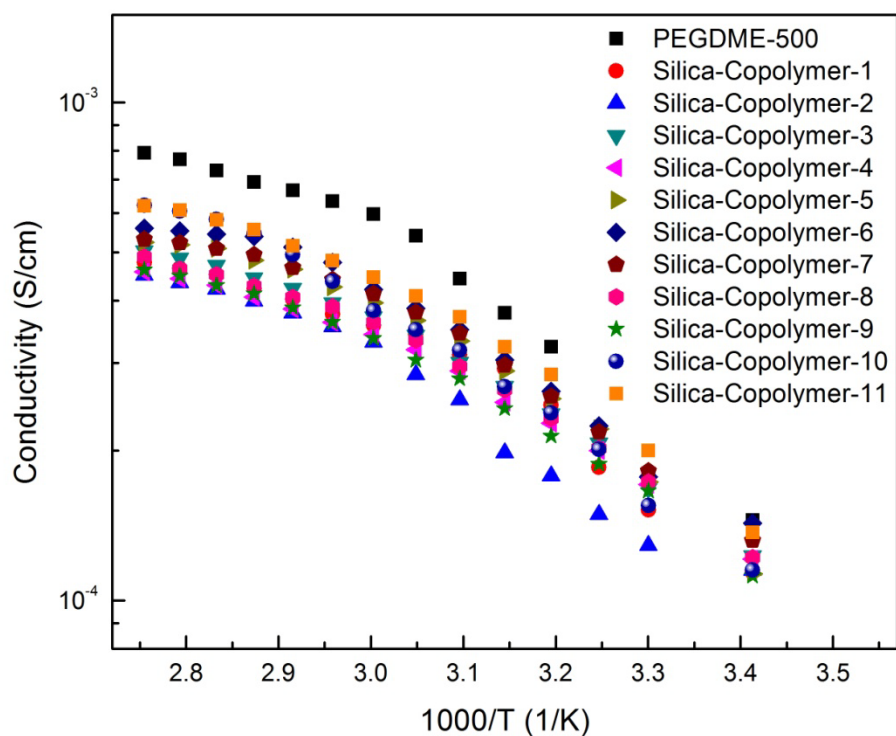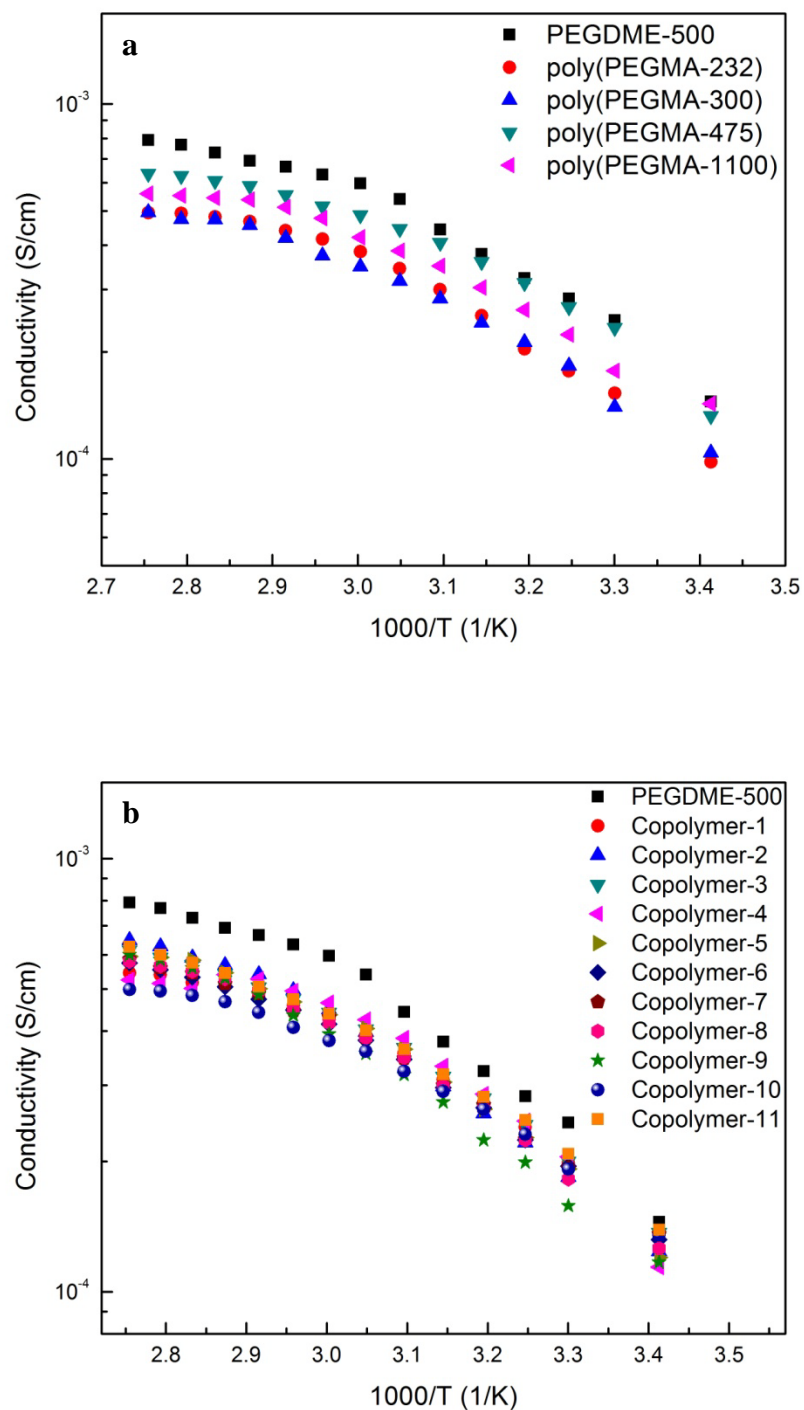
Figure 3-11   Temperature-dependent ionic conductivities of electrolytes formed by (a) free poly(PEGMA) homopolymers in PEGMDE containing LiI/I_2, and (b) free

poly(PEGMA) copolymers in PEGMDE containing LiI/I$_2$. The figure also shows data for PEGDME/ LiI/I$_2$ without modified particles.

3.3 Conclusions

To summarize, hybrid silica/polymer nanocomposites were synthesized by grafting various PEO based polymers onto silica nanoparticles via surface-initiated ATRP. Polymer electrolytes were prepared by blending silica-poly(PEGMA) particles with PEGDME-500 containing LiI/I$_2$ to creat potential candidates for electrolytes in DSSCs. The introduction of silica nanoparticles enhanced the electrolyte mechanical properties, making the electrolytes viscous gels. These solid-like polymer/inorganic hybrid electrolytes still show room temperature conductivity around 10^{-4} S/cm, only a 3-fold decrease compared to an electrolyte with only PEGDME-500 and LiI/I$_2$. Copolymerization of two PEGMA monomers circumvents the problem of PEO crystallization because a short PEO side chain interrupts the structure of the longer side chain. This lack of crystallization, however, only increases conductivity by a factor of two when comparing electrolytes containing nanoparticles modified with homo and copolymers. Conductivities of PEGDME-500/LiI/I$_2$ containing silica-copolymer electrolytes and corresponding free copolymers are nearly identical. However, the silica-copolymer electrolytes are highly viscous gels that are much more amenable to encapsulation. Our ongoing research will focus on utilizing these novel electrolytes in DSSCs or LIBs.

3.4   Experimental section

3.4.1   Materials

Lithium iodide (crystalline powder, 99.9%), cetyltrimethylammonium bromide (CTAB), copper (I) bromide (CuBr, 99.999%), ethyl 2-bromoisobutyrate (EBiB, 98%), methacryloyl chloride (97%), 10-undecen-1-ol (98%), 2-bromoisobutyryl bromide (98%), trichlorosilane (99%), tri(ethylene glycol) monomethyl ether (96%), and di(ethylene glycol) monomethyl ether (96%) were obtained from Aldrich and used as received. N, N, N', N'-ethylenediaminetetraacetic acid (disodium salt dehydrate, EDTA·2Na) was purchased from Spectrum. Triethylamine and hydroquinone were obtained from J. T. Baker Chemical and used as received. Iodine (Aldrich, 99.99%) and 2, 2-Bipyridine (bpy, Aldrich, 99%) were sublimed prior to use. Poly(ethylene glycol) methyl ether methacrylates (Aldrich, average M_n=300, 475, or 1100) were passed through an activated basic alumina column before use. Snowtex-XS (7-10 nm) was a gift from Nissan Chemical, and the colloidal silica was received as an aqueous dispersion in pH 9-10 water. All other chemicals and solvents were ACS reagent grade and used as received from commercial suppliers without further purification unless otherwise specified.

3.4.2   Instruments

^{1}H NMR spectra were obtained using Varian Inova 500 MHz instruments. Thermogravimetric analyses (TGA) were performed in air using a Perkin-Elmer TGA 7 Instrument, with a heating rate of 10 °C/min; samples were heated up to 850 °C after holding at 120 °C for 30 min prior to the temperature ramp. FT-IR spectra were collected with a Mattson Galaxy 300 spectrometer through KBr pellets.   Differential scanning

calorimetry (DSC) was carried out using a TA DSC Q100 instrument with a heating/cooling/heating cycle of 10 °C/min under nitrogen. Transmission electron microscopy (TEM) images were obtained with a high resolution JEOL100 CXII instrument with both digital and film image recording capabilities. Samples were spotted on copper grids coated with ultrathin polymer films (PELCO® TEM grid 01822). Electrical impedance spectroscopy (EIS) analysis was done with a Hewlett-Packard 4192A LF Impedance Analyzer to obtain temperature-dependent ionic conductivity data. Electrolytes were pipetted into a cell and resistance measurements were taken when voltage was passed through the cell at 5 ºC intervals from 30-90 ºC. The sample cell uses two steel disks as symmetrical electrodes separated by a sample 0.6 cm in radius and 0.02 cm in thickness. All measurements were conducted in a N_2-filled glove box.

3.4.3 Synthesis and characterization of initiator-coated silica nanoparticles (silica-initiator)

Silica - Initiator   **Silane Initiator**
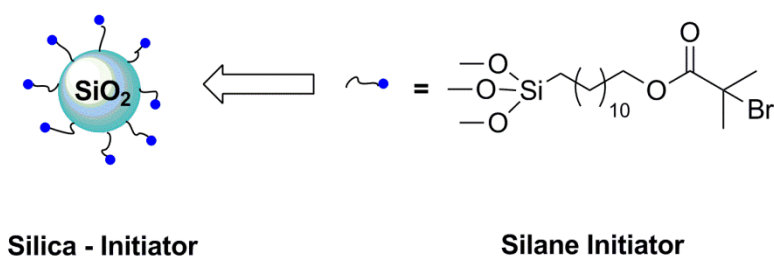
Figure 3-12   Initiator-coated silica nanoparticles (silica-initiator)

3.4.3.1 Preparation of silica-initiator nanoparticles

Particle preparation followed a literature procedure.[210] 1 g of cetyltrimethylammonium bromide (CTAB) was added into 20 mL of Snowtex-XS, and the mixture was stirred at room temperature for 30 min, during which the particles aggregated and precipitated from solution. Silica particles were collected by centrifugation and were then redispersed in 100 mL deionized water to remove CTAB residues. Particles were recollected by centrifugation, and the collecting/redispersing process was repeated 20 times to remove CTAB as completely as possible. Finally, silica particles were dried under high vacuum ($\leq$ 10 mTorr) at 70 °C overnight.

(11-(2-bromo-2 methyl) propionyloxy)undecyl-trichlorosilane was synthesized via a two-step literature procedure.[213] 10-undecen-1-ol (1.71g, 10mmol) and pyridine (0.96 mL, 12 mmol) were dissolved in 10 ml of distilled THF, followed by the addition of 2-bromoisobutyryl bromide (1.24 mL, 10 mmol) drop by drop over a period of 10 minutes. The mixture was stirred at room temperature under N_2 atmosphere overnight. Following dilution with 20 mL hexane, and washing with 3N HCl three times and distilled water three times, the organic phase obtained was dried over Na_2SO_4 and filtered under reduced pressure. Finally, solvent was removed and a colorless oily liquid product, 10-undecen-1-yl 2-bromo-2-methylpropionate, was obtained (2.63 g, 82.5% yield). ^{1}H NMR (500 MHz, CDCl$_3$): δ 1.22 – 1.41 (m, 12H), 1,60 – 1.70 (m, 2H), 1.92 (s, 6H), 1.97 – 2.06 (m, 2H), 4.15 (t, 2H), 4.86 – 5.02 (m, 2H), 5.85 – 5,72(m, 1H).

10-undecen-1-yl 2-bromo-2-methylpropionate (2 g, 6.27 mmol) and trichlorosilane (5 mL, 50.7 mmol) were added into a flame-dried flask, followed by the addition of Karstedt's catalyst (10 μL). The reaction took place at room temperature

overnight under N_2, and, the mixture was passed through a flash column to remove catalyst. Excess trichlorosilane was removed by vacuum distillation (60 °C, 100 mTorr), to give a colorless oil, (11-(2-Bromo-2-methyl)propionyloxy) undecyltrichlorosilane (1.81 g, 72% yield). ^{1}H NMR (500 MHz, CDCl$_3$): δ 1.21 – 1.41 (t, 2H), 1,46 – 1.75 (m, 4H), 1.92 (s, 6H), 4.15 (t, 2H).

Freshly prepared surface initiator, (11-(2-bromo-2 methyl) propionyloxy)undecyl-trichlorosilane, was dissolved in dry toluene, and stirred with silica nanoparticles under N_2 at 60 – 70 °C overnight. Initiator was in excess to ensure effective anchoring onto the surface of the silica nanoparticles. The initiator-coated particles were collected by centrifugation, dispersed into toluene, washed with pentane, and then recollected by centrifugation. The redispersion /wash/centrifugation/recollecting cycle was repeated at least 10 times to remove any free initiator from the solution or particle surface. The initiator-coated nanoparticles were finally dried under vacuum (10 mTorr) at 70 °C overnight.

3.4.3.2   Calculation   of   initiator   content   grafted   on   silica-initiator nanoparticles

After drying, TGA was conducted to determine the amount of initiator attached to the particles. TGA was performed under a dry air atmosphere, holding the temperature at 120 °C for 30 min before starting the temperature ramp at 10 °C/min up to 850 °C. The TGA data showed 23.7% weight loss, implying that 1 mg of initiator-coated nanoparticles contained 0.237 mg initiator. The molar mass of the initiator is 342.54 g/mol, so there are 6.9×10^{-7} mole of initiator per mg of silica-initiator. Thus, when

surface-initiated ATRP was conducted with 62 mg of initiator coated particles, the solution contained 0.042 mmol of initiator. Therefore, for each surface-initiated ATRP reaction, the monomer (2 mmol) to initiator ratio was roughly 47:1.

3.4.4 Surface-initiated ATRP of silica-poly(PEGMA) homopolymers

Silica-poly(PEGMA) Homopolymer
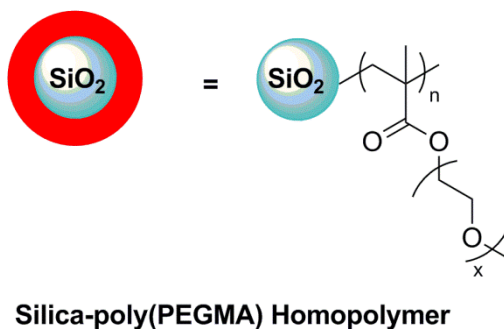
Figure 3-13   PEGMA homopolymer coated silica nanoparticles (silica-poly(PEGMA))

Synthesis of tri(ethylene glycol) methyl ether methacrylate.[221] Tri(ethylene glycol) monomethyl ether (13.7 g) and 20 mL of triethylamine (0.14 mol) were dissolved in 50 mL of diethyl ether in a three-neck round-bottom flask and placed in an ice bath. To this flask a solution containing 6.87 mL of methacryloyl chloride (0.07 mol) in 15 mL of ethyl ether was added dropwise over 15 minutes. The reaction was allowed to proceed overnight at room temperature under N_2. The mixture was filtered under reduced pressure to remove the precipitate, and the residue was purified by silica gel column chromatography (hexanes/ethyl acetate 1/2, v/v). After removal of the solvent, a small amount (ca. 3 mg) of hydroquinone was added to the product as a polymerization inhibitor. The product was further purified by vacumn distillation at 120 °C, 100 mTorr

to obtain a colorless liquid (11.29 g, 70% yield). ^{1}H NMR (500 MHz, CDCl$_3$): δ 1.92 (s, 3H), 3.37 (t, 3H), 3.64 (m, 10H), 4.28 (t, 2H), 5.55 (s, 1H), 6.11 (s, 1H).

Synthesis of di(ethylene glycol) methyl ether methacrylate.[221] This synthesis followed the same protocol described with the same molar ratios of reactants to obtain a colorless liquid (78% yield). ^{1}H NMR (500 MHz, CDCl$_3$): δ 1.93 (s, 3H), 3.36 (t, 3H), 3.64 (m, 8H), 4.28 (t, 2H), 5.55 (t, 1H), 6.11 (q, 1H).

Surface-initiated ATRP of tri(ethylene glycol) methyl ether methacrylate (Silica-poly(PEGMA-232)).[66] The monomer was first dissolved in methanol and passed through an activated basic alumina column to remove inhibitor. After removing the methanol, 0.464 g of tri(ethylene glycol) methyl ether methacrylate (2 mmol), 28 mg of 2, 2-bipyridine (bpy, 0.18 mmol), and 62 mg of initiator grafted-particles (ca. 0.042 mmol of initiators) were dissolved or dispersed in 1 mL of deionized water and 3 mL of methanol in a Schlenk flask. The mixture was ultrasonicated for 15-20 minutes. After 3 freeze-pump-thaw cycles, the Schlenk flask was filled with nitrogen, and 8 mg of CuBr (0.06 mmol) was added to the mixture, which became dark brown. After another freeze-pump-thaw cycle, the reaction was allowed to take place at room temperature for 12 hours. To quench the reaction, the Schlenk flask was opened and exposed to air, and the solution turned blue. The mixture was transferred to a 50-mL centrifuge tube and washed with an EDTA•2Na-saturated solution several times, until no blue color was observed. Subsequent washes employed deionized water 10 times and acetone 3 times. In each step the polymer-grafted silica particle was recollected by centrifugation. The product was dried under vacuum (≤ 10 mTorr) at 70 °C overnight. After drying, TGA was performed to determine the extent of polymer grafting on the particles.

Surface-initiated ATRP of silica-poly(PEGMA-188), silica-poly(PEGMA-300), silica-poly(PEGMA-475), and silica-poly(PEGMA-1100) followed the same protocol protocol with 2 mmol of monomer in the polymerization solution in all cases.

3.4.5 Surface-initiated ATRP of silica-copolymer
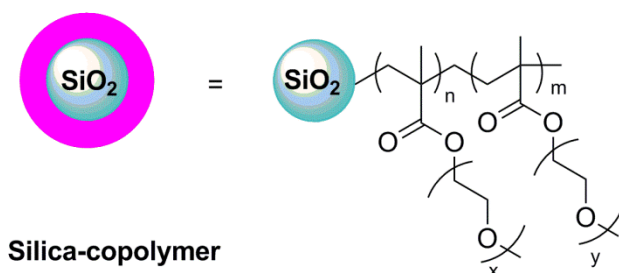
Figure 3-14   PEGMA copolymer coated silica nanoparticles

Surface-initiated ATRP of Silica-Copolymer-1 (Silica-poly(PEGMA-1100-*co*-PEGMA-232), 1:1). Two monomers for copolymerization, PEGMA-1100 and PEGMA-232, were dissolved separately in methanol and passed through an activated basic alumina to remove inhibitor. Copolymerization of PEGMA-1100 and PEGMA-232 at a 1:1 monomer ratio was carried out via surface-initiated ATRP. Initially, 1.1 g of poly(ethylene glycol) methyl ether methacrylate (M_n=1100, 1 mmol, PEGMA-1100), 0.232 g of tri(ethylene glycol) methyl ether methacrylate (1 mmol, PEGMA-232), 28 mg of 2, 2-bipyridine (bpy, 0.18 mmol), and 62 mg of initiator-modifies particles (ca. 0.042 mmol) were dissolved or dispersed in 1 mL of deionized water and 3 mL of methanol in a Schlenk flask. The mixture was ultrasonicated for 15-20 minutes. After 3 freeze-pump-thaw cycles the Schlenk flask was filled with N_2, and 8 mg of CuBr (0.06 mmol) was added to the solution, which became dark brown. After another freeze-pump-thaw cycle,

the reaction was allowed to proceed at room temperature for 12 hours. To quench the reaction, the Schlenk flask was exposed to air, and the solution turned blue. The mixture was transferred to a 50-mL centrifuge tube and washed with an EDTA•2Na saturated solution 3 times until no blue color was observed, deionized water 8-12 times, and acetone twice. In each step the polymer-grafted silica particle was recollected via centrifugation. The product was dried in vacuum at 60 °C overnight. After drying, TGA was performed to determine the extent of polymer grafting.

Surface-initiated ATRP of silica-copolymer-2 (silica-poly(PEGMA-1100-*co*-PEGMA-300), 1:1), silica-copolymer-3 (silica-poly(PEGMA-1100-*co*-PEGMA-475), 1:1), silica-copolymer-4 (silica-poly(PEGMA-300-*co*-PEGMA-475), 1:1), silica-copolymer-5 (silica-poly(PEGMA-1100-*co*-PEGMA-232), 3:7), silica-copolymer-6 (silica-poly(PEGMA-1100-*co*-PEGMA-300), 3:7), silica-copolymer-7 (silica-poly(PEGMA-1100-*co*-PEGMA-475), 3:7), silica-copolymer-8 (silica-poly(PEGMA-300-*co*-PEGMA-475), 3:7), silica-copolymer-9 (silica-poly(PEGMA-300-*co*-PEGMA-475), 7:3), silica-copolymer-10 (silica-poly(PEGMA-1100-*co*-PEGMA-300), 7:3) and silica-copolymer-11 (silica-poly(PEGMA-1100-*co*-PEGMA-475), 7:3) were conducted following the same protocol with the specified monomer ratios. In all cased the total amount of monomer in solution was 1 mmol. **Figure 3-7** and **Table 3-3** describe TGA profiles and weight loss.

3.4.6 ATRP of free poly(PEGMA) homopolymers and copolymers in solution
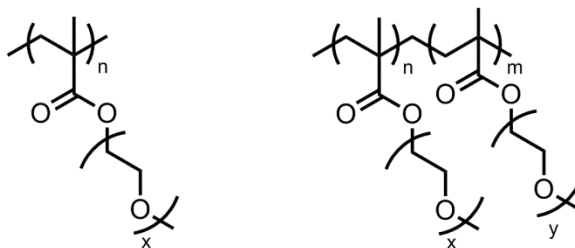
Figure 3-15 Free poly(PEGMA) homopolymers (left) and copolymers (right)

ATRP of free tri(ethylene glycol) methyl ether methacrylate (poly(PEGMA-232)) in solution. The monomer was dissolved in methanol and passed through an activated basic alumina column to remove inhibitor. After removing solvent, 1160 mg of tri(ethylene glycol) methyl ether methacrylate (5 mmol), 19.5 mg of ethyl 2-bromoisobutyrate (0.1 mmol, EBiB), and 62.5 mg of 2, 2-bipyridine (bpy, 0.4 mmol) were dissolved in 1 mL of deionized water and 3 mL of methanol in a Schlenk flask. The mixture was ultrasonicated for 15-20 minutes. After 3 freeze-pump-thaw cycles, the Schlenk flask was filled with nitrogen, 28.7 mg of CuBr (0.2 mmol) was added, and the solution immediately turned brown. After another freeze-pump-thaw cycle, the reaction was allowed to proceed at room temperature for 12 hours. To quench the reaction, the Schlenk flask was exposed to air, after which the solution turned blue. The mixture was diluted in deionized water and passed through an activated basic alumina column to remove copper catalyst. After removing solvent, the polymer was dried under vacuum ($\leqslant$ 10 mTorr) for 24 hours at 70 °C. Since no vinyl proton signal was observed in the ^{1}H NMR spectrum, indicating all monomers were consumed during polymerization, the

reaction conversion should be≥ 99%. The polymer (1.037 g, 89% yield) obtained was a colorless, highly viscous liquid.

ATRP of poly(PEGMA-188), poly(PEGMA-300), poly(PEGMA-475), and poly(PEGMA-1100) free polymers followed the same protocol using the same number of moles of monomer in each case.

ATRP of free copolymer-1 (poly(PEGMA-1100-*co*-PEGMA-232), 1:1), copolymer-2 (poly(PEGMA-1100-*co*-PEGMA-300), 1:1), copolymer-3 (poly(PEGMA-1100-*co*-PEGMA-475), 1:1), copolymer-4 (poly(PEGMA-300-*co*-PEGMA-475), 1:1), copolymer-5 (poly(PEGMA-1100-*co*-PEGMA-232), 3:7), copolymer-6 (poly(PEGMA-1100-*co*-PEGMA-300), 3:7), copolymer-7 (poly(PEGMA-1100-*co*-PEGMA-475), 3:7), copolymer-8 (poly(PEGMA-1100-*co*-PEGMA-475), 3:7), copolymer-9 (poly(PEGMA-300-*co*-PEGMA-475), 7:3), copolymer-10 (poly(PEGMA-1100-*co*-PEGMA-300), 7:3) and copolymer-11 poly(PEGMA-1100-*co*-PEGMA-475), 7:3) were conducted following the same protocol with different copolymerization ratio calculated. The total amount of monomer employed in all cases was 1 mmol.

3.4.7   Preparation of hybrid silica/polymer and free polymer electrolytes

Hybrid silica-poly(PEGMA) nanocomposite electrolyte preparation. Hybrid electrolytes were prepared by dissolving LiI and I_2 (10:1 mole ratio) in the host poly(ethylene glycol) dimethyl ether (PEGDME-500, M_n = 500) electrolyte, and then dispersing PEGMA/silica nanoparticles in this PEGDME. The mole ratio of PEGDME-500/LiI/I_2 was fixed at 100:10:1. Since the number of EO repeating units in PEGDME-500 is around 10, the EO to Li ratio is 100:1 in the PEGDME-500/LiI/I_2 mixture.

Specifically, 78 mg of I_2 (0.3 mmol) and 403.7 mg of LiI (3 mmol) were mixed into 15 g of PEGDME-500 (30 mmol) in a vial. The vial was sealed with parafilm, covered with aluminum foil, and the electrolyte was stirred overnight until the salt species dissolved. A clear, dark orange/brown liquid resulted. In this electrolyte, every 258 mg of liquid contained 5 mmol PEO (50 mmol EO), 0.5 mmol LiI, and 0.005 mmol I_2 (PEGDME-500/LiI/I_2 = 100/10/1). When dispersing nanoparticles in this electrolyte, to guarantee the same EO/Li ratio for all hybrid electrolytes, the mole ratio of PEGMA EO to the previously added lithium salt was fixed at 10:1 during each particle addition. Therefore, when including ethylene oxide units in both PEGDME-500 and silica-poly(PEGMA), the total EO/Li ratio was 110:1 for all hybrid electrolytes. The amount of poly(PEGMA)-coated silica to add to the electrolyte was calculated according to TGA data and molecular weight (for the copolymers, we assumed that the ratio of monomers incorporated into the polymer was the same as that in solution). Therefore, to make hybrid electrolyte, in every 258 mg of freshly prepared PEGDME-500/LiI/I_2 electrolyte, the following amount of hybrid particles were added (0.5 mmol EO from silica-poly(PEGMA) were added in all cases): 57.1 mg silica-poly(PEGMA-188), 43.1 mg silica-poly(PEGMA-232), 33.1 mg silica-poly(PEGMA-300), 29.4 mg silica-poly(PEGMA-475), 26.5 mg silica-poly(PEGMA-1100), 31.3 mg silica-poly(PEGMA-1100-*co*-PEGMA-232) (1:1), 28.6 mg silica-poly(PEGMA-1100-*co*-PEGMA-300) (1:1), 29.9 mg silica-poly(PEGMA-1100-*co*-PEGMA-475) (1:1), 31.4 mg silica-poly(PEGMA-300-*co*-PEGMA-475), 32.4 mg silica-poly(PEGMA-1100-*co*-PEGMA-232) (3:7), 29.1 mg silica-poly(PEGMA-1100-*co*-PEGMA-300) (3:7), 30.5 mg silica-poly(PEGMA-1100-*co*-PEGMA-475) (3:7), 30.3 mg silica-poly(PEGMA-300-*co*-PEGMA-475) (3:7),

31.5 mg silica-poly(PEGMA-300-*co*-PEGMA-475) (7:3), 27.2 mg silica-poly(PEGMA-1100-*co*-PEGMA-300) (7:3), 24.9 mg silica-poly(PEGMA-1100-*co*-PEGMA-475) (7:3). Electrolytes with silica-poly(PEGMA-1100), silica-poly(PEGMA-1100-*co*-PEGMA-300) (7:3) and silica-poly(PEGMA-1100-co-PEGMA-475) (7:3) were particularly viscous and solidified easily. A Wig-L-Bug was used to homogenize these particles in the PEGDME-500/LiI/I_2 electrolyte, while the other samples were stirred for 24 hours with a magnetic stirring bar in a parafilm-sealed, aluminum-covered vial. For a control experiment, a set of electrolytes containing PEGDME-500/LiI/I_2 with no particles but having the same EO/Li ratio was also prepared by adding 25 mg PEGDME-500 into 258 mg of previously prepared PEGDME-500/LiI/I_2 electrolyte.

Poly(PEGMA) free polymer electrolyte preparation. The mole ratio of PEGDME-500/LiI/I_2 was again fixed at 100:10:1, with EO:Li = 100:1 in the mixture. While dispersing free polymers into the system, the mole ratio of PEGMA EO to lithium salt was fixed at 10:1. Therefore, when including EO units in both PEGDME-500 and free poly(PEGMA), the total EO/Li ratio was fixed at 110:1 in all electrolytes. The amount of free poly(PEGMA) was calculated according to molecular weight. For every 258 mg of PEGDME-500/LiI/I_2 electrolyte, the following amounts of free polymers were added (0.5 mmol of EO in poly(PEGMA) in all cases): 38.8 mg poly(PEGMA-232), 29.9 mg poly(PEGMA-300), 26.5 mg poly(PEGMA-475), 23.9 mg poly(PEGMA-1100), 25.6 mg poly(PEGMA-1100-*co*-PEGMA-232) (1:1), 25.0 mg poly(PEGMA-1100-*co*-PEGMA-300) (1:1), 24.6 mg poly(PEGMA-1100-*co*-PEGMA-475) (1:1), 27.7 mg poly(PEGMA-300-*co*-PEGMA-475) (1:1), 27.4 mg poly(PEGMA-1100-*co*-PEGMA-232) (3:7), 26.0 mg poly(PEGMA-1100-*co*-PEGMA-300) (3:7), 25.1 mg poly(PEGMA-1100-

co-PEGMA-475) (3:7), 27.0 mg poly(PEGMA-300-*co*-PEGMA-475) (3:7), 28.4 mg poly(PEGMA-300-*co*-PEGMA-475) (7:3), 24.4 mg poly(PEGMA-1100-*co*-PEGMA-300) (7:3), or 24.3 mg poly(PEGMA-1100-*co*-PEGMA-475) (7:3). All these electrolytes were dark brown, viscous liquids.

3.4.8   Ionic conductivity measurements

Temperature-dependent ionic conductivity measurements were determined from electrical impedance analysis (EIS) using a homemade cell. The data were obtained with a Hewlett-Packard 4192A LF Impedance Analyzer over a frequency range of 5 Hz to 13 MHz with an applied oscillating voltage of 10 mV. The sample cell uses two steel disks as symmetrical electrodes separated by a 0.02 cm-thick sample in a Teflon collar. The sample radius is 0.6 cm. All electrolytes were pipetted into the cell, and impedance measurements were obtained at 5 ℃ intervals from 25 – 90 ℃. The sample was equilibrated at the pre-determined temperature for 15 minutes before each measurement. The resistance (*R*) can be obtained from a Nyquist plot (-imaginary impedance versue real impedance), where at the specific frequency the imaginary component of the complex impedance is zero (see more details in **Section 1.2.2.3** in Chapter 1). Ionic conductivity was calculated from **Equation 3-2**:

$$\sigma = 1/\rho = l/(R{\cdot}A)$$

where *l* (cm) refers to the measured distance and A (cm^2) is the cross-sectional area. To avoid moisture, all samples were dried under vacuum ($\leqslant$ 10 mTorr) at 70 °C for at least 48h. All conductivity measurements were conducted in the glove box.

4. Chapter 4   Summary and Future Work

4.1 Summary

The major objectives in this work have been to study the operational principals and limitations of solid-state polymer electrolytes for electrochemical devices, aiming to design novel polymer structures with optimized performance. Compared to liquid electrolytes, polymers exhibit high viscosity that serves low conductivity. However, the mobility of counterions ma be increased by lowering the polymer glass transition temperature (T_g), which enhances chain flexibility and raises polymer free volume.

In this dissertation, I synthesized and characterized two major types of low T_g polymers, followed by the preparation and analysis of their corresponding electrolytes.

Firstly, I employed polymer ionic liquids (PILs) with imidazolium-based cation sites and TFSI anions attached to flexible PEO tethering groups. To investigate how tethering groups affect electrochemical performance and physical properties of free ionic liquids (ILs) and PILs, a series of imidazolium-based IL model compounds and their corresponding PILs were first synthesized with various lengths of PEO attached on the imidazole. The thermophysical and electrochemical properties of the ionic liquids, including glass transition, melting, decomposition, viscosity, conductivity and rheological behavior were characterized. The solvent-free electrolytes present excellent conductivities that over 10^{-4} S/cm at room temperature. The characterization results also demonstrate that increasing the length of the PEO tethering group drastically alters the physical properties of PILs and enhances their conductivity. In addition, the ion transport mechanism is different with free IL small molecules and PILs. The charge carrier density is the dominant factor affecting conductivity in the former one and ion hopping follows

Arrhenius-type behavior, whereas ion mobility plays a more important role after polymerization and the ion conduction mechanism of PILs corresponds to the Vogel-Fulcher-Tammann (VFT) equation.

Secondly, I prepared a novel class of composite polymer electrolytes by first polymerizing poly(ethylene glycol) methyl ether methacrylate (PEGMA) from silica nanoparticles via surface-initiated atom transfer radical polymerization (ATRP), followed by blending hybrid nanoparticles with an optimized ratio of LiI/I_2 as potential candidates for electrolytes in dye-sensitized solar cells (DSSCs). Polymers were grafted from silica nanoparticles with controlled mass, architecture and functionality, which can create a network to prevent the viscous flow of low molecular weight PEO, thus, providing the required mechanical properties, while coordinating with lithium cations to maximize ionic conductivity. The inorganic nanoparticles led to electrolytes that macroscopically appear solid-state materials. To circumvent the problem of PEO crystallization, copolymerization of two PEGMA monomers was explored based on the idea that a short PEO side chain would interrupt the structure of the longer side chain. The hybrid electrolytes exhibit room temperature conductivity around 10^{-4} S/cm, making they suitable for practical application.

Both PILs and organic/inorganic nanocomposite solid-state polymer electrolytes present not only excellent thermal stability and high conductivity, but also a high viscosity amenable to encapsulation. Eventually, our ongoing research will focus on utilizing these novel electrolytes in energy devices.

4.2   Extensions and Future work

As shown in the previous chapters, introducing flexible tethering group with PILs is a successful method that leads to lower T_g and increase ionic conductivity. Based on this hypothesis, a new class of IL model compounds (**Scheme 4-1**) with PEO linkers between polymer backbone and imidazolium ring were synthesized, along with their corresponding PILs (**Scheme 4-2**).

1a, x = 3   **1b**, x = 3
2a, M = 400, x ≅ 9   **2b**, M = 400, x ≅ 9
3a, M = 600, x ≅ 14   **3b**, M = 600, x ≅ 14

1c, x = 3   **IL-3**, x = 3
2c, M = 400, x ≅ 9   **IL-9**, M = 400, x ≅ 9
3c, M = 600, x ≅ 14   **IL-14**, M = 600, x ≅ 14
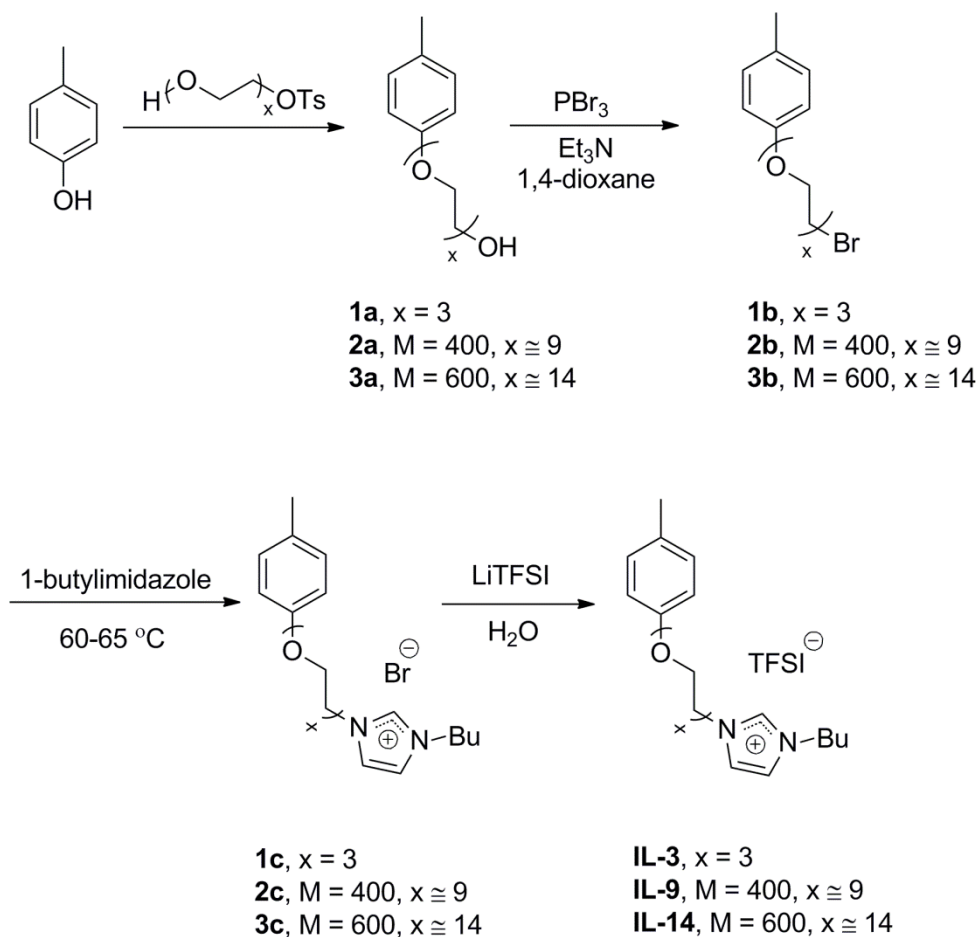
Scheme 4-1   Synthesis of a new class of imidazolium-based IL model compounds (M is the number average molecular weight of the PEO side chain given by the chemical manufactures; while x refers to a rough estimation of the number of PEO repeating units attached on the molecule.)

Table 4-1 DSC results of imidazolium based IL model compounds with chloride anion and TFSI anion

Compound	$T_g(°C)$	Compound	$T_g(°C)$
1c	-30.5	**IL-3**	-52.1
2c	-39.7	**IL-9**	-52.5
3c	-51.2	**IL-14**	-53.7
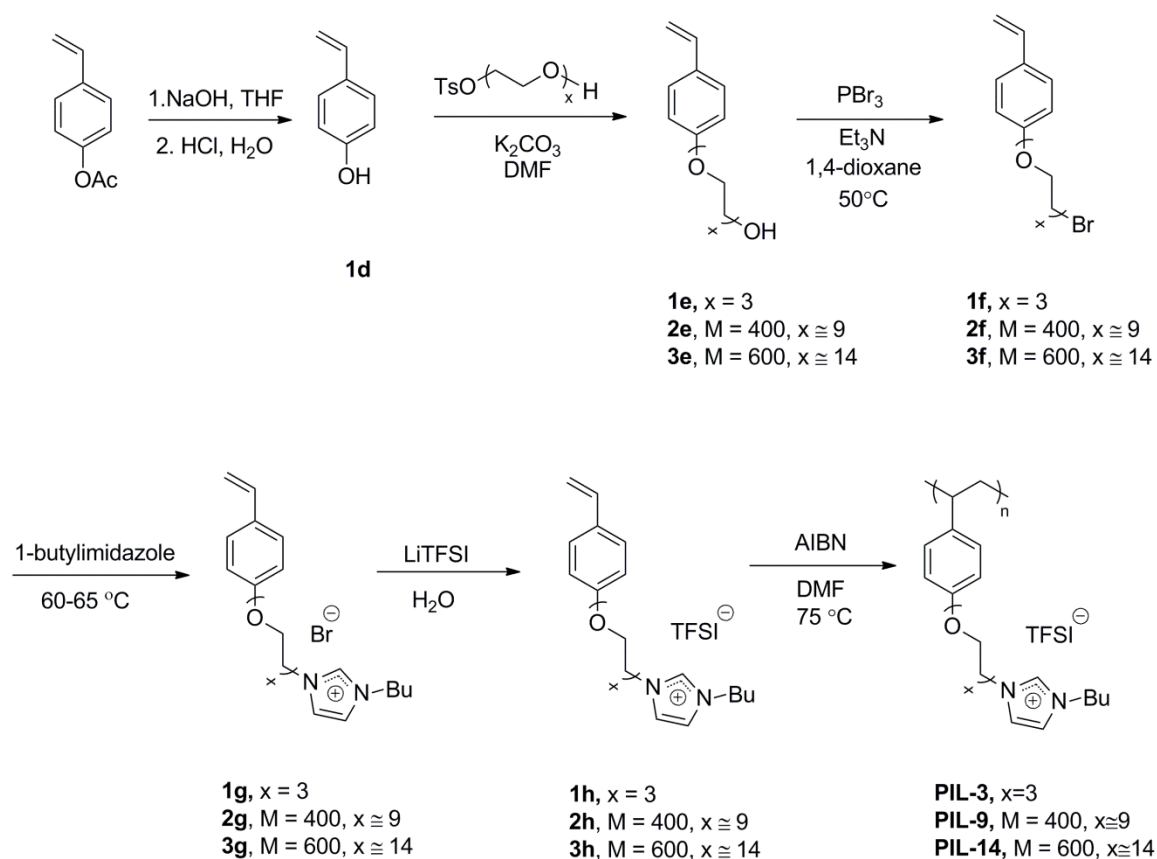
Scheme 4-2 Synthesis of a new class of imidazolium-based PILs

Table 4-1 shows the DSC results of ILs, presenting similar trend with ILs studied in Chapter 2. The value of T_g drops significantly as the length of PEO linker increases for compounds **1c – 3c**, and does not change too much with TFSI anion. This type of PILs was varied by altering the tethering group between the phenol and imidazolium rings, which may yield different results and optimized properties. In ongoing research in this project, DSC and impedance will be tested with the PILs to determine the optimized structure, and eventually test in DSSCs or LIBs.

REFERENCES

REFERENCES

(1)   Council, I. S. S.; United Nations Educational, S. C. O.: *World Social Science Report 2013 Changing Global Environments: Changing Global Environments*; OECD Publishing, 2013.

(2)   Snaith, H. J.; Schmidt-Mende, L. Advances in Liquid-Electrolyte and Solid-State Dye-Sensitized Solar Cells. *Advanced materials* **2007**, *19*, 3187-3200.

(3)   Aravindan, V.; Gnanaraj, J.; Madhavi, S.; Liu, H. K. Lithium-Ion Conducting Electrolyte Salts for Lithium Batteries. *Chemistry* **2011**, *17*, 14326-14346.

(4)   Linden, D.; Reddy, T. B.: *Handbook of Batteries*; McGraw-Hill, 2002.

(5)   Xu, K. Nonaqueous Liquid Electrolytes for Lithium-Based Rechargeable Batteries. *Chemical Reviews* **2004**, *104*, 4303-4418.

(6)   van Schalkwijk, W.; Scrosati, B.: *Advances in Lithium-Ion Batteries*; Springer, 2002.

(7)   Fry, A. J.: *Synthetic Organic Electrochemistry*; Wiley, 1989.

(8)   Scrosati, B. Recent Advances in Lithium Ion Battery Materials. *Electrochimica Acta* **2000**, *45*, 2461-2466.

(9)   Peled, E.; Golodnitsky, D.; Menachem, C.; Bar‑Tow, D. An Advanced Tool for the Selection of Electrolyte Components for Rechargeable Lithium Batteries. *Journal of The Electrochemical Society* **1998**, *145*, 3482-3486.

(10)   Yoshio, M.; Brodd, R. J.; Kozawa, A.: *Lithium-Ion Batteries: Science and Technologies*; Springer, 2010.

(11)   Ding, M. S.; Xu, K.; Jow, T. R. Liquid‑Solid Phase Diagrams of Binary Carbonates for Lithium Batteries. *Journal of The Electrochemical Society* **2000**, *147*, 1688-1694.

(12)   Wen, J. W.; Yu, Y.; Chen, C. H. A Review on Lithium-Ion Batteries Safety Issues: Existing Problems and Possible Solutions. *Mater. Express* **2012**, *2*, 197-212.

(13)   Blomgren, G. E. Electrolytes for Advanced Batteries. *Journal of Power Sources* **1999**, *81–82*, 112-118.

(14)   Campion, C. L.; Li, W.; Lucht, B. L. Thermal Decomposition of LiPF$_6$-Based Electrolytes for Lithium-Ion Batteries. *Journal of The Electrochemical Society* **2005**, *152*, A2327-A2334.

(15)   Agrawal, R. C.; Pandey, G. P. Solid Polymer Electrolytes: Materials Designing and All-Solid-State Battery Applications: An Overview. *Journal of Physics D: Applied Physics* **2008**, *41*, 223001.

(16)   Tarascon, J. M. Key Challenges in Future Li-Battery Research. *Philosophical transactions. Series A, Mathematical, physical, and engineering sciences* **2010**, *368*, 3227-3241.

(17)   Feldman, D. Polymer Electrolyte Reviews, J. R. MacCallum and C. A. Vincent, Eds., Elsevier Applied Science, New York, 1987, 351 pp. Price: $85.50. *Journal of Polymer Science Part C: Polymer Letters* **1988**, *26*, 371-372.

(18)   Wagner, A.; Kliem, H. Dispersive Ionic Space Charge Relaxation in Solid Polymer Electrolytes. II. Model and Simulation. *Journal of Applied Physics* **2002**, *91*, 6638.

(19)   MacCallum, J. R.; Vincent, C. A.: *Polymer Electrolyte Reviews*; Springer, 1989.

(20)   Quartarone, E.; Mustarelli, P.; Magistris, A. PEO-Based Composite Polymer Electrolytes. *Solid State Ionics* **1998**, *110*, 1-14.

(21)   Dias, F. B.; Plomp, L.; Veldhuis, J. B. J. Trends in Polymer Electrolytes for Secondary Lithium Batteries. *Journal of Power Sources* **2000**, *88*, 169-191.

(22)   Gombotz, W. R.: *Poly(ethylene Oxide) Surfaces: Synthesis, Characterization and Biological Interaction Studies*; University of Washington, 1988.

(23)   Armand, M. The History of Polymer Electrolytes. *Solid State Ionics* **1994**, *69*, 309-319.

(24)   Takahashi, Y.; Tadokoro, H. Structural Studies of Polyethers, (-(CH2)m-O-)n. X. Crystal Structure of Poly(ethylene oxide). *Macromolecules* **1973**, *6*, 672-675.

(25)   Takahashi, Y.; Sato, T.; Tadokoro, H.; Tanaka, Y. Crystal Structure of α-Gutta Percha: Modification of the Constrained Least-Squares Method. *Journal of Polymer Science: Polymer Physics Edition* **1973**, *11*, 233-248.

(26)   Chen, Y.; Baker, G. L.; Ding, Y.; Rabolt, J. F. Self-Assembly through Stepwise Crystalliztion. *Journal of the American Chemical Society* **1999**, *121*, 6962-6963.

(27)   Fenton, D. E.; Parker, J. M.; Wright, P. V. Complexes of Alkali Metal Ions with Poly(Ethylene Oxide). *Polymer* **1973**, *14*, 589.

(28)   Wright, P. V. Electrical Conductivity in Ionic Complexes of Poly(Ethylene Oxide). *British Polymer Journal* **1975**, *7*, 319-327.

(29)   Dickinson, T.: *Second International Meeting on Solid Electrolytes: St. Andrews, Scotland, September, 20-22, 1978*, 1978.

(30)   Vashishta, P.; Mundy, J. N.; Shenoy, G. K.: *Fast Ion Transport in Solids: Electrodes, and Electrolytes : Proceedings of the International Conference on Fast Ion Transport in Solids, Electrodes, and Electrolytes, Lake Geneva, Wisconsin, U.S.A., May 21-25, 1979*; North Holland, 1979.

(31)   Scrosati, B.; Siena, U. d.: *Second International Symposium on Polymer Electrolytes*; Elsevier Applied Science, 1990.

(32)   Gray, F. M.: *Solid Polymer Electrolytes: Fundamentals and Technological Applications*; Wiley, 1991.

(33)   Nei de Freitas, J.; Nogueira, A. F.; De Paoli, M.-A. New Insights into Dye-sensitized Solar Cells with Polymer Electrolytes. *Journal of Materials Chemistry* **2009**, *19*, 5279.

(34)   Lightfoot, P.; Mehta, M. A.; Bruce, P. G. Crystal Structure of the Polymer Electrolyte Poly(Ethylene Oxide)$_3$:LiCF$_3$SO$_3$. *Science* **1993**, *262*, 883-885.

(35)   Ratner, M. A.; Shriver, D. F. Ion Transport in Solvent-Free Polymers. *Chemical Reviews* **1988**, *88*, 109-124.

(36)   Müller‑Plathe, F.; van Gunsteren, W. F. Computer Simulation of a Polymer Electrolyte: Lithium Iodide in Amorphous Poly(Ethylene Oxide). *The Journal of Chemical Physics* **1995**, *103*, 4745-4756.

(37)   Nogueira, A. F.; Longo, C.; De Paoli, M. A. Polymers in Dye Sensitized Solar Cells: Overview and Perspectives. *Coordination Chemistry Reviews* **2004**, *248*, 1455-1468.

(38)   Berthier, C.; Gorecki, W.; Minier, M.; Armand, M. B.; Chabagno, J. M.; Rigaud, P. Microscopic Investigation of Ionic Conductivity in Alkali Metal Salts-Poly(Ethylene Oxide) Adducts. *Solid State Ionics* **1983**, *11*, 91-95.

(39)   Maccallum, J. R.; Smith, M. J.; Vincent, C. A. The Effects of Radiation-Induced Crosslinking on the Conductance of LiClO$_4$·PEO Electrolytes. *Solid State Ionics* **1984**, *11*, 307-312.

(40)   Chiodelli, G.; Ferloni, P.; Magistris, A.; Sanesi, M. Ionic Conduction and Thermal Properties of Poly(Ethylene Oxide)-Lithium Tetrafluoroborate Films. *Solid State Ionics* **1988**, *28–30, Part 2*, 1009-1013.

(41)   Maurya, K. K.; Srivastava, N.; Hashmi, S. A.; Chandra, S. Proton Conducting Polymer Electrolyte: II Poly Ethylene Oxide + NH$_4$l System. *J Mater Sci* **1992**, *27*, 6357-6364.

(42)   Quartarone, E.; Mustarelli, P. Electrolytes for Solid-State Lithium Rechargeable Batteries: Recent Advances and Perspectives. *Chemical Society reviews* **2011**, *40*, 2525-2540.

(43)   Capiglia, C.; Saito, Y.; Yamamoto, H.; Kageyama, H.; Mustarelli, P. Transport Properties and Microstructure of Gel Polymer Electrolytes. *Electrochimica Acta* **2000**, *45*, 1341-1345.

(44)   Noda, A.; Hayamizu, K.; Watanabe, M. Pulsed-Gradient Spin−Echo 1H and 19F NMR Ionic Diffusion Coefficient, Viscosity, and Ionic Conductivity of Non-Chloroaluminate Room-Temperature Ionic Liquids. *The Journal of Physical Chemistry B* **2001**, *105*, 4603-4610.

(45)   Wieczorek, W.; Florjanczyk, Z.; Stevens, J. R. Composite Polyether Based Solid Electrolytes. *Electrochimica Acta* **1995**, *40*, 2251-2258.

(46)   Feuillade, G.; Perche, P. Ion-Conductive Macromolecular Gels and Membranes for Solid Lithium Cells. *J Appl Electrochem* **1975**, *5*, 63-69.

(47)   Chintapalli, S.; Frech, R. Effect of Plasticizers on High Molecular Weight PEO-LiCF$_3$SO$_3$ Complexes. *Solid State Ionics* **1996**, *86–88, Part 1*, 341-346.

(48)   Tsuchida, E.; Ohno, H.; Tsunemi, K. Conduction of Lithium Ions in Polyvinylidene Fluoride and Its Derivatives—I. *Electrochimica Acta* **1983**, *28*, 591-595.

(49)   Watanabe, M.; Kanba, M.; Nagaoka, K.; Shinohara, I. Ionic Conductivity of Hybrid Films Based on Polyacrylonitrile and their Battery Application. *Journal of Applied Polymer Science* **1982**, *27*, 4191-4198.

(50)   Alamgir, M.; Abraham, K. M. Li Ion Conductive Electrolytes Based on Poly(vinyl chloride). *Journal of The Electrochemical Society* **1993**, *140*, L96-L97.

(51)   Choe, H. S.; Giaccai, J.; Alamgir, M.; Abraham, K. M. Preparation and Characterization of Poly(vinyl sulfone)- and Poly(vinylidene fluoride)-Based Electrolytes. *Electrochimica Acta* **1995**, *40*, 2289-2293.

(52)   Appetecchi, G. B.; Croce, F.; Scrosati, B. Kinetics and Stability of the Lithium Electrode in Poly(methylmethacrylate)-Based gel Gel Ectrolytes. *Electrochimica Acta* **1995**, *40*, 991-997.

(53)   Xue, Z.-M.; Zhou, W.; Ding, J.; Chen, C.-H. Electronic Structures and Molecular Properties of FLBDOB and its Derivatives: A Combined Experimental and Theoretical Study. *Electrochimica Acta* **2010**, *55*, 5342-5348.

(54)   Tarascon, J. M.; Gozdz, A. S.; Schmutz, C.; Shokoohi, F.; Warren, P. C. Performance of Bellcore's Plastic Rechargeable Li-ion Batteries. *Solid State Ionics* **1996**, *86–88, Part 1*, 49-54.

(55)   Croce, F.; Appetecchi, G. B.; Persi, L.; Scrosati, B. Nanocomposite Polymer Electrolytes for Lithium Batteries. *Nature* **1998**, *394*, 456-458.

(56)   Croce, F.; Curini, R.; Martinelli, A.; Persi, L.; Ronci, F.; Scrosati, B.; Caminiti, R. Physical and Chemical Properties of Nanocomposite Polymer Electrolytes. *The Journal of Physical Chemistry B* **1999**, *103*, 10632-10638.

(57)   Croce, F.; Settimi, L.; Scrosati, B. Superacid ZrO_2-added, Composite Polymer Electrolytes with Improved Transport Properties. *Electrochemistry Communications* **2006**, *8*, 364-368.

(58)   Weston, J. E.; Steele, B. C. H. Effects of Inert Fillers on the Mechanical and Electrochemical Properties of Lithium Salt-Poly(ethylene oxide) Polymer Electrolytes. *Solid State Ionics* **1982**, *7*, 75-79.

(59)   Croce, F.; Scrosati, B. Interfacial phenomena in polymer-electrolyte cells: lithium passivation and cycleability. *Journal of Power Sources* **1993**, *43*, 9-19.

(60)   Peled, E.; Golodnitsky, D.; Ardel, G.; Eshkenazy, V. The Sei Model— Application to Lithium-Polymer Electrolyte Batteries. *Electrochimica Acta* **1995**, *40*, 2197-2204.

(61)   Krawiec, W.; Scanlon Jr, L. G.; Fellner, J. P.; Vaia, R. A.; Vasudevan, S.; Giannelis, E. P. Polymer Nanocomposites: A New Strategy for Synthesizing Solid Electrolytes for Rechargeable Lithium Batteries. *Journal of Power Sources* **1995**, *54*, 310-315.

(62)   Khan, S. A.; Baker, G. L.; Colson, S. Composite Polymer Electrolytes Using Fumed Silica Fillers: Rheology and Ionic Conductivity. *Chemistry of Materials* **1994**, *6*, 2359-2363.

(63)   Fan, J.; Raghavan, S. R.; Yu, X.-Y.; Khan, S. A.; Fedkiw, P. S.; Hou, J.; Baker, G. L. Composite Polymer Electrolytes Using Surface-Modified Fumed Silicas: Conductivity and Rheology. *Solid State Ionics* **1998**, *111*, 117-123.

(64)   Raghavan, S. R.; Hou, J.; Baker, G. L.; Khan, S. A. Colloidal Interactions between Particles with Tethered Nonpolar Chains Dispersed in Polar Media: Direct Correlation between Dynamic Rheology and Interaction Parameters. *Langmuir* **1999**, *16*, 1066-1077.

(65)   Walls, H. J.; Zhou, J.; Yerian, J. A.; Fedkiw, P. S.; Khan, S. A.; Stowe, M. K.; Baker, G. L. Fumed Silica-Based Composite Polymer Electrolytes: Synthesis, Rheology, and Electrochemistry. *Journal of Power Sources* **2000**, *89*, 156-162.

(66)   Hu, H.; Yuan, W.; Zhao, H.; Baker, G. L. A Novel Polymer Gel Electrolyte: Direct Polymerization of Ionic Liquid from Surface of Silica Nanoparticles. *Journal of Polymer Science Part A: Polymer Chemistry* **2014**, *52*, 121-127.

(67)   Yuan, W.; Zhao, H.; Hu, H.; Wang, S.; Baker, G. L. Synthesis and Characterization of the Hole-Conducting Silica/Polymer Nanocomposites and Application in Solid-State Dye-Sensitized Solar Cell. *ACS Applied Materials & Interfaces* **2013**, *5*, 4155-4161.

(68)   Janna, K. M.: Polyelectrolytes for Batteries: Current State of Understanding. In *Polymers for Energy Storage and Delivery: Polyelectrolytes for Batteries and Fuel Cells*; ACS Symposium Series 1096; American Chemical Society, 2012; Vol. 1096; pp 1-17.

(69)   Kerr, J. B.: *Grafted Polyelectrolyte Membranes for Lithium Batteries and Fuel Cells*, 2003.

(70)   Bannister, D. J.; Davies, G. R.; Ward, I. M.; McIntyre, J. E. Ionic Conductivities for Poly(Ethylene Oxide) Complexes with Lithium Salts of Monobasic and Dibasic Acids and Blends of Poly(Ethylene Oxide) with Lithium Salts of Anionic Polymers. *Polymer* **1984**, *25*, 1291-1296.

(71)   Hardy, L. C.; Shriver, D. F. Preparation and Electrical Response of Solid Polymer Electrolytes with Only One Mobile Species. *Journal of the American Chemical Society* **1985**, *107*, 3823-3828.

(72)   Tsuchida, E.; Ohno, H.; Kobayashi, N. Single-Ion Conduction in Poly[(oligo(oxyethylene)methacrylate)-co-(alkali-metal methacrylates)]. *Macromolecules* **1988**, *21*, 96-100.

(73)   Doyle, M.; Fuller, T. F.; Newman, J. The Importance of the Lithium Ion Transference Number in Lithium/Polymer Cells. *Electrochimica Acta* **1994**, *39*, 2073-2081.

(74)   Asfour, F. H. Molecular Reinforced Polymers And Self Assembled Nanocomposites for Secondary Lithium Batteries. Michigan State University, 2003.

(75)   Ohno, H. Molten Salt Type Polymer Electrolytes. *Electrochimica Acta* **2001**, *46*, 1407-1411.

(76)   Armand, M.; Endres, F.; MacFarlane, D. R.; Ohno, H.; Scrosati, B. Ionic-Liquid Materials for the Electrochemical Challenges of the Future. *Nat Mater* **2009**, *8*, 621-629.

(77)   Green, M. D.; Long, T. E. Designing Imidazole-Based Ionic Liquids and Ionic Liquid Monomers for Emerging Technologies. *Polymer Reviews* **2009**, *49*, 291-314.

(78)   Zakeeruddin, S. M.; Grätzel, M. Solvent-Free Ionic Liquid Electrolytes for Mesoscopic Dye-Sensitized Solar Cells. *Advanced Functional Materials* **2009**, *19*, 2187-2202.

(79)   Hallett, J. P.; Welton, T. Room-Temperature Ionic Liquids: Solvents for Synthesis and Catalysis. 2. *Chemical Reviews* **2011**, *111*, 3508-3576.

(80)   Olivier-Bourbigou, H.; Magna, L.; Morvan, D. Ionic Liquids and Catalysis: Recent Progress from Knowledge to Applications. *Applied Catalysis A: General* **2010**, *373*, 1-56.

(81)   Ho, T. D.; Zhang, C.; Hantao, L. W.; Anderson, J. L. Ionic Liquids in Analytical Chemistry: Fundamentals, Advances, and Perspectives. *Analytical Chemistry* **2013**, *86*, 262-285.

(82)   Dupont, J.; Scholten, J. D. On the Structural and Surface Properties of Transition-Metal Nanoparticles in Ionic Liquids. *Chemical Society reviews* **2010**, *39*, 1780-1804.

(83)   Roosen, C.; Müller, P.; Greiner, L. Ionic Liquids in Biotechnology: Applications and Perspectives for Biotransformations. *Applied Microbiology and Biotechnology* **2008**, *81*, 607-614.

(84)   MacFarlane, D. R.; Tachikawa, N.; Forsyth, M.; Pringle, J. M.; Howlett, P. C.; Elliott, G. D.; Davis, J. H.; Watanabe, M.; Simon, P.; Angell, C. A. Energy Applications of Ionic Liquids. *Energy & Environmental Science* **2014**, *7*, 232-250.

(85)   1.4.1   Synthesis of PILsWalden, P. Molecular Weights and Electrical Conductivity of Several Fused Salts. *Bull. Acad. Imper. Sci.(St.-Petersbourg)* **1914**, *8*, 405-422.

(86)   Tokuda, H.; Tsuzuki, S.; Susan, M. A. B. H.; Hayamizu, K.; Watanabe, M. How Ionic Are Room-Temperature Ionic Liquids? An Indicator of the Physicochemical Properties. *The Journal of Physical Chemistry B* **2006**, *110*, 19593-19600.

(87)   Graenacher, C.: Cellulose Solution. Google Patents, 1934.

(88)   Chum, H. L.; Koch, V. R.; Miller, L. L.; Osteryoung, R. A. Electrochemical Scrutiny of Organometallic Iron Complexes and Hexamethylbenzene in a Room Temperature Molten Salt. *Journal of the American Chemical Society* **1975**, *97*, 3264-3265.

(89)   Wilkes, J. S.; Hussey, C. L.: *Selection of Cations for Ambient Temperature Chloroaluminate Molten Salts Using MNDO Molecular Orbital Calculations*; Directorate of Chemical Sciences, Frank J. Seiler Research Laboratory, Air Force Systems Command, 1982.

(90)   Plechkova, N. V.; Seddon, K. R. Applications of Ionic Liquids in the Chemical Industry. *Chemical Society reviews* **2008**, *37*, 123-150.

(91)   Wilkes, J. S.; Zaworotko, M. J. Air and Water Stable 1-Ethyl-3-Methylimidazolium Based Ionic Liquids. *Journal of the Chemical Society, Chemical Communications* **1992**, 965-967.

(92)   Bonhôte, P.; Dias, A.-P.; Papageorgiou, N.; Kalyanasundaram, K.; Grätzel, M. Hydrophobic, Highly Conductive Ambient-Temperature Molten Salts†. *Inorganic Chemistry* **1996**, *35*, 1168-1178.

(93)   Kapustinskii, A. F. Lattice Energy of Ionic Crystals. *Quarterly Reviews, Chemical Society* **1956**, *10*, 283-294.

(94)   Abdul-Sada, A. a. K.; Greenway, A. M.; Hitchcock, P. B.; Mohammed, T. J.; Seddon, K. R.; Zora, J. A. Upon the Structure of Room Temperature Halogenoaluminate Ionic Liquids. *Journal of the Chemical Society, Chemical Communications* **1986**, 1753-1754.

(95)   Hapiot, P.; Lagrost, C. Electrochemical Reactivity in Room-Temperature Ionic Liquids. *Chemical Reviews* **2008**, *108*, 2238-2264.

(96)   Ohno, H.: *Electrochemical Aspects of Ionic Liquids*; Wiley, 2011.

(97)   Le Bideau, J.; Viau, L.; Vioux, A. Ionogels, Ionic Liquid Based Hybrid Materials. *Chemical Society reviews* **2011**, *40*, 907-925.

(98)   Wilkes, J. S. A Short History of Ionic Liquids-from Molten Salts to Neoteric Solvents. *Green Chemistry* **2002**, *4*, 73-80.

(99)   Lu, W.; Fadeev, A. G.; Qi, B.; Smela, E.; Mattes, B. R.; Ding, J.; Spinks, G. M.; Mazurkiewicz, J.; Zhou, D.; Wallace, G. G.; MacFarlane, D. R.; Forsyth, S. A.; Forsyth, M. Use of Ionic Liquids for π-Conjugated Polymer Electrochemical Devices. *Science* **2002**, *297*, 983-987.

(100)   Marom, R.; Amalraj, S. F.; Leifer, N.; Jacob, D.; Aurbach, D. A Review of Advanced and Practical Lithium Battery Materials. *Journal of Materials Chemistry* **2011**, *21*, 9938.

(101)   Lewandowski, A.; Świderska-Mocek, A. Ionic Liquids as Electrolytes for Li-ion Batteries—An Overview of Electrochemical Studies. *Journal of Power Sources* **2009**, *194*, 601-609.

(102)   Borgel, V.; Markevich, E.; Aurbach, D.; Semrau, G.; Schmidt, M. On the Application of Ionic Liquids for Rechargeable Li Batteries: High Voltage Systems. *Journal of Power Sources* **2009**, *189*, 331-336.

(103)   Foropoulos, J.; DesMarteau, D. D. Synthesis, Properties, and Reactions of Bis((trifluoromethyl)sulfonyl) Imide, $(CF_3SO_2)_2NH$. *Inorganic Chemistry* **1984**, *23*, 3720-3723.

(104)   PÉTer, L.; Arai, J. Anodic Dissolution of Aluminium in Organic Electrolytes Containing Perfluoroalkylsulfonyl Imides. *Journal of Applied Electrochemistry* **1999**, *29*, 1053-1061.

(105)   Earle, M. J.; Esperanca, J.; Gilea, M. A.; Lopes, J. N. C.; Rebelo, L. P. N.; Magee, J. W.; Seddon, K. R.; Widegren, J. A. The Distillation and Volatility of Ionic Liquids. *Nature* **2006**, *439*, 831-834.

(106)   Benrabah, D.; Baril, D.; Sanchez, J.-Y.; Armand, M.; Gard, G. G. Comparative Electrochemical Study of New Poly(oxyethylene)-Li Salt Complexes. *Journal of the Chemical Society, Faraday Transactions* **1993**, *89*, 355-359.

(107)   Mecerreyes, D. Polymeric Ionic Liquids: Broadening the Properties and Applications of Polyelectrolytes. *Progress in Polymer Science* **2011**, *36*, 1629-1648.

(108)   Matsumoto, H.; Sakaebe, H.; Tatsumi, K. Preparation of Room Temperature Ionic Liquids Based on Aliphatic Onium Cations and Asymmetric Amide Anions and Their Electrochemical Properties as a Lithium Battery Electrolyte. *Journal of Power Sources* **2005**, *146*, 45-50.

(109)   Susan, M. A. B. H.; Kaneko, T.; Noda, A.; Watanabe, M. Ion Gels Prepared by in Situ Radical Polymerization of Vinyl Monomers in an Ionic Liquid and Their Characterization as Polymer Electrolytes. *Journal of the American Chemical Society* **2005**, *127*, 4976-4983.

(110)   Bruce, P. G.; Scrosati, B.; Tarascon, J.-M. Nanomaterials for Rechargeable Lithium Batteries. *Angewandte Chemie International Edition* **2008**, *47*, 2930-2946.

(111)   Marcilla, R.; Blazquez, J. A.; Fernandez, R.; Grande, H.; Pomposo, J. A.; Mecerreyes, D. Synthesis of Novel Polycations Using the Chemistry of Ionic Liquids. *Macromolecular Chemistry and Physics* **2005**, *206*, 299-304.

(112)   Kadokawa, J.-i.; Murakami, M.-a.; Kaneko, Y. A Facile Method for Preparation of Composites Composed of Cellulose and a Polystyrene-type Polymeric Ionic Liquid Using a Polymerizable Ionic Liquid. *Composites Science and Technology* **2008**, *68*, 493-498.

(113)   Sato, T.; Marukane, S.; Narutomi, T.; Akao, T. High Rate Performance of a Lithium Polymer Battery Using a Novel Lonic Liquid Polymer Composite. *Journal of Power Sources* **2007**, *164*, 390-396.

(114)   Mineo, P. G.; Livoti, L.; Giannetto, M.; Gulino, A.; Lo Schiavo, S.; Cardiano, P. Very Fast CO_2 Response and Hydrophobic Properties of Novel Poly(ionic liquid)s. *Journal of Materials Chemistry* **2009**, *19*, 8861-8870.

(115)   Hirao, M.; Ito, K.; Ohno, H. Preparation and Polymerization of New Organic Molten Salts; N-alkylimidazolium Salt Derivatives. *Electrochimica Acta* **2000**, *45*, 1291-1294.

(116)   Tang, J.; Tang, H.; Sun, W.; Radosz, M.; Shen, Y. Low-pressure CO_2 Sorption in Ammonium-based Poly(ionic liquid)s. *Polymer* **2005**, *46*, 12460-12467.

(117)   Supasitmongkol, S.; Styring, P. High CO_2 Solubility in Ionic Liquids and a Tetraalkylammonium-based Poly(ionic liquid). *Energy & Environmental Science* **2010**, *3*, 1961-1972.

(118)   Watanabe, M.; Yamada, S.-i.; Ogata, N. Ionic Conductivity of Polymer Electrolytes Containing Room Temperature Molten Salts based on Pyridinium Halide and Aluminium Chloride. *Electrochimica Acta* **1995**, *40*, 2285-2288.

(119)   Xiao, S.; Lu, X.; Lu, Q. Photosensitive Polymer from Ionic Self-Assembly of Azobenzene Dye and Poly(ionic liquid) and Its Alignment Characteristic toward Liquid Crystal Molecules. *Macromolecules* **2007**, *40*, 7944-7950.

(120)   Ogihara, W.; Washiro, S.; Nakajima, H.; Ohno, H. Effect of Cation Structue on the Electrochemical and Thermal Properties of Ion Conductive Polymers Obtained from Polymerizable Ionic Liquids. *Electrochimica Acta* **2006**, *51*, 2614-2619.

(121)   Pont, A.-L.; Marcilla, R.; De Meatza, I.; Grande, H.; Mecerreyes, D. Pyrrolidinium-based Polymeric Ionic Liquids as Mechanically and Electrochemically Stable Polymer Electrolytes. *Journal of Power Sources* **2009**, *188*, 558-563.

(122)   Appetecchi, G. B.; Kim, G. T.; Montanino, M.; Carewska, M.; Marcilla, R.; Mecerreyes, D.; De Meatza, I. Ternary Polymer Electrolytes Containing

Pyrrolidinium-based Polymeric Ionic Liquids for Lithium Batteries. *Journal of Power Sources* **2010**, *195*, 3668-3675.

(123) Wang, J.; Li, S.; Zhang, S. Novel Hydroxide-Conducting Polyelectrolyte Composed of an Poly(arylene ether sulfone) Containing Pendant Quaternary Guanidinium Groups for Alkaline Fuel Cell Applications. *Macromolecules* **2010**, *43*, 3890-3896.

(124) Fredlake, C. P.; Crosthwaite, J. M.; Hert, D. G.; Aki, S.; Brennecke, J. F. Thermophysical Properties of Imidazolium-based Ionic Liquids. *J. Chem. Eng. Data* **2004**, *49*, 954-964.

(125) Huddleston, J. G.; Visser, A. E.; Reichert, W. M.; Willauer, H. D.; Broker, G. A.; Rogers, R. D. Characterization and Comparison of Hydrophilic and Hydrophobic Room Temperature Ionic Liquids Incorporating the Imidazolium Cation. *Green Chemistry* **2001**, *3*, 156-164.

(126) Ohno, H.; Ito, K. Room-Temperature Molten Salt Polymers as a Matrix for Fast Ion Conduction. *Chemistry Letters* **1998**, *27*, 751-752.

(127) Yoshizawa, M.; Ohno, H. Synthesis of Molten Salt-type Polymer Brush and Effect of Brush Structure on the Ionic Conductivity. *Electrochimica Acta* **2001**, *46*, 1723-1728.

(128) Ohno, H.; Yoshizawa, M.; Ogihara, W. Development of New Class of Ion Conductive Polymers Based on Ionic Liquids. *Electrochimica Acta* **2004**, *50*, 255-261.

(129) Yoshizawa, M.; Hirao, M.; Ito-Akita, K.; Ohno, H. Ion Conduction in Zwitterionic-type Molten Salts and Their Polymers. *Journal of Materials Chemistry* **2001**, *11*, 1057-1062.

(130) Yoshizawa, M.; Ohno, H. Molecular Brush Having Molten Salt Domain for Fast Ion Conduction. *Chemistry Letters* **1999**, *28*, 889-890.

(131) Yoshizawa, M.; Ogihara, W.; Ohno, H. Novel Polymer Electrolytes Prepared by Copolymerization of Ionic Liquid Monomers. *Polymers for Advanced Technologies* **2002**, *13*, 589-594.

(132) Tang, H.; Tang, J.; Ding, S.; Radosz, M.; Shen, Y. Atom Transfer Radical Polymerization of Styrenic Ionic Liquid Monomers and Carbon Dioxide Absorption of the Polymerized Ionic Liquids. *Journal of Polymer Science Part A: Polymer Chemistry* **2005**, *43*, 1432-1443.

(133) Vijayakrishna, K.; Jewrajka, S. K.; Ruiz, A.; Marcilla, R.; Pomposo, J. A.; Mecerreyes, D.; Taton, D.; Gnanou, Y. Synthesis by RAFT and Ionic Responsiveness of

Double Hydrophilic Block Copolymers Based on Ionic Liquid Monomer Units. *Macromolecules* **2008**, *41*, 6299-6308.

(134)   Yuan, J.; Schlaad, H.; Giordano, C.; Antonietti, M. Double Hydrophilic Diblock Copolymers Containing a Poly(ionic liquid) Segment: Controlled Synthesis, Solution Property, and Application as Carbon Precursor. *European Polymer Journal* **2011**, *47*, 772-781.

(135)   Yang, J.; Sun, W.; Lin, W.; Shen, Z. Synthesis and Magnetic Properties of Comb-Like Copolymeric Complexes Based on Thiazole Ring and Ionic Liquid. *Journal of Polymer Science Part A: Polymer Chemistry* **2008**, *46*, 5123-5132.

(136)   Stathatos, E.; Jovanovski, V.; Orel, B.; Jerman, I.; Lianos, P. Dye-Sensitized Solar Cells Made by Using a Polysilsesquioxane Polymeric Ionic Fluid as Redox Electrolyte. *The Journal of Physical Chemistry C* **2007**, *111*, 6528-6532.

(137)   Vygodskii, Y. S.; Shaplov, A. S.; Lozinskaya, E. I.; Lyssenko, K. A.; Golovanov, D. G.; Malyshkina, I. A.; Gavrilova, N. D.; Buchmeiser, M. R. Conductive Polymer Electrolytes Derived from Poly(norbornene)s with Pendant Ionic Imidazolium Moieties. *Macromolecular Chemistry and Physics* **2008**, *209*, 40-51.

(138)   Burns, C. T.; Lee, S.; Seifert, S.; Firestone, M. A. Thiophene-based Ionic Liquids: Synthesis, Physical Properties, Self-Assembly, and Oxidative Polymerization. *Polymers for Advanced Technologies* **2008**, *19*, 1369-1382.

(139)   Lee, S.; Becht, G. A.; Lee, B.; Burns, C. T.; Firestone, M. A. Electropolymerization of a Bifunctional Ionic Liquid Monomer Yields an Electroactive Liquid-Crystalline Polymer. *Advanced Functional Materials* **2010**, *20*, 2063-2070.

(140)   Lu, J.; Yan, F.; Texter, J. Advanced Applications of Ionic Liquids in Polymer Science. *Progress in Polymer Science* **2009**, *34*, 431-448.

(141)   Ricks-Laskoski, H. L.; Snow, A. W. Synthesis and Electric Field Actuation of an Ionic Liquid Polymer. *Journal of the American Chemical Society* **2006**, *128*, 12402-12403.

(142)   Washiro, S.; Yoshizawa, M.; Nakajima, H.; Ohno, H. Highly Ion Conductive Flexible Films Composed of Network Polymers Based on Polymerizable Ionic Liquids. *Polymer* **2004**, *45*, 1577-1582.

(143)   Juger, J.; Meyer, F.; Vidal, F.; Chevrot, C.; Teyssié, D. Synthesis, Polymerization and Conducting Properties of an Ionic Liquid-type Anionic Monomer. *Tetrahedron Letters* **2009**, *50*, 128-131.

(144)   Ohno, H.; Yoshizawa, M.: Preparation and Properties of Polymerized Ionic Liquids as Film Electrolytes. In *Ionic Liquids IIIB: Fundamentals, Progress,*

Challenges, and Opportunities; ACS Symposium Series 902; American Chemical Society, 2005; Vol. 902; pp 159-170.

(145) Ito, K.; Nishina, N.; Ohno, H. Enhanced Ion Conduction in Imidazolium-type Molten Salts. *Electrochimica Acta* **2000**, *45*, 1295-1298.

(146) Li, M.; Yang, L.; Fang, S.; Dong, S. Novel Polymeric Ionic Liquid Membranes as Solid Polymer Electrolytes with High Ionic Conductivity at Moderate Temperature. *Journal of Membrane Science* **2011**, *366*, 245-250.

(147) G. Huddleston, J.; D. Rogers, R. Room Temperature Ionic Liquids as Novel Media for 'Clean' Liquid-Liquid Extraction. *Chemical Communications* **1998**, 1765-1766.

(148) Visser, A. E.; Swatloski, R. P.; Reichert, W. M.; Griffin, S. T.; Rogers, R. D. Traditional Extractants in Nontraditional SolventsGroups 1 and 2 Extraction by Crown Ethers in Room-Temperature Ionic Liquids†. *Industrial & Engineering Chemistry Research* **2000**, *39*, 3596-3604.

(149) Ngo, H. L.; LeCompte, K.; Hargens, L.; McEwen, A. B. Thermal Properties of Imidazolium Ionic Liquids. *Thermochimica Acta* **2000**, *357–358*, 97-102.

(150) Green, O.; Grubjesic, S.; Lee, S.; Firestone, M. A. The Design of Polymeric Ionic Liquids for the Preparation of Functional Materials. *Polymer Reviews* **2009**, *49*, 339-360.

(151) D. Holbrey, J.; R. Seddon, K. The Phase Behaviour of 1-Alkyl-3-Methylimidazolium Tetrafluoroborates; Ionic Liquids and Ionic Liquid Crystals. *Journal of the Chemical Society, Dalton Transactions* **1999**, 2133-2140.

(152) Hunley, M. T.; England, J. P.; Long, T. E. Influence of Counteranion on the Thermal and Solution Behavior of Poly(2-(dimethylamino)ethyl methacrylate)-Based Polyelectrolytes. *Macromolecules* **2010**, *43*, 9998-10005.

(153) Vygodskii, Y. S.; Mel'nik, O. A.; Shaplov, A. S.; Lozinskaya, E. I.; Malyshkina, I. A.; Gavrilova, N. D. Synthesis and Ionic Conductivity of Polymer Ionic Liquids. *Polym. Sci. Ser. A* **2007**, *49*, 256-261.

(154) Torriero, A. A. J.; Shiddiky, M. J. A.: *Electrochemical Properties and Applications of Ionic Liquids*; Nova Science Publishers, Incorporated, 2011.

(155) Ohno, H. Design of Ion Conductive Polymers Based on Ionic Liquids. *Macromolecular Symposia* **2007**, *249-250*, 551-556.

(156) Tarascon, J. M.; Armand, M. Issues and Challenges Facing Rechargeable Lithium Batteries. *Nature* **2001**, *414*, 359-367.

(157)   Batra, D.; Seifert, S.; Firestone, M. A. The Effect of Cation Structure on the Mesophase Architecture of Self-Assembled and Polymerized Imidazolium-Based Ionic Liquids. *Macromolecular Chemistry and Physics* **2007**, *208*, 1416-1427.

(158)   Nakajima, H.; Ohno, H. Preparation of Thermally Stable Polymer Electrolytes from Imidazolium-type Ionic Liquid Derivatives. *Polymer* **2005**, *46*, 11499-11504.

(159)   Ding, S.; Tang, H.; Radosz, M.; Shen, Y. Atom Transfer Radical Polymerization of Ionic Liquid 2-(1-Butylimidazolium-3-yl)ethyl Methacrylate Tetrafluoroborate. *Journal of Polymer Science Part A: Polymer Chemistry* **2004**, *42*, 5794-5801.

(160)   Hagfeldt, A.; Boschloo, G.; Sun, L.; Kloo, L.; Pettersson, H. Dye-Sensitized Solar Cells. *Chemical Reviews* **2010**, *110*, 6595-6663.

(161)   Grätzel, M. Recent Advances in Sensitized Mesoscopic Solar Cells. *Accounts of Chemical Research* **2009**, *42*, 1788-1798.

(162)   Meyer, W. H. Polymer Electrolytes for Lithium-Ion Batteries. *Advanced Materials* **1998**, *10*, 439-448.

(163)   Chen, H.; Choi, J.-H.; Salas-de la Cruz, D.; Winey, K. I.; Elabd, Y. A. Polymerized Ionic Liquids: The Effect of Random Copolymer Composition on Ion Conduction. *Macromolecules* **2009**, *42*, 4809-4816.

(164)   Lee, M.; Choi, U. H.; Colby, R. H.; Gibson, H. W. Ion Conduction in Imidazolium Acrylate Ionic Liquids and their Polymers. *Chemistry of Materials* **2010**, *22*, 5814-5822.

(165)   Li, X.; Eli, W.; Li, G. Solvent-Free Synthesis of Benzoic Esters and Benzyl Esters in Novel Brønsted Acidic Ionic Liquids under Microwave Irradiation. *Catalysis Communications* **2008**, *9*, 2264-2268.

(166)   Tokuda, H.; Hayamizu, K.; Ishii, K.; Susan, M. A. B. H.; Watanabe, M. Physicochemical Properties and Structures of Room Temperature Ionic Liquids. 1. Variation of Anionic Species. *The Journal of Physical Chemistry B* **2004**, *108*, 16593-16600.

(167)   Awad, W. H.; Gilman, J. W.; Nyden, M.; Harris Jr, R. H.; Sutto, T. E.; Callahan, J.; Trulove, P. C.; DeLong, H. C.; Fox, D. M. Thermal Degradation Studies of Alkyl-Imidazolium Salts and their Application in Nanocomposites. *Thermochimica Acta* **2004**, *409*, 3-11.

(168)   Crosthwaite, J. M.; Muldoon, M. J.; Dixon, J. K.; Anderson, J. L.; Brennecke, J. F. Phase Transition and Decomposition Temperatures, Heat Capacities and Viscosities of Pyridinium Ionic Liquids. *The Journal of Chemical Thermodynamics* **2005**, *37*, 559-568.

(169)   Chan, B.; Chang, N.; Grimmett, M. The Synthesis and Thermolysis of Imidazole Quaternary Salts. *Australian Journal of Chemistry* **1977**, *30*, 2005-2013.

(170)   Kroon, M. C.; Buijs, W.; Peters, C. J.; Witkamp, G.-J. Quantum Chemical Aided Prediction of the Thermal Decomposition Mechanisms and Temperatures of Ionic Liquids. *Thermochimica Acta* **2007**, *465*, 40-47.

(171)   Quartarone, E.; Mustarelli, P. Electrolytes for Solid-State Lithium Rechargeable Batteries: Recent Advances and Perspectives. *Chemical Society reviews* **2011**, *40*, 2525-2540.

(172)   Alba-Simionesco, C.; Fan, J.; Angell, C. A. Thermodynamic Aspects of the Glass Transition Phenomenon. II. Molecular Liquids with Variable Interactions. *The Journal of Chemical Physics* **1999**, *110*, 5262-5272.

(173)   Every, H.; Bishop, A. G.; Forsyth, M.; MacFarlane, D. R. Ion Diffusion in Molten Salt Mixtures. *Electrochimica Acta* **2000**, *45*, 1279-1284.

(174)   McFarlane, D. R.; Sun, J.; Golding, J.; Meakin, P.; Forsyth, M. High Conductivity Molten Salts Based on the Imide Ion. *Electrochimica Acta* **2000**, *45*, 1271-1278.

(175)   Nigmatullin, R. R.; Osokin, S. I.; Smith, G. New Approach in the Description of Dielectric Relaxation Phenomenon: Correct Deduction and Interpretation of the Vogel–Fulcher–Tamman Equation. *Journal of Physics: Condensed Matter* **2003**, *15*, 3481.

(176)   Bruce, P. G.; Vincent, C. A. Polymer Electrolytes. *Journal of the Chemical Society, Faraday Transactions* **1993**, *89*, 3187-3203.

(177)   Smedley, S. I.: *The Interpretation of Ionic Conductivity in Liquids*; Plenum Press: New York, 1980.

(178)   Ganapatibhotla, L. V. N. R.; Zheng, J.; Roy, D.; Krishnan, S. PEGylated Imidazolium Ionic Liquid Electrolytes: Thermophysical and Electrochemical Properties. *Chemistry of Materials* **2010**, *22*, 6347-6360.

(179)   Yu, G.; Zhao, D.; Wen, L.; Yang, S.; Chen, X. Viscosity of Ionic Liquids: Database, Observation, and Quantitative Structure-Property Relationship Analysis. *AIChE Journal* **2012**, *58*, 2885-2899.

(180) Viswanath, D. S.: *Viscosity of Liquids: Theory, Estimation, Experiment, and Data*; Springer, 2007.

(181) Peng, R.; Wang, Y.; Tang, W.; Yang, Y.; Xie, X. Progress in Imidazolium Ionic Liquids Assisted Fabrication of Carbon Nanotube and Graphene Polymer Composites. *Polymers* **2013**, *5*, 847-872.

(182) Galiński, M.; Lewandowski, A.; Stępniak, I. Ionic Liquids as Electrolytes. *Electrochimica Acta* **2006**, *51*, 5567-5580.

(183) Ekpe, U. J.; Sime, S. J. Properties of Molten Carboxylates. Part 2.-The Viscosities of Some Molten Lead and Zinc Carboxylates. *Journal of the Chemical Society, Faraday Transactions 1: Physical Chemistry in Condensed Phases* **1976**, *72*, 1144-1149.

(184) Ning, Z.; Fu, Y.; Tian, H. Improvement of Dye-Sensitized Solar Cells: What We Know and What We Need to Know. *Energy & Environmental Science* **2010**, *3*, 1170.

(185) O'Regan, B.; Grätzel, M. A Low-Cost, High-Efficiency Solar Cell Based on Dye-Sensitized Colloidal TiO_2 Films. *Nature* **1991**, *353*, 737-740.

(186) Halme, J.; Vahermaa, P.; Miettunen, K.; Lund, P. Device Physics of Dye Solar Cells. *Advanced materials* **2010**, *22*, E210-234.

(187) Armand, M.; Tarascon, J. M. Building Better Batteries. *Nature* **2008**, *451*, 652-657.

(188) Zou, H.; Wu, S.; Shen, J. Polymer/Silica Nanocomposites: Preparation, Characterization, Properties, and Applications. *Chemical Reviews* **2008**, *108*, 3893-3957.

(189) Qiao, J.; Chen, Y.; Baker, G. L. Polymer Electrolytes Based on Unsaturated Ethylene Oxide-Segmented Polymers. *Chemistry of Materials* **1999**, *11*, 2542-2547.

(190) Gazotti, W. A.; Spinacé, M. A. S.; Girotto, E. M.; De Paoli, M. A. Polymer Electrolytes Based on Ethylene Oxide–Epichlorohydrin Copolymers. *Solid State Ionics* **2000**, *130*, 281-291.

(191) Cao, Y.-C.; Xu, C.; Wu, X.; Wang, X.; Xing, L.; Scott, K. A Poly (Ethylene Oxide)/Graphene Oxide Electrolyte Membrane for Low Temperature Polymer Fuel Cells. *Journal of Power Sources* **2011**, *196*, 8377-8382.

(192) Anderman, M. Lithium-polymer batteries for electrical vehicles: A realistic view. *Solid State Ionics* **1994**, *69*, 336-342.

(193) Grajales, S. T.; Dong, X.; Zheng, Y.; Baker, G. L.; Bruening, M. L. Effects of Monomer Composition on CO₂-Selective Polymer Brush Membranes. *Chemistry of Materials* **2010**, *22*, 4026-4033.

(194) Kim, J.-B.; Bruening, M. L.; Baker, G. L. Surface-Initiated Atom Transfer Radical Polymerization on Gold at Ambient Temperature. *Journal of the American Chemical Society* **2000**, *122*, 7616-7617.

(195) Kim, J.-B.; Huang, W.; Bruening, M. L.; Baker, G. L. Synthesis of Triblock Copolymer Brushes by Surface-Initiated Atom Transfer Radical Polymerization. *Macromolecules* **2002**, *35*, 5410-5416.

(196) Pyun, J.; Jia, S.; Kowalewski, T.; Patterson, G. D.; Matyjaszewski, K. Synthesis and Characterization of Organic/Inorganic Hybrid Nanoparticles: Kinetics of Surface-Initiated Atom Transfer Radical Polymerization and Morphology of Hybrid Nanoparticle Ultrathin Films. *Macromolecules* **2003**, *36*, 5094-5104.

(197) Bombalski, L.; Min, K.; Dong, H.; Tang, C.; Matyjaszewski, K. Preparation of Well-Defined Hybrid Materials by ATRP in Miniemulsion. *Macromolecules* **2007**, *40*, 7429-7432.

(198) Braunecker, W. A.; Matyjaszewski, K. Controlled/Living Radical Polymerization: Features, Developments, and Perspectives. *Progress in Polymer Science* **2007**, *32*, 93-146.

(199) Moad, G.; Rizzardo, E.; Thang, S. H. Living Radical Polymerization by the RAFT Process. *Australian Journal of Chemistry* **2005**, *58*, 379-410.

(200) Moad, G.; Rizzardo, E.; Thang, S. H. Living Radical Polymerization by the RAFT Process—A First Update. *Australian Journal of Chemistry* **2006**, *59*, 669-692.

(201) Moad, G.; Rizzardo, E.; Thang, S. H. Living Radical Polymerization by the RAFT Process – A Second Update. *Australian Journal of Chemistry* **2009**, *62*, 1402-1472.

(202) Bartholome, C.; Beyou, E.; Bourgeat-Lami, E.; Chaumont, P.; Lefebvre, F.; Zydowicz, N. Nitroxide-Mediated Polymerization of Styrene Initiated from the Surface of Silica Nanoparticles. In Situ Generation and Grafting of Alkoxyamine Initiators. *Macromolecules* **2005**, *38*, 1099-1106.

(203) Konn, C.; Morel, F.; Beyou, E.; Chaumont, P.; Bourgeat-Lami, E. Nitroxide-Mediated Polymerization of Styrene Initiated from the Surface of Laponite Clay Platelets. *Macromolecules* **2007**, *40*, 7464-7472.

(204) Hawker, C. J.; Barclay, G. G.; Orellana, A.; Dao, J.; Devonport, W. Initiating Systems for Nitroxide-Mediated "Living" Free Radical Polymerizations: Synthesis and Evaluation. *Macromolecules* **1996**, *29*, 5245-5254.

(205) Hawker, C. J.; Bosman, A. W.; Harth, E. New Polymer Synthesis by Nitroxide Mediated Living Radical Polymerizations. *Chemical Reviews* **2001**, *101*, 3661-3688.

(206) Balazs, A. C.; Emrick, T.; Russell, T. P. Nanoparticle Polymer Composites: Where Two Small Worlds Meet. *Science* **2006**, *314*, 1107-1110.

(207) von Werne, T.; Patten, T. E. Atom Transfer Radical Polymerization from Nanoparticles: A Tool for the Preparation of Well-Defined Hybrid Nanostructures and for Understanding the Chemistry of Controlled/"Living" Radical Polymerizations from Surfaces. *Journal of the American Chemical Society* **2001**, *123*, 7497-7505.

(208) Sunday, D.; Curras-Medina, S.; Green, D. L. Impact of Initiator Spacer Length on Grafting Polystyrene from Silica Nanoparticles. *Macromolecules* **2010**, *43*, 4871-4878.

(209) Jiang, X.; Zhong, G.; Horton, J. M.; Jin, N.; Zhu, L.; Zhao, B. Evolution of Phase Morphology of Mixed Poly(tert-butyl acrylate)/Polystyrene Brushes Grafted on Silica Particles with the Change of Chain Length Disparity. *Macromolecules* **2010**, *43*, 5387-5395.

(210) Yuan, W.; Zhao, H.; Hu, H.; Wang, S.; Baker, G. L. Synthesis and Characterization of the Hole-Conducting Silica/Polymer Nanocomposites and Application in Solid-State Dye-Sensitized Solar Cell. *ACS applied materials & interfaces* **2013**, *5*, 4155-4161.

(211) Saha, S.; Bruening, M. L.; Baker, G. L. Facile Synthesis of Thick Films of Poly(methyl methacrylate), Poly(styrene), and Poly(vinyl pyridine) from Au Surfaces. *ACS applied materials & interfaces* **2011**, *3*, 3042-3048.

(212) Zhao, H. PhD Dissertation. 2013.

(213) Matyjaszewski, K.; Miller, P. J.; Shukla, N.; Immaraporn, B.; Gelman, A.; Luokala, B. B.; Siclovan, T. M.; Kickelbick, G.; Vallant, T.; Hoffmann, H.; Pakula, T. Polymers at Interfaces: Using Atom Transfer Radical Polymerization in the Controlled Growth of Homopolymers and Block Copolymers from Silicon Surfaces in the Absence of Untethered Sacrificial Initiator. *Macromolecules* **1999**, *32*, 8716-8724.

(214) Michael, G.; Ferch, H. Basic Characteristics of AEROSIL. *Degussa Technical Bulletin Pigment* **1998**.

(215)   Zhang, X.-W.; Fedkiw, P. S. Ionic Transport and Interfacial Stability of Sulfonate-Modified Fumed Silicas as Nanocomposite Electrolytes. *Journal of The Electrochemical Society* **2005**, *152*, A2413-A2420.

(216)   Gagne, M. R.; Stern, C. L.; Marks, T. J. Organolanthanide-Catalyzed Hydroamination. A kinetic, Mechanistic, and Diastereoselectivity Study of the Cyclization of N-unprotected Amino Olefins. *Journal of the American Chemical Society* **1992**, *114*, 275-294.

(217)   Ohshima, H.: *Electrical Phenomena at Interfaces and Biointerfaces: Fundamentals and Applications in Nano-, Bio-, and Environmental Sciences*; Wiley, 2012.

(218)   Association, N. F. P.; Engineers, S. o. F. P.: *SFPE Handbook of Fire Protection Engineering, Third Edition*; NFPA, National Fire Protection Association, 2002.

(219)   Wunderlich, B. Theory of Cold Crystallization of High Polymers. *The Journal of Chemical Physics* **1958**, *29*, 1395-1404.

(220)   Stowe, M. K.; Liu, P.; Baker, G. L. Star Poly(ethylene oxide) as a Low Temperature Electrolyte and Crystallization Inhibitor. *Chemistry of Materials* **2005**, *17*, 6555-6559.

(221)   Li, D.; Jones, G. L.; Dunlap, J. R.; Hua, F.; Zhao, B. Thermosensitive Hairy Hybrid Nanoparticles Synthesized by Surface-Initiated Atom Transfer Radical Polymerization. *Langmuir* **2006**, *22*, 3344-3351.